

Polymer Blending as a Surface Modification Technique to  
Alter the Wettability of Hydrophobic Electrospun Mats

by

Rafael SALLES KURUSU

MANUSCRIPT-BASED THESIS PRESENTED TO ÉCOLE DE  
TECHNOLOGIE SUPÉRIEURE IN PARTIAL FULFILLMENT FOR THE  
DEGREE OF DOCTOR OF PHILOSOPHY  
Ph.D.

MONTREAL, DECEMBER 19, 2016

ÉCOLE DE TECHNOLOGIE SUPÉRIEURE  
UNIVERSITÉ DU QUÉBEC

© Copyright 2016 reserved by Rafael SALLES KURUSU

© Copyright reserved

It is forbidden to reproduce, save or share the content of this document either in whole or in parts. The reader who wishes to print or save this document on any media must first get the permission of the author.

**BOARD OF EXAMINERS**  
**THIS THESIS HAS BEEN EVALUATED**  
**BY THE FOLLOWING BOARD OF EXAMINERS**

Professor Nicole R. Demarquette, Thesis Supervisor  
Mechanical Engineering Department at École de technologie supérieure

Professor Simon Joncas, President of the Board of Examiners  
Automated Manufacturing Engineering Department at École de technologie supérieure

Professor Éric David, Member of the jury  
Mechanical Engineering Department at École de technologie supérieure

Professor Ricardo Zednik, Member of the jury  
Mechanical Engineering Department at École de technologie supérieure

Professor Basil Favis, External Evaluator  
École Polytechnique de Montréal

**THIS THESIS WAS PRESENTED AND DEFENDED**  
**IN THE PRESENCE OF A BOARD OF EXAMINERS AND PUBLIC**  
**ON DECEMBER 12, 2016**  
**AT ÉCOLE DE TECHNOLOGIE SUPÉRIEURE**



## ACKNOWLEDGMENT

First, I would like to thank Professor Nicole for the opportunity to be the first graduate student to join the group at ÉTS. I will always appreciate the time, guidance and especially the trust and freedom I had to conduct my project and to make my own mistakes and discoveries.

I would also like to express my gratitude to the *École de Technologie Supérieure* for the generous scholarship I received to pursue my studies during these four years. I hope I have met the expectations and I also hope that this type of program to support foreign students will continue to exist.

Among people from ÉTS, I would like to thank Professor Éric David for his help throughout the whole project; Professor Sophie Lerouge, whose classes inspired me to change the direction of my project and her students (Mathieu, Audrey, Fatemeh and Jessica) for the help with experiments; Professor Sylvain Cloutier and his students (Jaime, Felipe and Charles) for helping me with film fabrication; Professors Natalia Nuño, Ricardo Zednik and Simon Joncas for agreeing to evaluate this work during exams or defense. I would also like to thank the technicians Radu, Olivier, Nabil, Claude-Daniel and Michel for their practical help.

I would like to thank Professor Basil Favis from *École Polytechnique* for agreeing to evaluate this thesis; Professor Ali Dolatabadi and his student Navid for the high-speed imaging experiments at Concordia University; Patricia at *Université de Montréal* for the help with AFM experiments and Josianne for all the XPS at *Polytechnique*.

I would like to express my gratitude to all the students and interns from our research group during this time: Anthony, Camille, Carlos, Chris, Emna, Foued, Marwa, Victor and Zahra. I wish you the best of luck on your path.

I could not forget the people who have made the life in Montreal or elsewhere much more interesting and have helped me to cope with difficult times. Glenn and Odile, for the talks, beers, food, festivals, etc. People from ÉTS that I got to know better outside: Audrey, Fernando, Felipe, Jaime, Oana, Thomas, Rafael, Leice, Julie, Mauricio and Scheyla. All the French-speaking people I bothered during lunch, in special Patrice, Martin, Thibault and Romain. Also, Mary's friends from Polytechnique and Canarail and all my Brazilian friends for being present even by distance.

A special thanks to my parents, my brother and my sister and all the family for their love and support.

And, of course, I would like to thank Mary for being there, for pushing me when needed, for absolutely everything. And our little one, who, as I write this section, is about to start his journey in this world. Thanks for putting things in perspective, or, as a materials scientist would say, for helping me find the right magnification.

# LES MÉLANGES DE POLYMÈRES COMME TECHNIQUE DE TRAITEMENT DE SURFACE POUR ALTÉRER LA MOUILLABILITÉ DES TAPIS ÉLECTROFILÉS

Rafael SALLES KURUSU

## RÉSUMÉ

Dans cette thèse, l'utilisation des mélanges de polymères comme technique de modification de surface pour contrôler la mouillabilité des tapis électrofilés a été étudiée. Dans la première étape, une matrice hydrophobe (SEBS) a été mélangée avec un copolymère amphiphile (PEO-PPO-PEO) et les résultats ont montré que l'hydrophilisation a été réalisée avec 15% en poids de PEO-PPO-PEO avec une grande ségrégation à la surface. Cependant, cette composition a présenté des propriétés de surface non homogènes. Une analyse microscopique a révélé que la composition à 20% en poids de PEO-PPO-PEO a présenté une morphologie particulière avec des grains interconnectés qui a augmenté la rugosité de la surface des films et des fibres et qui a contribué aux propriétés de surface plus homogènes. Dans l'étape suivante, trois types de copolymères PEO-PPO-PEO avec des poids moléculaires et des contenus de PEO différents ont été utilisés pour hydrophiliser le SEBS. La ségrégation à la surface a augmentée dans les mélanges de SEBS avec des molécules PEO-PPO-PEO plus petites et avec une proportion plus élevée de blocs hydrophobes PPO. L'hydrophilisation a été réalisée avec aussi peu que 5% en poids de PEO-PPO-PEO et la saturation de la surface a également été observée. L'imagerie à grande vitesse et les mesures à effet de mèche ont montré que le temps d'étalement et de remontée capillaire varient grandement en fonction du niveau de la ségrégation et le type de PEO-PPO-PEO utilisé dans les mélanges. La dernière partie de cette thèse est une comparaison des mélanges des polymères hydrophobes soit avec un polymère hydrophile (PEO) ou avec des polymères amphiphiles (PEO-PPO-PEO) pour atteindre l'hydrophilisation. Les résultats ont montré que la présence des blocs PPO avec une faible énergie de surface a augmenté considérablement la ségrégation des polymères PEO-PPO-PEO vers la surface tandis que les mélanges avec PEO pur ont présenté une diminution de PEO dans la surface. De manière surprenante, la ségrégation de PEO-PPO-PEO a continué pendant plusieurs semaines à température ambiante. Les résultats théoriques ont montré que la morphologie d'équilibre pour le système SEBS/PPO correspond à une couche de PPO (mouillage complet) sur le SEBS, ce qui confirme les résultats expérimentaux de la couverture complète dans certains mélanges ainsi que les résultats de vieillissement. La capacité de la matrice de permettre le mouvement de PEO-PPO-PEO a également été analysée en comparant la ségrégation de ce copolymère à l'intérieur du SEBS et du PS pur. Dans le premier, la ségrégation a été élevée en raison d'une plus grande fraction de volume libre à la température ambiante tandis que dans le dernier aucune ségrégation au fil du temps n'a été observée.

**Mot-clés :** mélanges de polymères, mouillabilité, électrofilage, modification de surface



# **POLYMER BLENDING AS A SURFACE MODIFICATION TECHNIQUE TO ALTER THE WETTABILITY OF HYDROPHOBIC ELECTROSPUN MATS**

Rafael SALLES KURUSU

## **ABSTRACT**

In this thesis, blending as a surface modification technique to change the wettability of hydrophobic electrospun mats was investigated. In the first step, SEBS, chosen as the hydrophobic matrix was blended with amphiphilic PEO-PPO-PEO copolymer. The results showed that hydrophilization was achieved with 15 wt% of PEO-PPO-PEO in the SEBS/PEO-PPO-PEO mats with great surface segregation. But although hydrophilic, this composition presented nonuniform surface coverage and wettability. A microscopic analysis revealed that the composition with 20 wt% of PEO-PPO-PEO presented a peculiar rough interconnected grain-like morphology on the surface of the films and fibers that contributed to more homogeneous surface properties. In the next step, three different types of commercially available PEO-PPO-PEO copolymers with different molecular weight and PEO content were used to hydrophilize SEBS. Segregation to the surface increased in the blends of SEBS with smaller PEO-PPO-PEO molecules with higher proportion of hydrophobic PPO blocks. Hydrophilization was achieved with as little as 5 wt% of PEO-PPO-PEO and complete surface saturation was also observed at higher PEO-PPO-PEO contents. Blends with liquid PEO-PPO-PEO presented leaching when in contact with water. High-speed imaging and wicking measurements were performed to distinguish between different hydrophilic mats, and the results showed that the spreading time and wicking rate varied greatly according to the level of segregation and the type of PEO-PPO-PEO used in the blends. The last part of this thesis is a comparison of blending hydrophobic polymers with either hydrophilic PEO or amphiphilic PEO-PPO-PEO polymers to achieve hydrophilization. The results showed that the presence of low surface energy PPO blocks greatly increased the segregation of PEO-PPO-PEO. Blends with pure PEO presented surface depletion and hydrophilization was not achieved in the range of compositions tested (0-20 wt%). Surprisingly, the segregation of PEO-PPO-PEO continued over weeks at room temperature. Theoretical results showed that the equilibrium morphology for the SEBS/PPO system corresponds to a complete wetting layer of PPO over SEBS, which supports the experimental results of complete coverage for some of the SEBS/PEO-PPO-PEO blends and also the aging results that showed a continued segregation to form a PPO layer. The ability of the matrix to allow PEO-PPO-PEO movement over time was also analyzed by comparing the segregation of this copolymer inside SEBS and pure PS. The former presented major segregation due to a higher fraction of free volume at room temperature while the latter practically presented no segregation over time.

**Keywords:** polymer blends, electrospinning, wettability, surface modification



## TABLE OF CONTENTS

	Page
INTRODUCTION .....	1
0.1 Research Hypothesis .....	2
0.2 Objectives .....	2
CHAPTER 1 SURFACE MODIFICATION TO CONTROL THE WETTABILITY OF ELECTROSPUN MATS .....	 5
1.1 Introduction.....	5
1.1.1 Applications of mats with controlled wetting behavior.....	7
1.1.1.1 Membranes for separation/filtration .....	8
1.1.1.2 Sensing applications.....	9
1.1.1.3 Self-cleaning surfaces and antifouling membranes .....	9
1.1.1.4 Tissue engineering and drug delivery .....	10
1.2 Basic principles.....	11
1.2.1 Electrospinning process .....	11
1.2.2 Wettability of electrospun mats .....	13
1.3 Surface modification methods .....	18
1.3.1 Post-treatments.....	20
1.3.1.1 Plasma.....	20
1.3.1.2 Wet chemistry .....	27
1.3.1.3 Grafting.....	34
1.3.1.4 Coating.....	40
1.3.2 One-step surface modification .....	48
1.3.2.1 Nanoparticles .....	48
1.3.2.2 Blending.....	55
1.4 Future prospects and conclusions .....	65
CHAPTER 2 ARTICLES ORGANIZATION.....	67
CHAPTER 3 BLENDING AND MORPHOLOGY CONTROL TO TURN HIGHLY HYDROPHOBIC SEBS ELECTROSPUN MATS SUPERHYDROPHILIC .....	  69
3.1 Introduction.....	70
3.2 Experimental .....	73
3.3 Results and discussion .....	75
3.4 Conclusions.....	86
3.5 Acknowledgements.....	87

CHAPTER 4	WETTING OF HYDROPHILIC ELECTROSPUN MATS PRODUCED BY BLENDING SEBS WITH PEO-PPO-PEO COPOLYMERS OF DIFFERENT MOLECULAR WEIGHT .....	89
4.1	Introduction.....	90
4.2	Experimental.....	92
4.3	Results and discussion .....	94
4.4	Conclusions.....	106
4.5	Acknowledgements.....	107
CHAPTER 5	SURFACE PROPERTIES EVOLUTION IN ELECTROSPUN POLYMER BLENDS BY SEGREGATION OF HYDROPHILIC OR AMPHIPHILIC MOLECULES.....	109
5.1	Introduction.....	109
5.2	Experimental.....	112
5.3	Results and discussion .....	113
5.4	Conclusions.....	126
5.5	Acknowledgements.....	127
CHAPTER 6	DISCUSSION.....	129
6.1	Wetting of electrospun mats .....	129
6.2	Electrospinning of SEBS and SEBS/PEO-PPO-PEO blends .....	130
6.3	Hydrophilization of SEBS with PEO-PPO-PEO .....	131
6.4	Morphology evolution of electrospun blends .....	132
CONCLUSIONS AND RECOMMENDATIONS .....		135
7.1	Main findings and conclusions.....	135
	7.1.1 Summary and conclusions of Chapter 3.....	135
	7.1.2 Summary and conclusions of Chapter 4.....	136
	7.1.3 Summary and conclusions of Chapter 5.....	137
	7.1.4 Main Conclusion .....	139
7.2	Recommendations .....	139
ANNEX I	ABOUT THE AUTHOR - ACADEMIC ACHIEVEMENTS.....	141
LIST OF BIBLIOGRAPHICAL REFERENCES.....		144

## LIST OF TABLES

	Page
Table 1.1 – Plasma treatment used to alter the wettability of electrospun mats .....	22
Table 1.2 – Wet-chemistry methods to change the wettability of electrospun mats ....	29
Table 1.3 – Grafting strategies and the effect on the wetting behavior of electrospun mats .....	35
Table 1.4 – Surface modification by coating or adsorption.....	41
Table 1.5 – Nanoparticles to change surface properties of electrospun mats .....	49
Table 1.6 – Blending as a surface modification technique .....	57
Table 3.1 - Mechanical properties of electrospun mats.....	86
Table 4.1 - Main features of the PEO-PPO-PEO copolymers used in the present study	92
Table 5.1 – Surface energy values calculated by the Owens-Wendt method, and taken from literature as indicated .....	118
Table 5.2 – Interfacial tension, spreading coefficients and possible morphologies for the polymer blends using either hydrophilic PEO or amphiphilic PEO-PPO-PEO as surface modifying polymers in a SEBS or PS matrix .....	119



## LIST OF FIGURES

	Page
Figure 1.1 – Possible applications of electrospun mats with controlled wettability (a) PAN electrospun membrane used for oil-water separation after surface modification (X. Li, Wang, Wang, Cheng, & Wang, 2014); (b) Schematic apparatus of a humidity sensing system where electrospun fibers are deposited on the electrode inside the humidity chamber (Xianfeng, Bin, Jianyong, Moran, & Fukui, 2010); (c) water droplets deposited on superhydrophobic electrospun PS-PDMS/PS blends (Minglin Ma, Hill, Lowery, Fridrikh, & Rutledge, 2005); (d) Fluorescence micrograph showing myoblast cells in a PLGA/gelatin/ $\alpha$ -elastin electrospun mat used for tissue engineering (M. Li et al., 2006); (e) Three different strategies to load drugs on the surface of electrospun fibers (Yoo, Kim, & Park, 2009). .....	7
Figure 1.2 – Schematic of the electrospinning process with the main material and processing parameters that will influence the final wettability. ....	13
Figure 1.3 – Basics of wetting: (a) A droplet deposited on a perfectly flat surface forming an equilibrium contact angle $\theta_E$ according with the energies involved; (b) Wetting on rough surfaces, characterized by the observed contact angle $\theta^*$ , showing the transition from Wenzel to Cassie-Baxter state, defined by a critical contact angle $\theta_c$ . .....	14
Figure 1.4 – Wetting in porous structures: (a) Critical contact angle as a function of roughness and solid fraction; (b) typical switching mechanism in porous structures like electrospun mats, from hydrophobic (Cassie-Baxter state) to complete absorption of water by simple chemical modification. ....	15
Figure 1.5 – Measuring the advancing and receding contact angle by (a) increasing or decreasing the drop volume or (b) tilting the surface until the drop starts to slide or roll.....	17
Figure 1.6 – Evaluating the wettability of hydrophilic mats: (a) wicking measurements on a mat strip to analyze the liquid rise dynamics; (b) high-speed imaging to observe the dynamics of droplet impact. ....	18
Figure 1.7 – Schematic showing the main approaches to modify.....	19

Figure 1.8 –	Schematic showing surface hydrophilization by plasma treatment (Oh & Lee, 2013).....	21
Figure 1.9 –	PVDF electrospun mats treated by plasma and the (a) influence of plasma power on the contact angle; (b) mat morphology as a function of applied power: no treatment (b.1), 240 W (b.2), 360 W (b.3) and 480 W (b.4) (Correia et al., 2015).....	24
Figure 1.10 –	Electrospun PCL mats treated by plasma with (a) and without (b) an aluminum oxide template (c) (Jeon & Kim, 2014).....	26
Figure 1.11 –	Effect of plasma treatment on the wettability of electrospun PCL mats: (a) untreated mat; (b) treated without the aluminum oxide template; (c) treated with template; (d) comparison of water absorption capacity (Jeon & Kim, 2014). .....	26
Figure 1.12 –	Hydrolysis and aminolysis reactions to introduce hydrophilic groups on the surface of PLGA (Croll, O'Connor, Stevens, & Cooper-White, 2004). .....	28
Figure 1.13 –	Proposed wetting mechanism for (a, b) PVA-silanol fibers after silanization with strong adhesion due to the low receding contact angle; (c, d) PVA/silica-silanol fibers after silanization showing air pockets that helps to increase the receding contact angle (Pisuchpen et al., 2011).....	33
Figure 1.14 –	The main approaches to graft polymers on a surface: (a) grafting-to, in which the macromolecules are grafted to functional groups and (b) grafting-from, in which polymerization occurs directly on the surface (Araki, 2013).....	34
Figure 1.15 –	PVDF electrospun mat: (a) untreated, (b) top surface after plasma exposure, (c) top surface after MMA grafting and (d) bottom surface after MMA grafting (Kaur et al., 2007). .....	38
Figure 1.16 –	Atomic force microscopy images showing the grafted layers on PMMA-co-BIEM fibers grafted with (a) PMAPS, (b) PHEMA and (c) PFA-C8-grafted (Yano et al., 2011). .....	39
Figure 1.17 –	Wettability of PS nanofibrous mats with solid fibers (PS-sNF) as a function of coating time in PDOPA solution: (1) Contact angle evolution for (a) uncoated mats, (b) PS mats coated for 15 minutes (PS-sNF-15), (c) PS mats coated for 90 minutes; (2) Moisture transport behavior for the same compositions, showing the water content on the top surface of the mat where the liquid is sprayed and on the bottom surface to evaluate the transport ability (Dong et al., 2014).....	45

Figure 1.18 –	SEM images and respective contact angle of PMMA/O-MMT composite fibers (a) untreated and sputter-coated with TiO <sub>2</sub> with (b) 80 W, (c) 100 W, (d) 120 W and (e) 200 W of sputter power. TEM image of (a) showing nanoclay domains (Q. Wang et al., 2011). ....	47
Figure 1.19 –	Dual-morphology with thicker and spiderweb-like thinner nanofibers found in electrospun nanocomposites of (a) TPU/Tourmaline (95/05 wt%) (Tijing et al., 2012) (Reproduced with permission from Elsevier Ltd, UK) and (b) PA6/HAp (90/10 wt%) (Abdal-hay, Pant, et al., 2013). .....	52
Figure 1.20 –	Wicking behavior of PAN/fumed silica composite mats as a function of additive (A150 or R805) concentration: (a) water uptake as a function of time; (b) total absorbed water after wicking; (c) wicking height as a function of time (Dufficy et al., 2015). .....	54
Figure 1.21 –	Schematic of blending immiscible polymers by electrospinning and some of the possible bulk and surface morphologies. ....	56
Figure 1.22 –	Contact angle results for PS/PVME fibers, miscible and immiscible, and miscible films (Valiquette & Pellerin, 2011). .....	60
Figure 1.23 –	Effect of blending on the mat morphology: (a) Pure PET and (b) PET/PVA (20/1 proportion) blend (G. Li et al., 2013) (Reproduced with permission from Elsevier Ltd, UK); (c) Pure PCL and (d) PCL/n-chitin (95:05) blend (Ji et al., 2014). .....	62
Figure 1.24 –	Amount of oxygen at the surface of SEBS/PEO-PPO-PEO electrospun fibers prepares with different PEO-PPO-PEO (F127, P123, and L61). From bottom to top, the solid lines show the theoretical amount of oxygen according to the bulk composition, pure L61, pure P123 and pure F127 (Rafael S. Kurusu & Demarquette, 2016). .....	64
Figure 3.1 –	Water contact angle for the electrospun mats (black diamonds) and dip-coated films (open circles) as a function of F127 concentration in the SEBS/F127 blends. The insert shows the vials containing each solution..	76
Figure 3.2 –	Water droplet fast spreading for the superhydrophilic SEBS/F127_20 electrospun mat. ....	76
Figure 3.3 –	Electrospun fibers observed by SEM with 100x magnification: (a) pure SEBS and (b) SEBS/F127_20. Scale bars correspond to 200 μm. ....	77

Figure 3.4 –	XPS results: (a) Measured % of oxygen atoms converted in wt% of F127 vs. bulk wt% of F127 for the electrospun mats (black diamonds) and dip-coated films (open circles); (b) High resolution XPS spectra for the electrospun SEBS/F127 mats with 5, 10, 15 and 20 wt% of F127. ....	80
Figure 3.5 –	Dip-coated films observed by transmitted light microscopy at 1000x magnification: (a) Pure SEBS, and increasing F127 concentration to (b) 5 wt% (c) 10 wt% (d), 15 wt% (e) 20 wt% (f) and pure F127. Scale bars correspond to 20 $\mu\text{m}$ .....	82
Figure 3.6 –	Dip-coated films observed by SEM in secondary electrons mode and 1000x magnification for the (a) SEBS/F127_20 blend, and (b) pure F127. Scale bars correspond to 20 $\mu\text{m}$ .....	83
Figure 3.7 –	SEM images of (a) Pure SEBS, (b) SEBS/F127_15 and (c) SEBS/F127_20 at 10.000x magnification. The scale bars correspond to 1 $\mu\text{m}$ . ....	84
Figure 3.8 –	AFM experimental scheme for electrospun fibers with a scan area of 500nmX500nm; (a-d) Phase images of (a) Pure SEBS, (b) region 1 of SEBS/F127_15, (c) region 2 of SEBS/F127_15, and (d) SEBS/F127_20.....	85
Figure 3.9 –	Schematic simplified illustrations of a water drop in contact with electrospun mats for the hydrophobic and superhydrophilic compositions. ....	86
Figure 4.1 –	Water contact angle results for all electrospun mats as a function of PEO-PPO-PEO content. The insert is a plot of the hemi-wicking condition (J. Bico et al., 2001), the critical contact angle $\theta_c$ as a function of roughness $r$ for different values of solid/liquid interface fraction ( $\phi_s$ ).....	94
Figure 4.2 –	(a) spreading and imbibition experiments methodology and results for the contact angle $\theta$ as a function of time; (b) drop impact images showing the last frame before impact as the first image and the total time for absorption as the final image for F127_20, P123_20 and L61_20 (top to bottom).....	97
Figure 4.3 –	Results for the wicking measurements: (a) example of the experiments pictures and the results for height as a function of time; (b) the square of height ( $h^2$ ) versus time; (c) Diffusion coefficient $D$ and total time to reach the maximum height as a function of PEO-PPO-PEO content. ....	99

Figure 4.4 –	(a) SEM micrographs of the samples containing 5 and 20 wt% of PEO-PPO-PEO (scale bar = 20 $\mu\text{m}$ ) and (b) the results of fiber diameter as a function of PEO-PPO-PEO content for all samples. ....	102
Figure 4.5 –	(a) X-ray photoelectron spectroscopy (XPS) survey spectra for pure SEBS, F127_20, P123_20, L61_20 and pure PEO-PPO-PEO; (b) XPS results of the atomic percentage of oxygen as a function of blend bulk composition. The straight lines are theoretical values based on the chemical structure of each molecule. ....	103
Figure 4.6 –	Wicking results as a function of the number of EO segments in each side of the PEO-PPO-PEO molecules. ....	104
Figure 4.7 –	L61_20 fibers: (a) L61 leaching observed by optical microscopy, in which the arrows indicate the water front advancing direction (scale bar = 10 $\mu\text{m}$ ); (b) SEM image of the same composition showing broken fibers (scale bar = 30 $\mu\text{m}$ ). ....	106
Figure 5.1 –	Mat morphology and static contact angle results for (a) pure SEBS, (b) F127_20, (c) P123_20 and (d) PEO_20. ....	114
Figure 5.2 –	XPS results: (a) Survey spectra for pure PEO-PPO-PEO and pure SEBS showing the photoemission peaks of C 1s and O 1s. (a) Surface chemical composition of SEBS/PEO-PPO-PEO or SEBS/PEO blends after processing (day 1) as a function of PEO-PPO-PEO (F127 or P123) or PEO concentration (0, 5, 10, 15 and 20 wt%). ....	115
Figure 5.3 –	XPS aging results: (a) Survey results showing PEO or PEO-PPO-PEO (F127 or P123) segregation to the surface over time in the SEBS blends; (b) High-resolution spectra showing intensity increase in the –C-O- peak over time. ....	116
Figure 5.4 –	Possible blend surface morphologies according to surface energy values and spreading coefficients. Polymer 1 (orange) is the SEBS matrix and polymer 2 (green) represents either PEO or PEO-PPO-PEO. ....	119
Figure 5.5 –	Edge of a cut mat and cross section of a fiber after washing: (a) and (b) PEO_20; (c) and (d) P123_20. Scale bars = 20 $\mu\text{m}$ in (a) and (c); 2 $\mu\text{m}$ in (b) and (d). ....	123

Figure 5.6 –	Schematic illustrations: (a) solutions containing SEBS and PEO-PPO-PEO with pictures of representative solutions; (b) surface enrichment and hydrophilization mechanism with amphiphilic PEO-PPO-PEO and pure PEO (out of scale); (c) Aging mechanism showing PEO-PPO-PEO molecules that continue to segregate to the surface over time after solidification. ....	124
Figure 5.7 –	Evolution in oxygen content over time for the blends containing 5 and 10 wt% of P123 in SEBS or PS matrix.....	126

## LIST OF ABBREVIATIONS

AA	Acrylic acid
AFM	Atomic Force Microscopy
ATRP	Atom transfer radical polymerization
BIEM	2-(2-bromoisobutyryloxy) ethyl methacrylate (BIEM)
CA	Cellulose acetate
CF <sub>4</sub>	Tetrafluoromethane
CNC	Cellulose nanocrystal
CNT	Carbon nanotubes
CS	Chondroitin sulfate
DOPA	Dopamine
DTMS	Decyltrimethoxysilane
ECM	Extra cellular matrix
F108	Pluronic F108 (PEO-PPO-PEO)
F127	Pluronic F127 (PEO-PPO-PEO)
FAS	Fluoroalkylsilane
FPU	Flourinated Polyurethane
GO	Graphene oxide
HA	Hyaluronic acid
HAp	Hydroxyapatite
HCL	Hydrochloric acid
iCVD	Initiated chemical vapor deposition
L61	Pluronic L61 (PEO-PPO-PEO)
LCST	Lower critical solution temperature
LiClO <sub>4</sub>	Lithium perchlorate
MAA	Methyl methacrylate
M <sub>w</sub>	Weight Average Molecular Weight

MWCNT	Multiwalled carbon nanotubes
NaIO <sub>4</sub>	Sodium periodate
NaOH	Sodium hydroxide
NIPAAm	N-isopropylacrylamide
O-MMT	Organically modified montmorillonite (O-MMT)
P123	Pluronic P123 (PEO-PPO-PEO)
PA6	Polyamide 6
PAA	Poly(acrylic acid)
PAN	Polyacrylonitrile
PANi	Polyaniline
PBLG	poly( $\gamma$ -benzyl-L-glutamate)
PCL	Poly( $\epsilon$ -caprolactone)
PDLLA	Poly(DL-lactide)
PDMS	Poly(styrene-b-dimethylsiloxane)
PDOPA	Polydopamine
PEG	Poly(ethylene glycol)
PEI	Polyethyleneimine
PEO	Poly(ethylene oxide)
PEO-PPO-PEO	Poly(ethylene oxide)-b-poly(propylene oxide)-b-poly(ethylene oxide)
PET	Polyethylene terephthalate
PFA-C8	Poly(2-(perfluorooctyl)ethyl acrylate)
PFDTs	Perfluorodecyltrichlorosilane
PGA	Poly(glycolic acid)
PHA	Polyhydroxyalkanoates
PHBV	Poly(3-hydroxybutyrate-co-3-hydroxyvalerate)
PHEMA	Poly(2-hydroxyethyl methacrylate)
PLA	Poly(lactide)
PLACL	Poly(l-lactic acid)-co-poly( $\epsilon$ -caprolactone)
PLCL	Poly( $\epsilon$ -caprolactone-co-lactide)
PLGA	Poly(lactic-co-glycolic acid)

PLLA	Poly(l-lactic acid)
PMAPS	Poly(3-(N-2-methacryloyloxyethyl-N,N-dimethyl ammonatopropanesulfonate)
PMIA	Poly(m-phenylene isophthalamide)
PMMA	Poly(methyl methacrylate)
PNIPA	Poly(N-isopropylacrylamide)
PNIPAAm	poly(N-isopropylacrylamide)
POSS	Polyhedral Oligomeric Silsesquioxane
PP	Polypropylene
PPFEMA	Poly(perfluoroalkyl ethyl methacrylate)
PPO	Poly(propylene oxide)
PS	Polystyrene
PSMA	Polystyrene/maleic anhydride
Psu	Polysulfone
PTFE	Polytetrafluoroethylene (Teflon)
PU	Polyurethane
PVA	Poly(vinyl alcohol)
PVB	Polyvinyl butyral
PVDF	Poly(vinylidene fluoride)
PVDFhfp	Poly(vinylidene fluoride-co-hexafluoropropylene)
PVME	Poly(vinyl methyl ether)
PVP	Polyvinylpyrrolidone
QCM	Quartz crystal microbalance
RC	Regenerated cellulose
SEBS	Poly(styrene)-b-poly(ethylene-butylene)-b-poly(styrene)
SEM	Scanning Electron Microscopy
SiCl <sub>4</sub>	Silicon tetrachloride
SS	Silk sericin protein

TBAB	Tetrabutylammonium
TEOS	Tetraethylorthosilicate
TiO <sub>2</sub>	Titanium dioxide
TPU	Thermoplastic polyurethane
XPS	X-ray photoelectron spectroscopy
ZnO	Zinc Oxide
β-TCP	β-tricalcium phosphate

## LIST OF SYMBOLS

D	Diffusion coefficient
d	Fiber diameter
f	Distance between fibers (Chapter 4) or free volume fraction (Chapter 5)
$f_g$	Free volume fraction at the glass transition temperature
h	Height
r	Roughness factor (Chapter 1) or radius (Chapter 4)
t	Time
T	Temperature
$T_g$	Glass transition temperature
v	Drop volume
We	Weber number
$\alpha_2$	Difference between the thermal expansion coefficient above and below the glass transition temperature
$\gamma$	Surface tension or surface energy (Chapter 5)
$\gamma^d$	Dispersion component of surface energy
$\gamma^p$	Polar component of surface energy
$\gamma_{SL}$	Surface energy between the solid and the liquid
$\gamma_{SV}$	Energy between the solid and the air/vapour
$\eta$	Liquid viscosity
$\theta^*$	Observed contact angle
$\theta_{ADV}$	Advancing contact angle
$\theta_c$	Critical contact angle
$\theta_E$	Equilibrium contact angle
$\theta_{REC}$	Receding contact angle
$\theta_{tilt}$	Tilt angle
$\rho$	Density
$\varphi_S$	Solid fraction



## INTRODUCTION

Electrospinning is a polymer processing technique that has gained much attention due to its ability to produce porous structures that have potential applications in a wide range of technologies, including filtration, separation, sensing, tissue engineering and drug delivery. The electrospinning process is based on the formation of micro or nanofibers from a polymer solution under an electric field. The solution is usually directed through a nozzle charged with a few kilovolts with controlled flow rate. If the solution properties such as viscosity, surface tension and conductivity, and the processing parameters such as voltage, flow rate and distance to a grounded collector are well adjusted, a thin jet erupts from the solution droplet at the tip of the nozzle. This charged jet travels towards the grounded collector and as it travels bending, due to electrostatic interactions, and solvent evaporation occur. Solid fibers are then deposited on the collector as a nonwoven mat of randomly aligned fibers. The electrospun mat has an interconnected porous structure with high surface area-to-volume ratio whose pore size can be tuned according to the fiber diameter. The control of surface properties is therefore particularly important for this type of structure. The interaction between the solid fibers with aqueous fluids, or wettability, is one of the surface properties that have a great impact in many applications. As an example, mats used in tissue engineering, also known as scaffolds, present better cell attachment and proliferation if the fibers are hydrophilic, *i.e.*, have a greater tendency to be wet by water. Hydrophobic mats can be used as oil-water separation membranes to block the passage of water while letting oil pass.

In many cases, the appropriate polymer for electrospinning does not have the desired surface properties and thus surface modification is required. Many polymers used in biomedical applications, for example, are naturally hydrophobic and need to undergo a hydrophilization process to improve their performance. The electrospun mats can be treated by plasma or a

wet-chemistry method to create hydrophilic groups on the surface of the fibers, or they can be coated with a hydrophilic material, for instance. Sometimes, however, the post-treatment can deteriorate the fibers and consequently the mat structure or simply fail to reach deeper fiber layers inside the mat.

Surface modification can be also performed during electrospinning in a one-step process. The incorporation of a second polymer to the electrospinning solution, or blending, can significantly alter the surface properties of the resulting fibers provided that the modifying polymer is present on the surface after the process. The hydrophilization of electrospun mats by blending has been achieved in some studies found in literature, but there is still a lack of understanding about the basics of wetting of porous structures, the role of blend morphology and energy factors that contribute more to the surface segregation of the surface modifying polymer. Most of the work used hydrophilization only as a step before testing for a specific application. From a materials science perspective there are still a lot of unanswered questions.

## **0.1 Research Hypothesis**

Within the context outlined above, the hypothesis is that surface modification of electrospun mats, in particular the hydrophilization of hydrophobic mats, can be achieved in a one-step process, that is, together with electrospinning by controlling the location of surface modifying agents and thus obtaining a homogeneous surface treatment.

## **0.2 Objectives**

The main objective of this thesis is to **develop a one-step method to achieve and control the hydrophilicity of hydrophobic electrospun mats** that could be an alternative surface modification method and also circumvent some of the problems associated with post-treatments such as fiber degradation and lack of penetration. Many research topics such as the electrospinning process, multiphase systems and wetting of porous structures are

involved and many parameters such as the surface segregation, morphology and chemical composition have to be understood. The specific objectives of this thesis are thus defined as:

1. Evaluate polymer blending with an amphiphilic PEO-PPO-PEO copolymer as a method to achieve hydrophilization of SEBS, chosen as the hydrophobic matrix, by preparing and thoroughly characterizing the system SEBS/PEO-PPO-PEO (chemical composition, morphology, contact angle) produced by electrospinning and dip-coating;
2. Fabricate and characterize electrospun mats of SEBS/PEO-PPO-PEO blends with three types of commercially available PEO-PPO-PEO copolymers, with different molar masses and PPO/PEO ratio, and evaluate the possibility of tuning the surface properties in terms of segregation, wettability and robustness of the treatment;
3. Evaluate different characterization techniques to distinguish between different hydrophilic mats, given the limitation of a single contact angle measurement to evaluate the wettability of hydrophilic porous structures;
4. Understand the fundamental mechanisms involved in surface segregation during and after electrospinning by preparing blends of SEBS and PS with pure PEO, which has a relative high surface energy, and amphiphilic PEO-PPO-PEO, which has a low surface energy PPO block. Compare segregation of the same polymer inside different matrices.



## CHAPTER 1

### SURFACE MODIFICATION TO CONTROL THE WETTABILITY OF ELECTROSPUN MATS

The performance of electrospun mats in many applications is greatly affected by their interaction with water. Superhydrophobic mats can be used as separation membranes while superhydrophilic mats are usually preferred for tissue engineering. In many cases, however, the polymer used to produce the fibers does not have the appropriate surface properties, which need to be tuned. This review covers the main surface modification techniques used to change the wetting behavior of mats produced by electrospinning. Some basic aspects of the electrospinning process, as well of the wetting theories, are also presented as a starting point for the discussion, highlighting the common wetting switching mechanism found in highly porous structures like electrospun mats. The techniques are classified as post-treatments, or after-electrospinning, and one-step during electrospinning.

#### 1.1 Introduction

The interconnected porous structures produced by electrospinning are increasingly interesting to a vast array of applications. These nonwoven mats are formed by polymer fibers with diameter generally ranging from hundreds of nanometers to a few micrometers. In the most common scenario the fibers are randomly deposited and the geometry of the mat depends on the average distance between fibers and fiber diameter, which influence the pore size (Lowery, Datta, & Rutledge, 2010). Mats can be composed of cylindrical fibers with uniform diameter or different morphologies like ribbon-shaped or beads-on-string fibers. Considering the generally high surface area-to-volume ratio of these mats, the control of surface properties is crucial and can be achieved by controlling the geometry of the mat and the surface chemical composition and morphology of the fibers. The wettability is one of the

most important surface properties that needs to be understood and controlled, in light of the many possible applications in which the fibers interact with water or an aqueous medium.

In general terms, wettability determines if a material has more or less affinity with water and so a polymer can be either naturally hydrophilic or hydrophobic. In the case of perfectly flat films, this property is defined only by the chemical composition of the outermost molecular layers and the characterization of wettability is usually done by the measurement of water contact angle on the surface. However, electrospun mats are composed of fibers and interconnected air pores and can be seen as a rough surface in the hydrophobic case and as porous structure in the hydrophilic case. According to wetting theories (José Bico, Thiele, & Quéré, 2002; Callies & Quere, 2005; Shirtcliffe, McHale, Newton, Perry, & Roach, 2005), these characteristics favor more extreme cases of high static contact angle values for mats made of hydrophobic polymers and near-zero contact angle values for water-absorbing mats made of hydrophilic polymers (C. H. Kim, Khil, Kim, Lee, & Jahng, 2006; G. Li, Zhao, Lv, Shi, & Cao, 2013; Valiquette & Pellerin, 2011).

However, many times the appropriate polymer for processing or with the desired bulk properties does not present the ideal wetting behavior so that surface modification for hydrophobization/hydrophilization is needed. Also, surface modification enables the tuning of both bulk and surface properties of the materials, making them more functional. Changing the surface properties of electrospun mats can be done after processing by different techniques such as plasma treatment, wet-chemistry methods, coating, etc, adding at least one more step after electrospinning to achieve the desired properties. But surface modification can also be done during electrospinning by incorporating nanoparticles or blending with surface modifying polymers that segregate to the surface, for example.

The present work is a review of the main surface modification techniques used for electrospun mats aiming to change their wettability. The principles of the main techniques are presented and discussed with examples, highlighting the advantages and drawbacks of each technique. This review is intended to be an introduction for researchers and engineers

working with electrospinning and looking for options to tune the wettability of mats for a given application.

### 1.1.1 Applications of mats with controlled wetting behavior

There are several applications in which it is necessary to control the affinity of electrospun membranes with water. Figure 1.1 shows some examples that are briefly discussed below.

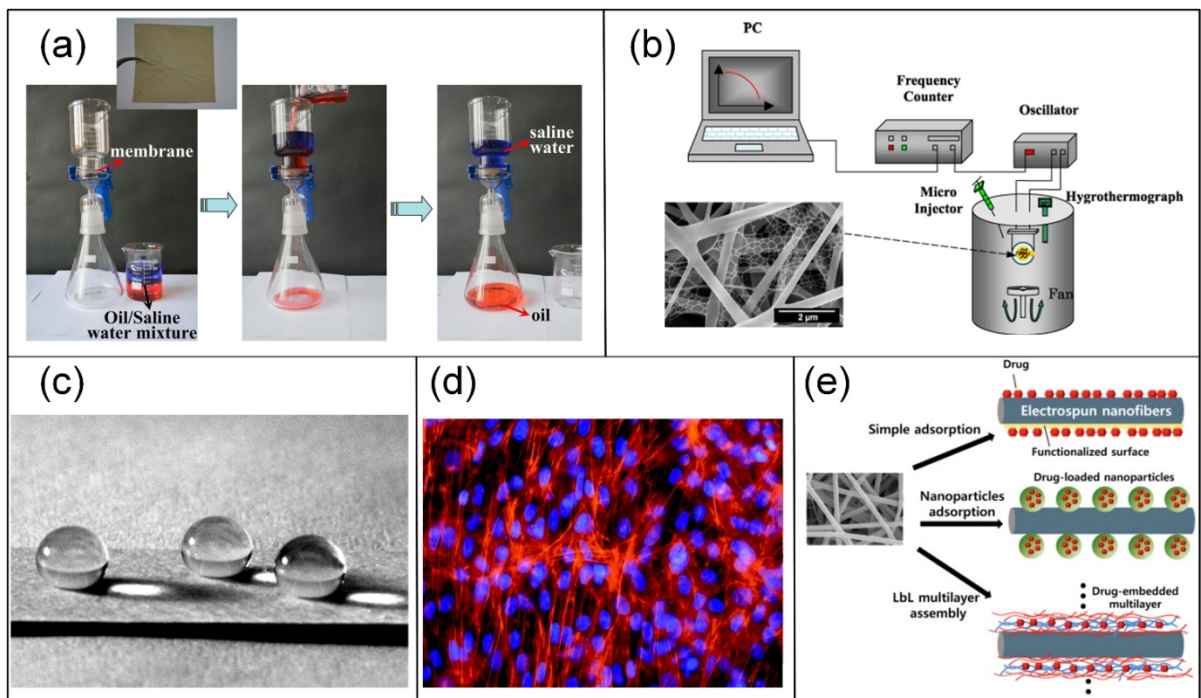


Figure 1.1 – Possible applications of electrospun mats with controlled wettability (a) PAN electrospun membrane used for oil-water separation after surface modification (X. Li, Wang, Wang, Cheng, & Wang, 2014); (b) Schematic apparatus of a humidity sensing system where electrospun fibers are deposited on the electrode inside the humidity chamber (Xianfeng, Bin, Jianyong, Moran, & Fukui, 2010); (c) water droplets deposited on superhydrophobic electrospun PS-PDMS/PS blends (Minglin Ma, Hill, Lowery, Fridrikh, & Rutledge, 2005); (d) Fluorescence micrograph showing myoblast cells in a PLGA/gelatin/ $\alpha$ -elastin electrospun mat used for tissue engineering (M. Li et al., 2006); (e) Three different strategies to load drugs on the surface of electrospun fibers (Yoo, Kim, & Park, 2009).

### 1.1.1.1 Membranes for separation/filtration

Perhaps the clearest example of application in which wettability is important is the use of porous membranes to separate immiscible liquids such water and oils or other type of contaminants related to environmental problems (Darmanin & Guittard, 2014; Xue, Cao, Liu, Feng, & Jiang, 2014). Oils have lower values of surface tension (ranging around 20 to 40 mN/m) (Grynyov et al., 2016) when compared to water (surface tension of 72 mN/m) so that it is easier to wet a surface with oil and thus the most common approach for water/oil separation is the use hydrophobic or superhydrophobic and superoleophilic membranes that let oil pass through but block the passage of water (Figure 1.1a) (Darmanin & Guittard, 2014; Xue et al., 2014). PS is the most commonly investigated polymer to produce electrospun membranes for oil-water separation. It can be easily dissolved in different solvents and the microstructure of the fibers can be tuned by altering different material properties and processing parameters such as molecular weight, solvent type, concentration and relative humidity (M. W. Lee et al., 2013; J. Lin, Ding, Yang, Yu, & Sun, 2012; J. Lin, Y. Shang, et al., 2012; Pai, Boyce, & Rutledge, 2009; Wu et al., 2012). As an example, hydrophobic PS electrospun mats with highly porous fibers showed a drastic increase in oil absorption capacity when compared to commercial nonwoven PP mats with thicker and non-porous fibers (J. Lin, B. Ding, et al., 2012; J. Lin, Y. Shang, et al., 2012; Wu et al., 2012). In other cases, surface modification such as the incorporation of nanoparticles is needed to improve the hydrophobicity and consequently the separation efficiency of the electrospun polymer (Tai, Gao, Tan, Sun, & Leckie, 2014; Tuteja et al., 2007).

Wettability is also critical in water filtration technology, in which hydrophilic electrospun mats can be used to control the passage of water while blocking particles. Moreover, the pore size of electrospun mats can be tuned to be smaller than in commercial fibrous filtration membranes, which drastically increases filtration efficiency while the interconnected structure maintains the appropriate permeability (B. Sun et al., 2014). Mats of PVDF or PSu, for instance, are interesting for water treatment due to their good mechanical properties and chemical resistance, but their hydrophobicity decreases the flow of water through the

membrane. The incorporation of surface-modification molecules makes the mat more hydrophilic and enables higher water-flux rates at lower pressures (Kaur, Rana, Matsuura, Sundarrajan, & Ramakrishna, 2012).

#### **1.1.1.2 Sensing applications**

Sensing applications can also benefit from the large specific area of electrospun mats, presenting higher sensitivity than flat films. Hydrophilic fibers, for example, can be deposited on a QCM electrode to act as humidity sensors, as shown in the apparatus illustrated in Figure 1.1b. The principle is based on the adsorption of water molecules on the surface of the fibers deposited on the QCM electrode that will induce a response variation of the quartz crystal and lead to a change in the resonance frequency and therefore on the measured mass (Marx, 2003; X. Wang, Ding, Yu, & Wang, 2011; Xianfeng et al., 2010). In addition to the large surface area, the ideal material must be sensitive to humidity and electrical signals. Examples include electrospun PA6 mats deposited on QCM electrodes and impregnated with sensing PEI, which outperformed flat films with higher sensitivity and faster response time in the detection range of 2-95% of relative humidity (X. Wang et al., 2011), and PEO mats doped with LiClO<sub>4</sub> that also outperformed flat films, but in this case the fibers were damaged after the measurement, making it a disposable humidity sensor (Aussawasathien, Dong, & Dai, 2005).

#### **1.1.1.3 Self-cleaning surfaces and antifouling membranes**

Superhydrophobic electrospun mats (Figure 1.1c) can also be employed as a self-cleaning surface, not only repelling water but also using rolling water droplets to clean the surface from dust particle, for example (Sas, Gorga, Joines, & Thoney, 2012). The lotus leaf found in nature exhibits this behavior and a lot of effort has been put to mimic its microstructure composed of micro and nanoroughness that makes the water droplets bounce and roll (Jiang,

Zhao, & Zhai, 2004). Mats with beads-on-string morphology produced by electrospinning can show similar properties but water repellency is more stable by combining these geometric features with low surface energy materials on the surface (Tuteja et al., 2007).

In the opposite case, hydrophilization also reduces the accumulation of proteins, bacteria and other organisms, known as fouling (Banerjee, Pangule, & Kane, 2011; Huang et al., 2014). One of the most common approaches to avoid fouling is the use of hydrophilic surfaces containing PEO/PEG due to the high hydrophilicity, flexibility, and mobility of its chains (Y.-q. Wang et al., 2005). Many surface modifications methods can be used to impart PEO on the surface of electrospun mats, from grafting to blending, and they are mainly concentrated on biomedical applications.

#### **1.1.1.4 Tissue engineering and drug delivery**

The resemblance of electrospun mats with the natural ECM makes them a natural fit as a substrate for tissue engineering (Agarwal, Wendorff, & Greiner, 2008; Zeng et al., 2003). The natural ECM is composed, among many other components, of hydrophilic carbohydrate polymers. Hydrophilicity increases cell affinity so that hydrophobic polymers used in tissue engineering such as PLA, PHAs or PCL need to undergo surface modification (Liang, Hsiao, & Chu, 2007). By incorporating minerals in PCL (Araujo et al., 2008) or PHBV (Ito et al., 2005) mats to mimic the ECM found in bone structures, for instance, the resulting hydrophilic mats presented increased cell attachment and proliferation. Figure 1.1d shows an example of cells in a PLGA scaffolds blended with gelatin and elastin, a natural protein (M. Li et al., 2006). Another promising biomedical application where the wettability is important is drug delivery. Drugs can be incorporated on the surface of electrospun fibers in different ways (Figure 1.1e), or they can be embedded in the matrix with different morphologies (Sill & von Recum, 2008). The wetting behavior of the polymer matrix must be tailored to enable a better drug encapsulation (Zeng et al., 2003). Amphiphilic block-copolymers, for example, can form micelles used to encapsulate hydrophobic drugs and at the same time increase the dispersions inside a hydrophilic matrix (Rösler, Vandermeulen, & Klok, 2012), or they can be used to tune drug release rate (K. Kim et al., 2004).

## **1.2 Basic principles**

### **1.2.1 Electrospinning process**

Electrospinning is a technique in which polymer fibers are formed, generally from a solution, under an electrical field. In the most basic apparatus, the solution is placed inside a syringe and directed through a charged syringe needle. Raised to a high potential, the drop formed at the needle tip is elongated until a thin jet erupts and travels towards a grounded collector. The jet experiences bending instabilities and solvent evaporation before the solid fibers reach the collector deposited as a nonwoven mat (Reneker & Yarin, 2008; Rutledge & Fridrikh, 2007). The charged drop deformation phenomenon and jet eruption was described by Zeleny (1917) (Zeleny, 1917). Later, the theory was further developed by Taylor (1964), who described the conditions for the droplet instability in high fields that leads to the formation of a conic shape before the eruption. Taylor hypothesized that the electric field is locally greater at the vertex of the cone, as an explanation for this region to be the first to accelerate, and for the fact that is possible to generate fibers thinner than the capillary from which the solution ejects (Taylor, 1964). However, it was not until the mid-nineties that this technology experienced a resurgence, with the work of Doshi and Reneker (1996) as an example that showed the formation of polymer fibers from different solution, with different diameters and cross-sections, which had the potential for many applications(Doshi, 1995). After that, the number of publications on electrospinning increased dramatically. Although the phenomena involved is a complex interplay of solution characteristics such as rheological properties, surface tension, conductivity and evaporation rate, with the processing parameters like applied voltage, flow rate, distance to the collector, temperature and humidity, the basic apparatus is easy to assemble in a laboratory and the technique has proven to be remarkably versatile.

A non-woven mat composed of randomly aligned fibers is the most common type of structure obtained by electrospinning. Alternatively, rotating or air-gap collectors can produce aligned fibers and a processing variation called near-field electrospinning with a collector with controlled movement enables the design of mats with more precise geometry (D. Li, Wang, & Xia, 2003; Persano et al., 2013; D. Sun, Chang, Li, & Lin, 2006). Nevertheless, for this review's purpose, we consider an electrospun mat as an interconnected porous membrane in which the pores are formed by fibers randomly deposited. Mat morphology (mat geometry) is defined by fiber diameter/shape and fiber deposition. Many factors influence the final fiber diameter including the polymer choice, solvent type, evaporation rate, dielectric constant, solution viscosity and surface tension, electric field intensity, and others (Figure 1.2). The final fiber diameter, therefore, can be tuned and range from a hundred nanometers to a few micrometers. All these parameters also influence the shape of the fibers, which can be uniform with circular cross-section, ribbon-shaped fibers, wrinkled fibers, etc. The competition between "fluid forces" such as viscosity and surface tension and electric forces defines if particles (electrospraying) or fibers (electrospinning) will be obtained, with the beads-on-string morphology in-between these two limits (Deitzel, Kleinmeyer, Harris, & Beck Tan, 2001; Reneker & Yarin, 2008; Rutledge & Fridrikh, 2007). Fiber surface morphology is also highly influenced by materials and processing parameters. The choice of polymer, solvent system and relative humidity can create either smooth or porous fibers (Pai et al., 2009). Different blend morphologies (Rafael S. Kurusu & Demarquette, 2015), interactions between solvents and non-solvents (Pai et al., 2009), incorporation of nanoparticles (M. Ma et al., 2007), are some of the possibilities to alter the fiber surface roughness and chemical composition, the two factors that will influence its wetting behavior.

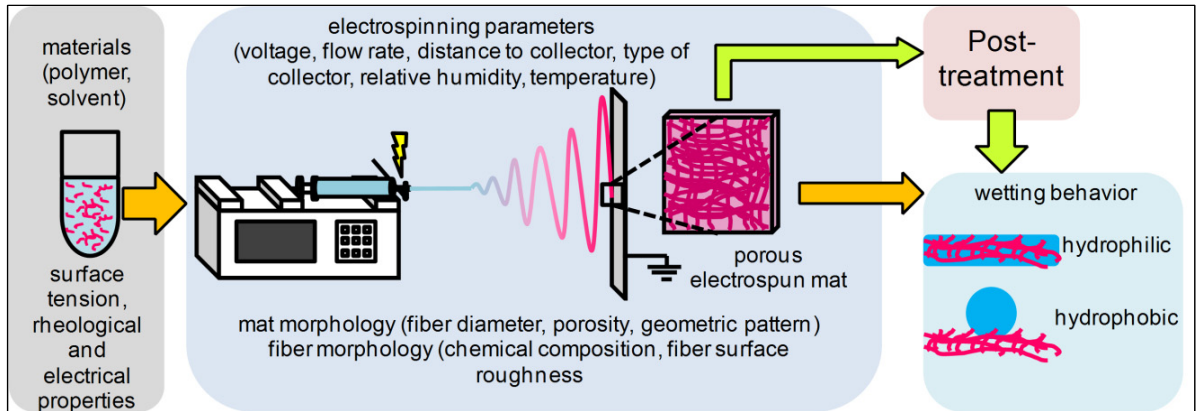


Figure 1.2 – Schematic of the electrospinning process with the main material and processing parameters that will influence the final wettability.

### 1.2.2 Wettability of electrospun mats

When a droplet of water is placed on a flat surface a contact angle  $\theta_E$  is formed, representing the equilibrium of all the interfacial energies involved and indicating the affinity of the surface with water (Figure 1.3a). If  $\theta_E$  is lower than  $90^\circ$  the surface is hydrophilic; if greater than  $90^\circ$ , hydrophobic. The introduction of roughness tends to amplify the original characteristic of the surface and so rough surfaces of hydrophobic materials have higher values of static contact angle when compared to the flat film. By increasing the roughness, the static contact angle increases as the droplet fills the whole surface area (Wenzel state, Figure 1.3b) up to a critical value in which the energy associated with the formation of air pockets under the droplet (Figure 1.3b) becomes lower than the energy related to following the whole solid surface (Callies & Quere, 2005). Air is trapped underneath and the droplet is deposited on a composite surface of air and solid (Cassie and Baxter state, Figure 1.3b) with even higher values of contact angle. In the hydrophilic case, the contact angle decreases while the droplet fills the roughness and the critical value marks the start of water impregnation by capillary action. The surface becomes wet ahead of the contact line and the

droplet is deposited on a composite surface of liquid and solid (J. Bico, Tordeux, & Quéré, 2001).

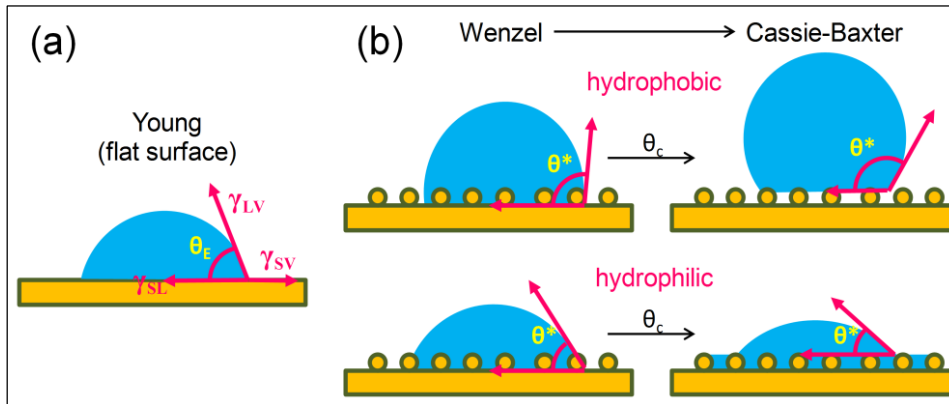


Figure 1.3 – Basics of wetting: (a) A droplet deposited on a perfectly flat surface forming an equilibrium contact angle  $\theta_E$  according with the energies involved; (b) Wetting on rough surfaces, characterized by the observed contact angle  $\theta^*$ , showing the transition from Wenzel to Cassie-Baxter state, defined by a critical contact angle  $\theta_c$ .

Fundamental studies on wetting are commonly performed with surfaces of well defined geometry. Parameters like roughness ( $r$ ), the ratio of the real surface area to the projected flat surface, and surface solid fraction  $\phi_s$  are known and can be finely tuned, which makes the wetting transitions easier to observe. Porous structures like electrospun mats tend to have high values of roughness ( $r \rightarrow \infty$ ) and low values of surface solid fraction. The consequence is that hydrophobic materials (equilibrium contact angle  $> 90^\circ$ ) produce electrospun mats with much higher static contact angle values (Cassie and Baxter state) while hydrophilic materials (equilibrium contact angle  $< 90^\circ$ ) produce mats that absorb water by capillary action, or wicking, resulting in a final contact angle of practically zero, although the advancing front never reaches zero on partially wettable materials (José Bico et al., 2002). For the purpose of this review, contact angle of zero means that the surface completely absorbed the water droplet during contact angle measurements. Hemi-wicking is the appropriate term to describe the phenomenon because as the liquid fills the roughness, it leaves behind dry islands and thus is not a perfect wicking. The condition for hemi-wicking (José Bico et al., 2002; J. Bico et al., 2001) as a function of roughness and solid fraction is presented in Figure 1.4a and

considering the usual high roughness of electrospun mats, the critical contact angle that defines the onset of imbibition is always practically  $90^\circ$ , regardless of the solid fraction  $\phi_s$ , as shown in Figure 1.4. This explains the switching mechanism (Figure 1.4b) often observed during static contact angle measurements of electrospun mats with different compositions. From hydrophobic with high static contact angle values to superhydrophilic absorbing structures (Rafael S. Kurusu & Demarquette, 2015; Shirtcliffe et al., 2005).

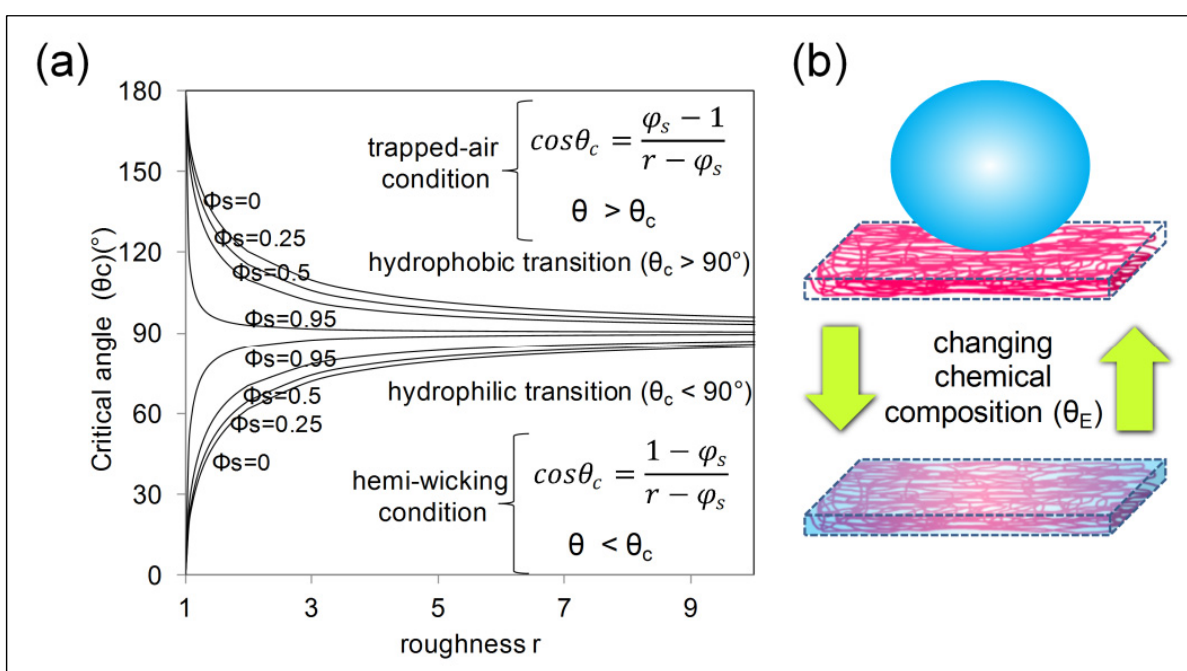


Figure 1.4 – Wetting in porous structures: (a) Critical contact angle as a function of roughness and solid fraction; (b) typical switching mechanism in porous structures like electrospun mats, from hydrophobic (Cassie-Baxter state) to complete absorption of water by simple chemical modification.

Hydrophobic electrospun mats can be seen as a surface with high roughness and the fiber and pore diameter will define an average solid fraction, knowing that randomly aligned mats with thinner fibers have smaller pores (Lowery et al., 2010). Fiber surface chemical composition will define the wettability of the solid part so that polymers with lower surface energy

generate more hydrophobic mats (M. Ma, R. M. Hill, et al., 2005). One of the criteria for superhydrophobicity, observed contact angle higher than  $150^\circ$ , can be achieved even with weakly hydrophilic materials (equilibrium water contact angle on a flat film smaller than but close to  $90^\circ$ ) depending on the surface re-entrant geometry (Herminghaus, 2000; Kota, Li, Mabry, & Tuteja, 2012), but this is a metastable state and the more robust superhydrophobic surfaces are produced by a combination of geometry, such as mats containing “beads on a string” morphology, and chemistry by using low surface energy materials (Tuteja et al., 2007). Still, high values of static contact angle do not make a surface water-repellent.

To truly characterize superhydrophobicity, the difference between the advancing and the receding contact angle, called contact angle hysteresis, has to be smaller than  $10^\circ$ . The experiment is usually done in two ways (Figure 1.5). In the first (Figure 1.5a), the advancing contact angle is measured using a droplet of water deposited on the surface that is continually filled until the contact line between surface, water and air moves outward. To access the receding angle, the opposite is done by extracting liquid from the droplet until the contact line moves inward. The second alternative (Figure 1.5b) is to tilt the surface until the droplet slides and measure both advancing and receding angles. A rough surface with high values of static contact angle and contact angle hysteresis will present a round water drop attached on the surface even if the mat is turned upside down, in a phenomenon described as petal effect (Feng et al., 2008). This type of surface avoids the water penetration but does not repel water. True water repellent surfaces will present low contact angle hysteresis, regardless of the static contact angle. Water will bounce or slide on those surfaces. The majority of studies presented in this review, however, do not take into account the contact angle hysteresis, relying only on static contact angle measurements to verify if the electrospun mats will be penetrated by an aqueous fluid.

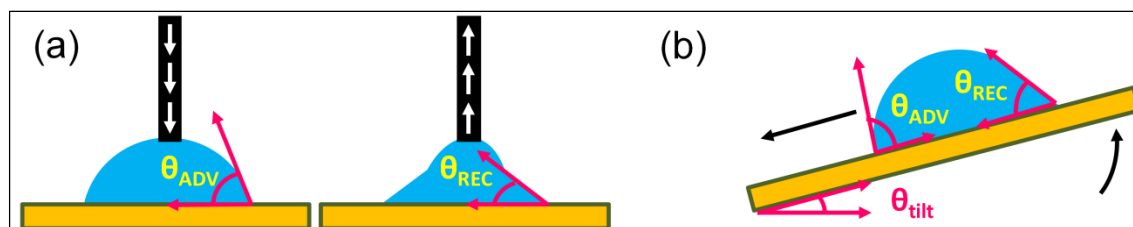


Figure 1.5 – Measuring the advancing and receding contact angle by (a) increasing or decreasing the drop volume or (b) tilting the surface until the drop starts to slide or roll.

In hydrophilic mats, capillary action will lead to a static contact angle of practically zero so that this measurement is not enough to fully characterize the mat or to access the difference between different hydrophilic materials, helping only to attest if an aqueous fluid will penetrate the mat. Wicking experiments can be performed to further describe the dynamics of wetting in these mats (Figure 1.6a). Different hydrophilic materials can exhibit great difference in absorption rate or capacity, which will certainly affect the performance for some applications (Rafael S. Kurusu & Demarquette, 2016). Another alternative to compare different hydrophilic materials is the observation, which sometimes requires the use of high-speed imaging, of the dynamics of droplet spreading or impact on the surfaces (Figure 1.6b) (Rafael S. Kurusu & Demarquette, 2016; Z. Wang, Espín, Bates, Kumar, & Macosko, 2016). Differences in water absorption time indicate nonuniform surface properties (Cécile & Hsieh, 2010). As in the hydrophobic case, most studies presented in this review use mainly the static contact angle measurements to evaluate if the electrospun mat is hydrophilic. Studies in filtration science seem to pay more attention to the absorption time during contact angle measurements.

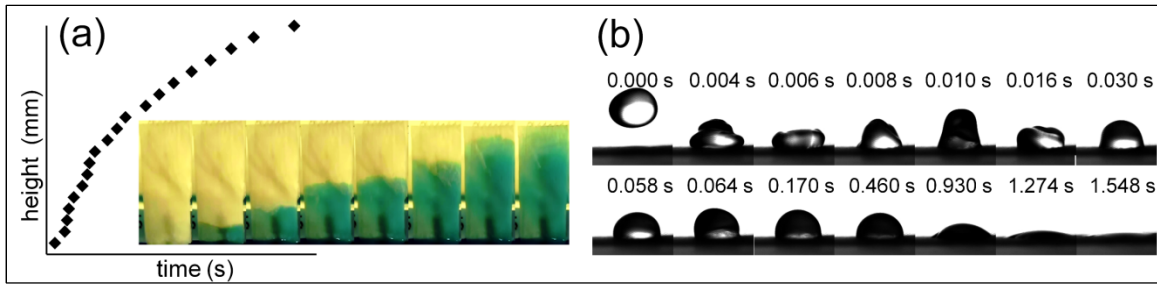


Figure 1.6 – Evaluating the wettability of hydrophilic mats: (a) wicking measurements on a mat strip to analyze the liquid rise dynamics; (b) high-speed imaging to observe the dynamics of droplet impact.

### 1.3 Surface modification methods

In the recent literature, surface modification is used to achieve the adequate performance for a given application and therefore most articles are not only focused on changing the wettability or understanding the mechanisms behind the wetting behavior. Still, in all the studies cited below the effects of surface modification methods on the wettability of electrospun mats were at least briefly investigated.

Considering that biomedical applications represent the greatest research interest in electrospun scaffolds, one of the major goals of surface modification is to hydrophilize the surfaces. Hydrophilic surfaces are known to have better biocompatibility and the ability to avoid biofouling. A surface treatment such as plasma, hydrolysis or aminolysis can produce polar groups such as carboxyl, hydroxyl and amines on the surface to improve the hydrophilicity. Another approach is to incorporate hydrophilic polymers or nanoparticles to the fibers. In contrast, surface hydrophobization has also been investigated to create superhydrophobic surfaces or membranes, for example, and it can be achieved by the introduction of low surface energy groups on the surface like fluorine-containing groups, or mixing with hydrophobic polymers or nanoparticles. Surface modification can be chemical such as the introduction of functional groups by plasma treatment or wet-chemistry reactions, or yet grafted polymers covalently bonded to the surface. Physical modification methods

include coating, adsorption or blending. Figure 1.7 shows the main routes to change the wettability of electrospun mats based on recent literature. The methods are divided in two main groups in the following sections: (i) post-treatments performed after electrospinning (plasma, wet-chemistry, grafting and coating); (ii) one-step treatments performed during electrospinning (nanocomposites and blends). This division was meant to emphasize a big difference between these two approaches: for the methods performed after electrospinning the penetration of the treatment will be an important factor while for the methods performed during electrospinning the modification is ideally achieved in every mat layer.

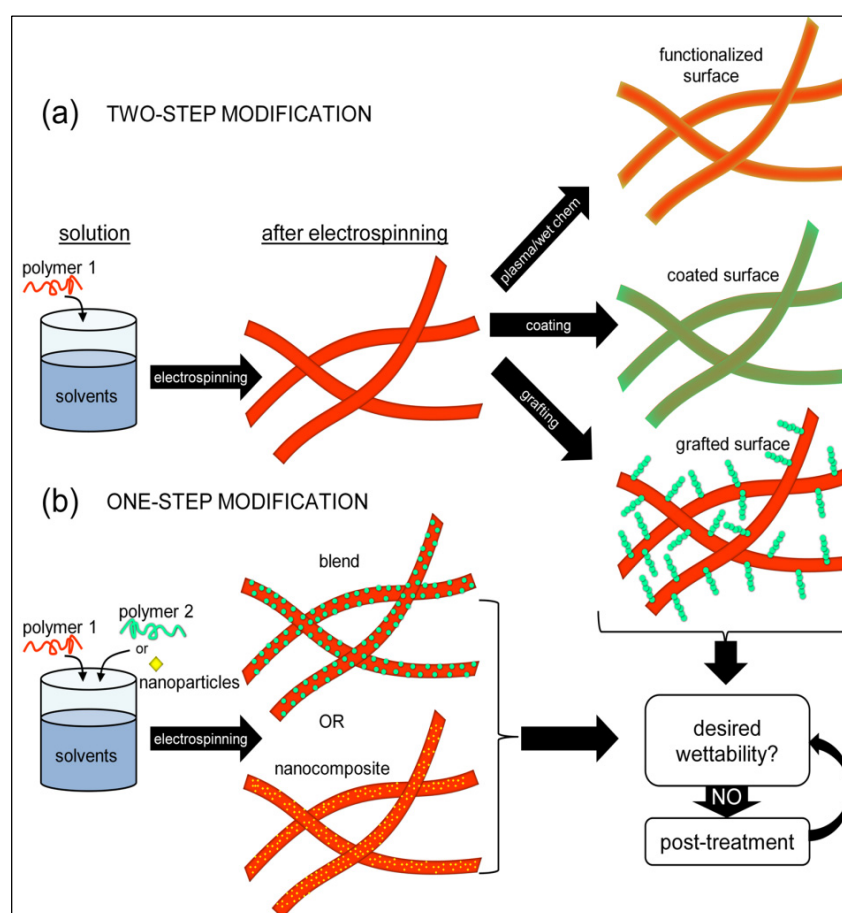


Figure 1.7 – Schematic showing the main approaches to modify the surface of electrospun mats.

### **1.3.1 Post-treatments**

#### **1.3.1.1 Plasma**

Plasma is a partially ionized gas formed by the same number density of negative and positive charge carriers (Strobel, Lyons, & Mittal, 1994), which can be created by heating the gas to extremely high temperatures or subjecting it to strong electromagnetic fields. Plasmas present collective behavior and are electrically conductive, responding to the presence of electromagnetic fields. Plasma processes were originally used to either etch a surface (removing material) or for the deposition of thin films. Surface treatment using plasmas can also modify only a few molecular layers with no significant amount of deposition or etching (Strobel et al., 1994).

Plasmas can be divided in thermal/high-temperature/hot plasma and non-thermal/low temperature/cold plasma. The former is characterized by very high temperatures and therefore is not suitable for temperature-sensitive materials like polymers (Morent, De Geyter, Desmet, Dubruel, & Leys, 2011). The advent of nonthermal/low-temperature/cold plasma processes, in which the gas molecules and ions are closer to the room temperature allowed the use of plasma treatments for polymers, reducing the risk of thermal degradation. Glow discharge is a source of nonthermal plasma formed by the passage of an electric current between two electrodes through a low-pressure gas. This type of plasma was originally used for etching and creating patterns on surfaces or to deposit thin films, usually operated in direct-current powering mode, which requires an electrically conductive sample to act as the negatively charged electrode (cathode). Alternatively, glow discharges can also be operated in radio-frequency mode, and in this case the treatment can be used for non-conductive materials like polymers thus broadening the possible applications of the technique. A thorough review on this type of plasma can be found in literature (Winchester & Payling, 2004). Corona discharge is another source of nonthermal plasma used for polymers, formed by the ionization of a fluid surrounding an electrically charged conductor under a strongly nonuniform electric field at atmospheric pressure (Desmet et al., 2009; Strobel et al.,

1994). The nonuniform electric field appears when one of the electrodes is much smaller than the distance between electrodes. A sharp electrode around which a glow is formed is normally used to treat the mats. Treatment by plasma can be used directly to create functional groups at the surface of the substrates, to etch, to cross-link, or to simply prepare the surface for another treatment such as coating or grafting. Plasma can also be used indirectly to graft polymers but this process will be discussed in more detail in the grafting section of this review. The introduction of hydrophilic polar groups like hydroxyl, carboxyl, amino, carbonyl, on the surface is the most common objective of plasma surface modification. The presence of these groups on the surface of hydrophobic polymer fibers will help to make the mats more hydrophilic and therefore more biocompatible for several biomedical applications. Figure 1.8 shows the simple generation of functional groups or radicals that can react with air or pure O<sub>2</sub> and produce hydrophilic groups. Table 1.1 summarizes recent studies that used plasma treatment to change the wettability of electrospun mats.

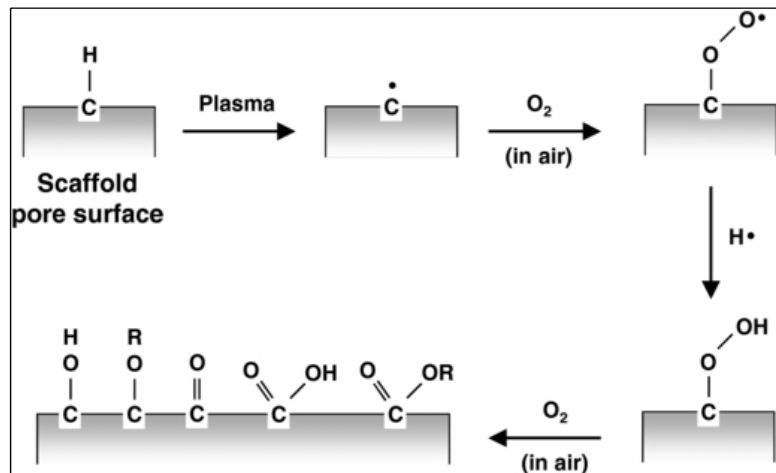


Figure 1.8 – Schematic showing surface hydrophilization by plasma treatment (Oh & Lee, 2013).

Table 1.1 – Plasma treatment used to alter the wettability of electrospun mats

Polymer	Treatment/Modification	Wettability characterization	Application	ref
PA 6	Cold gas plasma treatment (O <sub>2</sub> ) / Hydroxyl and carboxyl groups on the surface	Environmental scanning electron microscopy: increased hydrophilicity on individual fibers	Surface modification	(Wei, Gao, Hou, & Wang, 2005)
PCL	Remote plasma treatment with radio-frequency glow discharge (Ar)	Contact angle: untreated (82±4.1°) and treated (wicking)	Tissue engineering	(Y. Duan et al., 2007)
PLLA	Plasma treatment (air)	Contact angle: untreated (63±10.5°) and treated (32±5.5°) (Aligned fibers)	Tissue engineering	(Corey et al., 2008)
PCL	Radio-frequency glow discharge plasma treatment (Ar)	Contact angle: untreated (113±5°) and treated (wicking)	Tissue engineering	(Yang, Wolke, & Jansen, 2008)
PLACL and PLACL/gelatin	Radio-frequency glow discharge plasma (air)/ Polar groups introduced	Contact angle: untreated PLACL (121°) and treated PLACL (wicking), untreated PLACL/gelatin (129°) and treated PLACL/gelatin (wicking)	Tissue engineering	(Chandrasekaran, Venugopal, Sundarajan, & Ramakrishna, 2011)
CA and RC	Low-pressure plasma with trifluoromethane	Contact angle: untreated CA and RC (<25° to wicking) and treated CA (153.8±2.5°) and RC (154.8±0.7°)	Superhydrophobic textile	(Thorvaldsson et al., 2012)
PLACL	Radio-frequency glow discharge plasma treatment (air)	Contact angle: untreated PLACL (129.3±2.8°) and treated (52.6±9.6°)	Tissue engineering	(Bishi et al., 2013)
PLLA	Non-thermal atmospheric pressure corona discharge plasma (N <sub>2</sub> ) / Carboxyl groups	Contact angle: untreated PLLA (121.5±1.7°) and treated PLLA (wicking) / Droplet absorption time around 70 seconds / Water uptake capacity: untreated (10%), treated (> 300%)	Tissue engineering	(Dolci et al., 2014)

Table 1.1 (continuation) - Plasma treatment used to alter the wettability of electrospun mats

Polymer	Treatment/Modification	Wettability characterization	Application	ref
PCL	Radio-frequency glow discharge with selective exposure (O <sub>2</sub> )	Contact angle: instantly after deposition, untreated PCL (117±4°), treated without template (110±2.5°) and treated with template (114.5±2.5°); after 300 seconds, untreated PCL (102±2°), treated without template (8±1°) and treated with template (23±3°) / Water uptake capacity: untreated PCL (≈50%), treated without template (> 500%) and treated with template (> 400%)	Tissue engineering	(Jeon & Kim, 2014)
PVDF	Radio-frequency glow-discharge plasma (O <sub>2</sub> ) / Carboxyl groups	Contact angle: untreated PVDF (134±6°) and treated PVDF (wicking, with a minimum power and treatment time)	Surface modification	(Correia et al., 2015)
PET	Atmospheric pressure corona discharge (air), low-pressure radio-frequency plasma (Ar/O <sub>2</sub> or O <sub>2</sub> ), microwave plasma ashing (O <sub>2</sub> or O <sub>2</sub> /CF <sub>4</sub> ) / Polar groups (hydroxyl, carbonyl, carboxyl)	Contact angle: untreated PET (137±3°) and treated PET (wicking) / Wicking time (2 cm height): untreated PET (no wicking), treated with low-pressure plasma with Ar/O <sub>2</sub> or O <sub>2</sub> (4.5 and 5s), treated with corona discharge (8.5s), treated with microwave plasma ashing with O <sub>2</sub> or O <sub>2</sub> /CF <sub>4</sub> (8.5 and 9s)	Tissue engineering	(Savoji, Lerouge, Aji, & Wertheimer, 2015)
PLLA	Microwave plasma treatment (CF <sub>4</sub> )	Contact angle: untreated PLLA (116±3°) and treated PLLA at 100W/5 min (32±3.6°), 100W/min (wicking), 150W/5 min (wicking), 150W/10 min (≈60°), 200 W or more (> 120°)	Surface modification	(Yue et al., 2015)
PS	Plasma treatment (air) / Hydroxyl groups introduced	Contact angle: untreated PS (139±2.7° to 161±2.6°, according to fiber morphology) and treated (wicking)	Surface modification	(Yuan, Choi, & Kim, 2016)

Nonthermal radio frequency glow discharge plasma is the widely used method for introduction of hydrophilic functional groups. Many hydrophobic electrospun mats of biodegradable polymer such as PCL (Yang et al., 2008), PLLA (Dolci et al., 2014) and PLACL (Chandrasekaran et al., 2011) were hydrophilized after the introduction of polar groups by the treatment, as revealed by contact angle experiments. PVDF is another hydrophobic polymer that in many cases needs to undergo surface modification to broaden its many possible applications in different fields including tissue engineering, filtration and sensing. In a recent study, defluorination and oxidation were promoted by radio frequency glow discharge plasma and all the treated PVDF mats presented increased C-O bond content at the surface. It was also observed that there was a minimal treatment time, around 60 seconds, above which the mats attained superhydrophilicity. Analogous behavior was observed with the plasma power used, with a minimum of 360 W to hydrophilize the mats (Figure 1.9a). The increased applied power also caused some etching that led to melting and merging of fibers in the outer layer (Figure 1.9b) (Correia et al., 2015).

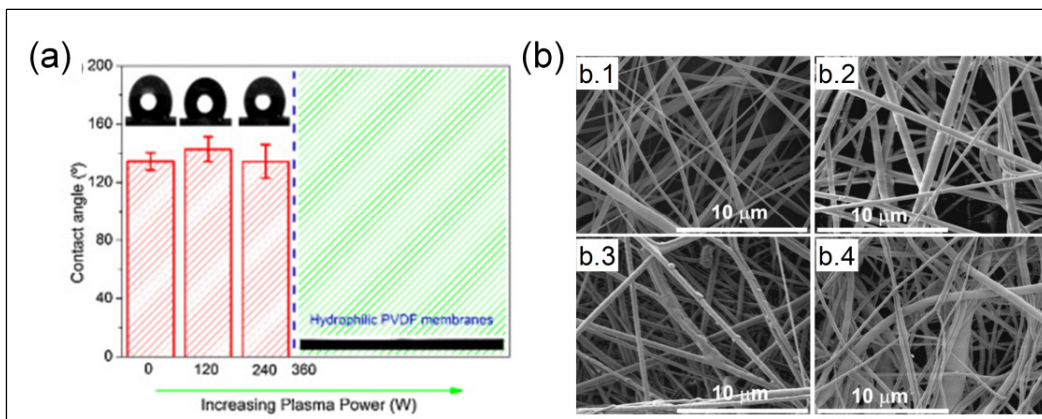


Figure 1.9 – PVDF electrospun mats treated by plasma and the (a) influence of plasma power on the contact angle; (b) mat morphology as a function of applied power: no treatment (b.1), 240 W (b.2), 360 W (b.3) and 480 W (b.4) (Correia et al., 2015).

Duan et. al. (2007) used a remote radio-frequency plasma treatment at varying distances from the source by using a narrow and long chamber in an attempt to minimize unwanted etching of PCL mats. After that the mats were treated with a solution to produce a collagen coating that mimics the natural ECM. The mats treated at longer distances, up to a critical value, presented higher amount of coated collagen, and it was concluded that this was due to reduced etching and other negative side effects of the plasma treatment, which negatively affect the adhesion of coatings. Both the plasma-treated and collagen-coated mats presented wicking and complete droplet absorption (Y. Duan et al., 2007).

In other cases, controlled etching can be the objective of a plasma treatment. The use of a template to produce selective plasma-exposure under oxygen was recently employed to modify the surface of PCL mats. The idea was to use an anodic aluminum oxide plate with holes of 800 nanometers in diameter (Figure 1.10c) in order to produce nanoroughness on the fibers surface. Mats treated with the template preserved the mat structure (Figure 1.10) and were hydrophilized with increased water uptake (Figure 1.11) and cell attachment when compared to untreated mats and mats treated without the template (Jeon & Kim, 2014). In another example, electrospun PET mats were treated by three different plasma etching techniques: atmospheric pressure corona discharge; low-pressure radio frequency plasma; and microwave plasma ashing. With the exception of the latter, the other two processes produced increased roughness on the fibers surfaces due to etching. All treatments caused a decreased in mechanical properties (tensile strength and young's modulus) and fiber diameter, but were effective to hydrophilize the mats and improve cell adhesion and growth when compared to untreated mats. The wicking time was slightly lower for the low pressure radio frequency plasma-treated mats (Savoji et al., 2015).

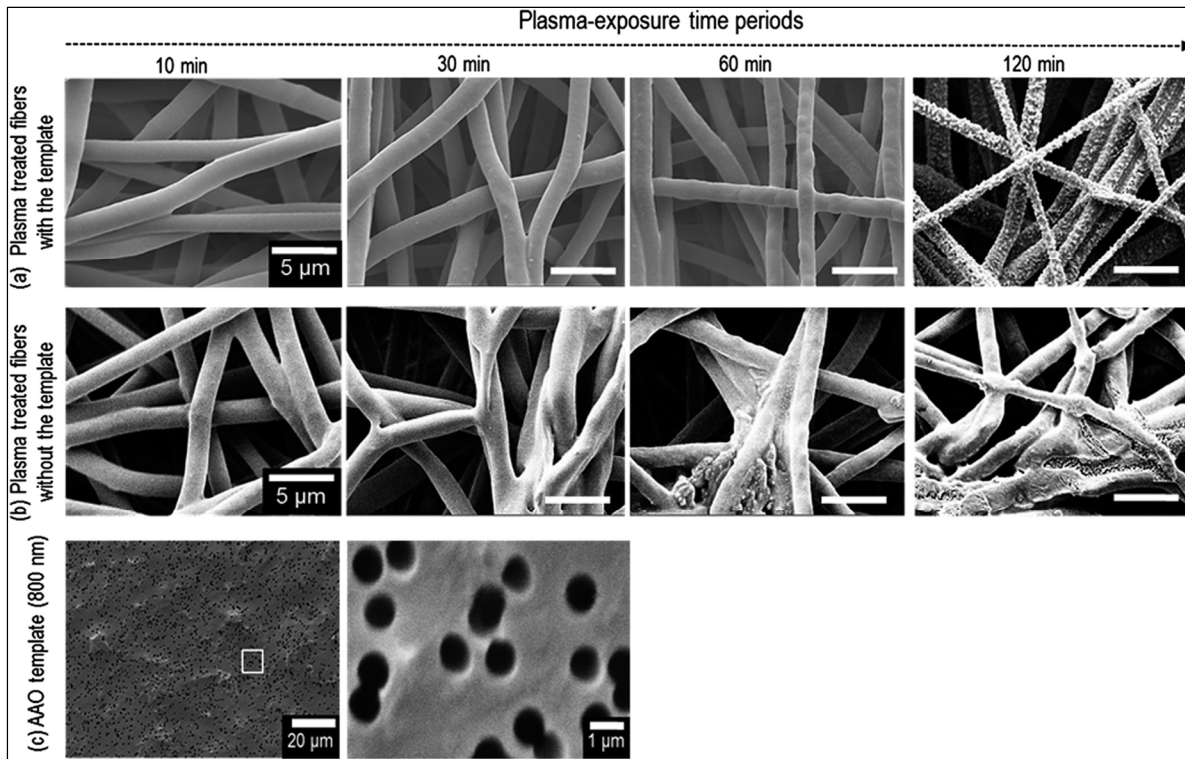


Figure 1.10 – Electrospun PCL mats treated by plasma with (a) and without (b) an aluminum oxide template (c) (Jeon & Kim, 2014).

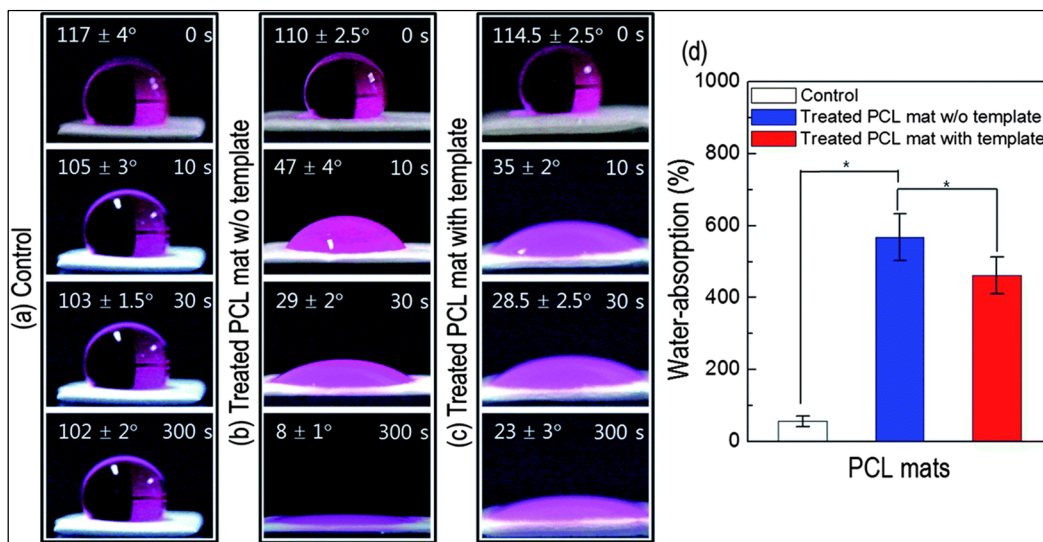


Figure 1.11 – Effect of plasma treatment on the wettability of electrospun PCL mats: (a) untreated mat; (b) treated without the aluminum oxide template; (c) treated with template; (d) comparison of water absorption capacity (Jeon & Kim, 2014).

As mentioned in the previous example, the use of the so-called nonthermal atmospheric pressure plasma with corona discharge is an interesting process variation in which there is no need to treat the mat inside a chamber with controlled pressure. A sharp corona discharge electrode was used to treat mats of hydrophobic PLLA, which absorbed the water droplet in a little more than one minute due to the presence of carboxyl groups on the surface produced by the treatment. Water absorption experiments were also performed by soaking mats of pre-defined dimension in deionized water, which revealed that all the treated PLLA mats presented similar water uptake percentage regardless of the aging time after the treatment (Dolci et al., 2014).

The examples above show that plasma treatment can be performed with different processing variations with advantages that include the ability to create a fine layer with properties completely different from the bulk and the absence of solvents. Ideally, the method is based on the controlled degradation of these few surface layers. Excessive etching and ablation can be a problem while treating electrospun mats, especially for fibers of small diameter that can be more easily degraded. Another possible drawback is the penetration of the treatment in deep layers of the nonwoven mats (Desmet et al., 2009; Yoo et al., 2009).

### **1.3.1.2 Wet chemistry**

Wet chemistry methods involve a reaction between a surface to be modified and a chemical compound in solution. The chemical modification is usually followed by increase in roughness and hydrophobicity/hydrophilicity, depending on the application. A typical example is the hydrolysis of polyesters in which water reacts with the ester groups and generates hydrophilic polar groups (Desmet et al., 2009). Aminolysis is another typical example of reaction in which hydrophobic groups can be replaced by more hydrophilic amine groups. Figure 1.12 shows both the hydrolysis and aminolysis reaction of polyester

PLGA and the resulting functional groups. Table 1.2 summarizes some of the recent work on wet-chemical surface modification methods.

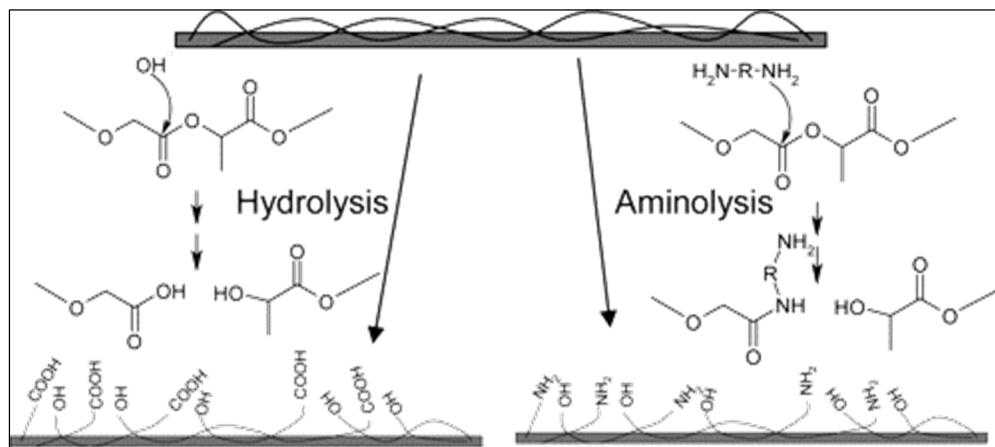


Figure 1.12 – Hydrolysis and aminolysis reactions to introduce hydrophilic groups on the surface of PLGA (Croll, O'Connor, Stevens, & Cooper-White, 2004).

Table 1.2 – Wet-chemistry methods to change the wettability of electrospun mats

Polymer	Treatment / Modification	Wettability Characterization	Application	ref
CA	Hydrolysis in NaOH/water/ethanol solution to remove acetyl groups and obtain a RC mat	Water flux: higher for RC mats at different pressures compared to commercial cellulose membranes	Affinity membrane	(Z. Ma, Kotaki, & Ramakrishna, 2005)
PSMA	Aminolysis in hydrazine or ethylenediamine solution to induce cross-linking of maleic anhydride group / Hydroxyl groups were produced	Wicking: used to calculate contact angle of the solid part indirectly for untreated PSMA ( $77.0 \pm 31.3^\circ$ ) and treated with hydrazine ( $69.0 \pm 9.6^\circ$ ) or ethylenediamine; and water absorption capacity for hydrazine-treated (89% of total pore volume and ethylenediamine-treated (79% of total pore volume)	Surface modification	(Cécile & Hsieh, 2010)
PDLLA	Aminolysis / amino groups	Contact angle: untreated PDLLA ( $132.2 \pm 1.5^\circ$ ) and treated ( $106.7^\circ$ )	Tissue engineering	(Cui et al., 2010)
PVA/silica composite	Silanization in FAS solution preceded by calcination to produce a silica mat	Contact angle: static / hysteresis for untreated PVA/silica or silica mats (wicking) and treated silica mats ( $\approx 141^\circ/10^\circ$ , $147^\circ/8^\circ$ and $154^\circ/7^\circ$ , for different mat morphologies)	Superhydrophobic surface	(Guo et al., 2010)
CA and CA/MWCNT	Hydrolysis in aqueous NaOH solution to remove acetyl groups and obtain a RC mat	Wicking (dynamic wetting): wetting force and water absorption increased in the following order: treated cellulose, cellulose/0.11 wt% of MWCNT and cellulose/0.55 wt% of MWCNT	Surface modification	(Lu & Hsieh, 2010)
PVA and PVA/TEOS composite	Hydrolysis to form silanol groups by exposure to $\text{SiCl}_4$ vapor and air humidity followed by vapor-phase silanization with FAS	Contact angle: advancing / receding contact angle for PVA-Silanol ( $167.6 \pm 3.8^\circ / 0^\circ$ ) and PVA/Silica-Silanol ( $157.3 \pm 1.5^\circ / 98.3 \pm 4^\circ$ )	Superhydrophobic surface	(Pisuchpen, Chaimngoen, Intasanta, Supaphol, & Hoven, 2011)

Table 1.2 (continuation) - Wet-chemistry methods to change the wettability of electrospun mats

Polymer	Treatment / Modification	Wettability Characterization	Application	ref
PVA/silica gel/silica nanoparticles	Silanization in FAS solution and drying in air to allow hydrolysis of the methoxy groups in FAS molecules. Treatment preceded by calcination to produce a silica mat / Si-O-Si bonds formed	Contact angle: treated mats with 0, 9.7, 19.4 and 38.8 wt% of silica nanoparticles (140°, 148°, 150° and 155°, respectively) / sliding angle for treated mat with 38.8 wt% of silica nanoparticles (3°)	Superhydrophobic surface	(F. Zhao et al., 2011)
PBLG	Hydrolysis in aqueous NaOH solution / Carboxyl groups generated	Contact angle: untreated PBLG (125.9°) and hydrolyzed for 2h (87.3°), 24h (31.1°) and 48h (wicking)	Tissue engineering	(Hakamada, Ohgushi, Fujimura-Kondo, & Matsuda, 2012)
PAN	Aminolysis followed by immobilization of Ag nanoparticles	Contact angle: static / hysteresis for treated mats (146.1±0.5° / 22.0±0.7° to 171.1±2.3° / 3.0±0.6°, depending on immobilization time)	Oil-water separation	(X. Li et al., 2014)
Thiolated PLGA (PLGA-SH) and catechol-conjugated 8-arm PEG (8cPEGa) blends	Immersion in NaIO <sub>4</sub> solution to induce cross-linking with catechol-thiol reactions or catechol-catechol conjugation	Contact angle: untreated/cross-linked PLGA/8cPEGa blends with the blending ratio 100/0, 90/10, 70/30 and 50/50 (97.8±0.2°/97.1±0.6°, 97.2±0.6°/49.3±0.4°, 93.5±0.5°/19.0±0.7° to wicking in 15s, 93.7±0.7°/19.0±0.6° to wicking in 15s, respectively)	Antifouling membranes	(H. S. Kim, Ham, Son, Messersmith, & Yoo, 2013)
PCL/CA blends	Hydrolysis in NaOH/water/ethanol solution to remove acetyl groups and obtain a RC mat	Contact angle: untreated / treated PCL/CA membranes with 80, 60, 40 and 20 wt% of CA (130.5±0.3°/9.5±0.4°, 130.1±0.1°/12.1±0.2°, 129.1±0.2°/13.5±1.1°, 124.2±0.4°/18.5±1.6°, respectively)	Tissue engineering	(Joshi et al., 2015)

During polyester hydrolysis the scission of ester bonds generates carboxyl and hydroxyl groups from degraded polymers at the very surface and this will contribute to mat hydrophilization. However, hydrolysis with only water is too slow so that a dilute acid or alkali is used to accelerate the reaction. Aqueous solutions containing NaOH have been used to promote the hydrolysis of CA electrospun mats and generate a RC mat, which presented increased hydrophilicity (Joshi et al., 2015), water absorption (Lu & Hsieh, 2010) and permeability to water (Z. Ma, M. Kotaki, & S. Ramakrishna, 2005).

In some cases two or more wet-chemistry methods can be combined to achieve the desired wettability, such as the recent use of aminolysis followed by Ag immobilization in solution to modify electrospun PAN mats. The amine groups on the surface produced by the first treatment were used to absorb  $[\text{Ag}(\text{NH}_3)_2]^+$  ions with a plating technique to immobilize Ag nanoclusters. The resulting mats had rough surfaces due to the presence of nanoparticles that led to superhydrophobicity with high values of contact angle and low values of contact angle hysteresis (X. Li et al., 2014). Aminolysis was also used to induce cross-linking of the maleic anhydride groups of electrospun PSMA mats by treating them in either hydrazine or ethylenediamine solution. The contact angle of the solid part of the fibers was calculated indirectly by analysing the wicking dynamics on mat strips. Untreated PSMA fibers presented contact angle of  $77^\circ$  but with a very high standard deviation, revealing a heterogeneous wettability, while the mats treated with hydrazine or ethylenediamine presented contact angle of  $69^\circ$  and  $46^\circ$ , respectively, with lower standard deviation. Treated mats presented much higher water absorption capacity, which showed that the hydrophilization was effective (Cécile & Hsieh, 2010).

Silanization is also a common wet-chemical surface modification method in which hydroxyl groups react with silanes to form covalent Si-O-Si bonds at the surface. In a series of recent studies, this reaction was used to introduce FAS on the surface of silica fibers (Guo et al., 2010; F. Zhao et al., 2011). The principle of the surface modification with FAS involves the

silanization of the surface with the silane group present in FAS to form a layer of low surface energy fluorine-based chains that increases the hydrophobicity of the mat. In the cited examples, PVA/silica nanofibers were prepared by electrospinning and the resulting mats were calcined at high temperatures (800 °C) to produce silica mats, which were immersed in a FAS solution and dried in air leading to hydrolysis to produce hydroxyl groups and allow silanization. The resulting fluorinated silica mats showed high values of water and oil contact angle (higher than 100°) but only the mats with beads-on-string morphology, produced with the smaller concentration of PVA during electrospinning, showed superhydrophobicity with water contact angle higher than 150° and low contact angle hysteresis of 7°. Upon annealing at different temperatures up to 450°C the contact angle decrease but the mat remained hydrophobic. At 500°C, the mat became superhydrophilic due to the complete degradation of FAS chains, restoring the wetting behavior of untreated silica mats (Guo et al., 2010). It was also found that the water contact angle increased with the addition of silica nanoparticles to the PVA/silica solutions before electrospinning, reaching over 150° with the highest nanoparticle content due to increased roughness (F. Zhao et al., 2011). In another study, PVA and PVA/silica mats were previously exposed to SiCl<sub>4</sub> vapor and then to air humidity to allow hydrolysis and form silanol groups. The resultant mats passed through vapor-phase silanization with a FAS. After the treatment with FAS, PVA-silanol fibers merged together forming a dense layer with high values of advancing contact angle but low values of receding contact angle, which increased water adhesion (Figure 1.13a and Figure 1.13b). PVA/silica-silanol mats presented fibrous structures with air pockets and lower values of contact angle hysteresis (Figure 1.13c and Figure 1.13d) (Pisuchpen et al., 2011).

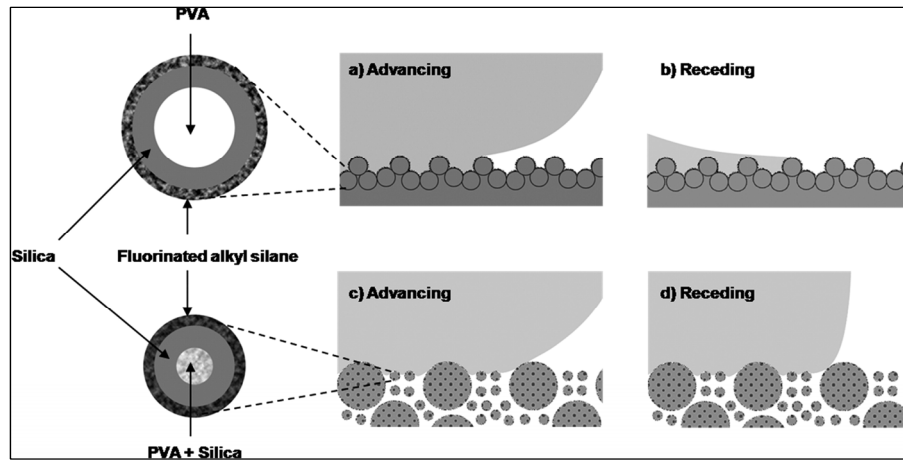


Figure 1.13 – Proposed wetting mechanism for (a, b) PVA-silanol fibers after silanization with strong adhesion due to the low receding contact angle; (c, d) PVA/silica-silanol fibers after silanization showing air pockets that helps to increase the receding contact angle (Pisuchpen et al., 2011).

There are also other examples of more specific reactions in wet chemistry. Biocompatible thiolated PLGA (PLGA-SH) and catechol-conjugated 8-arm PEG (8cPEGa) were blended at different ratios in solutions used in electrospinning and the resulting mats were then treated in  $\text{NaIO}_4$  solution to induce cross-linking with catechol-thiol reactions or catechol-catechol conjugation. The untreated mats presented no difference in contact angle measurements (between  $93^\circ$  and  $98^\circ$ ) regardless of the 8cPEGa content, and it was assumed that the washing procedure before the experiment removed the non-crosslinked 8cPEGa leading to contact angles similar to pure PLGA-SH. Cross-linked samples presented greater reduction in contact angle and when the amount of 8cPEGa reached 30 and 50 wt% the water droplet was absorbed by the mat in about 15 seconds (H. S. Kim et al., 2013).

Like plasma, wet-chemistry methods are based on the controlled degradation of the surface to form new functional groups that can contribute to change the surfaces' wettability. They can be easy to perform and can penetrate in deeper layers of the mat, being an alternative to plasma to modify the surface of thick mats. Some of the disadvantages include nonspecific

reactions and irregular etching that can lead to nonuniform or nonreproducible treatments and loss in mechanical properties due to degradation (Desmet et al., 2009). Also, in many cases the use of another solvent-based method after electrospinning is not desirable (Strobel et al., 1994). Grafting can also be performed via wet chemistry reaction, as will be discussed in the next section.

### 1.3.1.3 Grafting

A surface with grafted polymers can be obtained using two main approaches: Grafting-to or grafting-from. In the grafting-to (or grafting onto) method, a pre-prepared end-functionalized polymer must react with a solid surface, with appropriate chemistry or modification, to produce the polymer brushes (Figure 1.14a). In the grafting-from approach, initiators immobilized on the solid surface enable polymerization of a monomer that can produce high grafting density and film thickness (Figure 1.14b) (Yano et al., 2011; Zhou, Liu, Xie, & Zheng, 2011). Table 1.3 summarizes the recent literature on grafting polymers to control the wettability of electrospun mats.

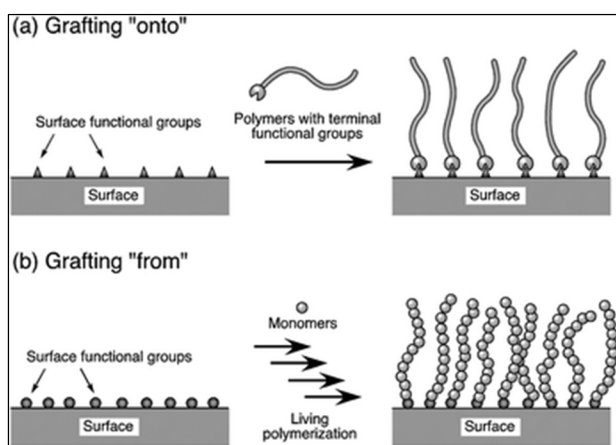


Figure 1.14 – The main approaches to graft polymers on a surface: (a) grafting-to, in which the macromolecules are grafted to functional groups and (b) grafting-from, in which polymerization occurs directly on the surface (Araki, 2013).

Table 1.3 – Grafting strategies and the effect on the wetting behavior of electrospun mats

Polymer	Treatment/modification	Wettability Characterization	Application	ref
PET	Grafting-from polymerization of MAA monomers in solution with Ce(IV) to oxidize the hydroxyl groups obtained by wet-chemistry and initiate the grafting	Contact angle: untreated PET (advancing 144°, receding 15°), grafted mats (wicking)	Tissue engineering	(Z. Ma, Kotaki, Yong, He, & Ramakrishna, 2005)
PVDF	Grafting-from polymerization of MMA monomer on plasma-treated mats	Contact angle: untreated mats (132 ±9°) and grafted membranes (62° to wicking in <5 s) / Water flux: decreased for grafted membranes	Filtration	(Kaur et al., 2007)
PGA, PLGA and PLLA	Grafting-to in situ polymerization of AA monomer during plasma treatment	Contact angle (in films only): untreated (61 ±1.59°) and grafted PGA (37 ±1.0°), untreated (71±1.2°) and grafted PLGA (42±0.9°), untreated (75 ±1.8°) and grafted PLLA (45 ±1.4°)	Tissue engineering	(K. Park, Ju, Son, Ahn, & Han, 2007)
PDLLA	Grafting-to with chitosan solution of mats treated by aminolysis	Contact angle: untreated PDLLA (137.6±3.1°) and grafted (wicking)	Tissue engineering	(Cui et al., 2010)
PMMA-co-BIEM	Grafting-from polymerization in solution with HEMA, MAPS or FA-C8 monomers	Contact angle: PFA-C8-grafted (150°), PHEMA-grafted (wicking) and PMAPS-grafted (wicking)	Surface modification	(Yano et al., 2011)
PET	Grafting-from polymerization of NIPAAm in solution on PET mats treated by wet-chemistry	Contact angle: untreated PET (≈125°) and grafted PET below the LCST of PNIPAAm (≈125° to wicking in 40s) and above the LCST of PNIPAAm (≈124°)	Responsive membrane	(Özçam, Roskov, Genzer, & Spontak, 2012)
PVDF	Grafting-from polymerization of AA or MAA monomers with and without initiators on plasma-treated mats	Contact angle: grafted membranes (wicking in <20 s) depending on treatment conditions) / Water flux: decreased for grafted membranes	Filtration	(Savoji, Rana, Matsuura, Tabe, & Feng, 2013)

Table 1.3 (continuation) - Grafting strategies and the effect on the wetting behavior of electrospun mats

Polymer	Treatment/modification	Wettability Characterization	Application	ref
PP	Grafting-from polymerization with AA monomer on plasma-treated mats (two stacked membranes)	Contact angle: untreated PP (137°), treated top and bottom surface of the first membrane (90° to wicking in <8s), top surface of the second membrane (around 110° to 45° in 30s), bottom surface of the second membrane ( $\approx 120^\circ$ ) / Water flux: increased for grafted membranes	Filtration	(Z.-P. Zhao, Li, Li, Wang, & Zhang, 2013)
TPU	Grafting-to polymerization of EG monomer during plasma treatment	Contact angle: untreated TPU ( $114 \pm 2.8^\circ$ ) and grafted TPU ( $110 \pm 0.4^\circ$ ) / Water uptake capacity: untreated TPU ( $\approx 130\%$ ) and grafted TPU ( $\approx 180\%$ ) after 24h	Antibacterial wound dressing	(Hacker, Karahaliloglu, Seide, Denkbaz, & Gries, 2014)

Among the “grafting-from” methods, a plasma treatment can be used to create functionalities on the surface that can act as initiators for polymerization. In this process the monomers are not subjected to plasma and that is why the method can be called postirradiation grafting (Desmet et al., 2009). This method was used to reduce the pore size of electrospun PVDF membranes to broaden their use in filtration (Kaur et al., 2007). The top surface of PVDF mats were first treated with radio-frequency glow discharge plasma and then exposed to air to enable the formation of oxides and peroxides on the surface. The next step was the graft polymerization in a solution containing MMA monomer. Grafted mats presented rapid wicking and also smaller pores than untreated mats. Figure 1.15 shows the effect of every step of the treatment on the mat morphology. After the plasma-treatment (Figure 1.15b), the top surface of the mat presented thinner fibers but preserved the typical open structure of electrospun membranes. The top surface morphology drastically changed after grafting (Figure 1.15c), with thicker fibers that looked swollen and smaller pores. The bottom surface presented unaltered morphology after grafting (Figure 1.15d) indicating lack of penetration of the plasma treatment (Kaur et al., 2007). In another study to evaluate the treatment penetration, two PP electrospun membranes of 200  $\mu\text{m}$  thickness were stacked and then the top surface of the first membrane was exposed to plasma. After this treatment the mats underwent AA polymerization in solution. Contact angle measurements of the treated stacked membranes revealed fast droplet absorption for both the top and bottom surface of the first membrane, while the top surface of the second membrane showed only a decrease in contact angle values from around  $110^\circ$  to  $45^\circ$  in 30 seconds and the bottom surface of the second membrane remained hydrophobic with contact angle around  $120^\circ$ , thus revealing again the limits of the treatment penetration (Z.-P. Zhao et al., 2013).

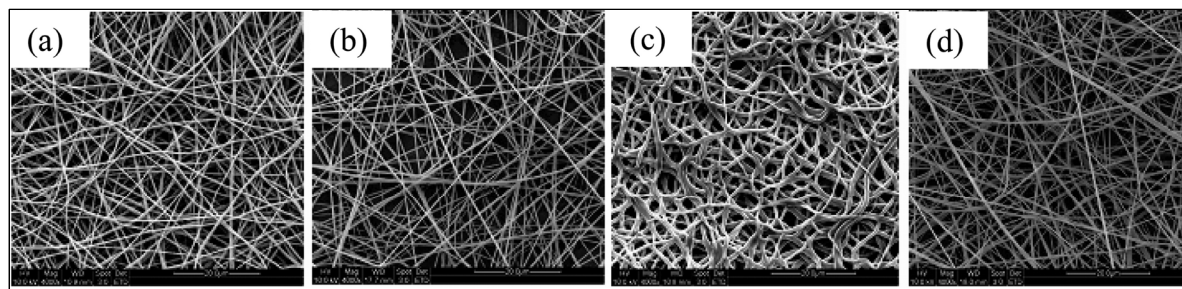


Figure 1.15 – PVDF electrospun mat: (a) untreated, (b) top surface after plasma exposure, (c) top surface after MMA grafting and (d) bottom surface after MMA grafting (Kaur et al., 2007).

In a study that involved the grafting-from method performed directly in solution, PET electrospun membranes were grafted with either PMMA or gelatin, and the penetration of the treatment was verified by the higher density of carboxyl groups in mats with increased thickness, revealing that the chosen treatment was effective to reach deeper layers of the mat. The original PET electrospun mat presented an advancing contact angle of  $144^\circ$  and receding contact angle of  $15^\circ$ , making it hydrophobic but also sticky. Both PMMA-grafted and gelatin-grafted mats presented wicking and resulting contact angle of zero. The latter also improved the proliferation of endothelial cells. (Z. Ma, M. Kotaki, T. Yong, et al., 2005). The effectiveness of the grafting treatment may also be evaluated directly on individual fibers. Figure 1.16 shows the results of an AFM analysis performed on the cross-sections of electrospun PMMA-co-BIEM fibers grafted with three different monomers (MAPS, HEMA and FA-C8), also by a grafting-from method in solution. Regarding wettability, untreated PMMA-co-BIEM mats presented contact angle of  $127^\circ$ , PFA-C8-grafted mats showed contact angle of  $150^\circ$ , while PMAPS-grafted or PHEMA-grafted mats presented wicking and low values of contact angle (Yano et al., 2011).

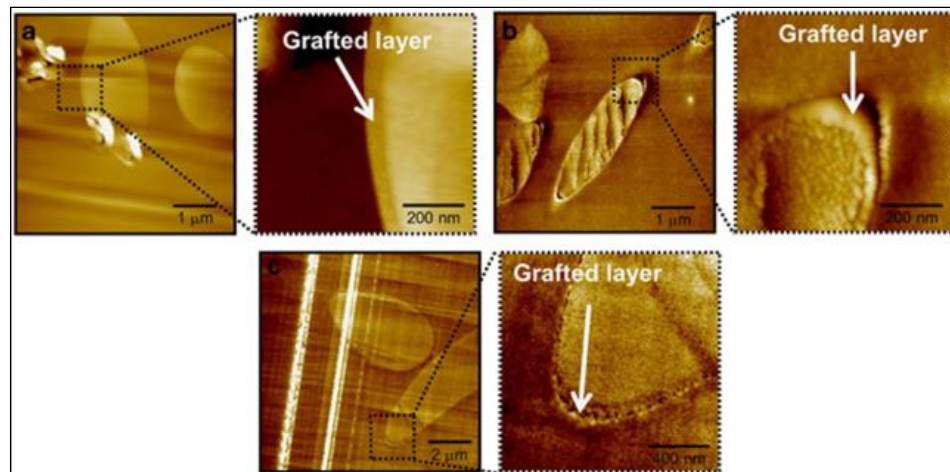


Figure 1.16 – Atomic force microscopy images showing the grafted layers on PMMA-co-BIEM fibers grafted with (a) PMAPS, (b) PHEMA and (c) PFA-C8-grafted (Yano et al., 2011).

Other grafting approaches include the treatment of the monomers by plasma. In the plasma syn-irradiation method the monomer is first adsorbed on the surface, which is then treated by plasma leading to the formation of a surface composed of cross-linked polymer. Plasma polymerization is a “grafting-to” method in which the monomer in vapor phase is injected in the plasma chamber, where it will be converted in reactive fragments and produce polymers still in the gas phase. These polymers are then deposited/grafted on the surface. Recent examples include the treatment of different biodegradable polymers (PLLA, PGA and PLGA) by plasma followed by polymerization of AA monomer to form a grafted layer of PAA. The treatment introduced carboxyl groups on the fibers surface that enhanced cell adhesion and proliferation. The analysis of contact angle was only performed in films of the same composition but the results indicated increased hydrophilicity (K. Park et al., 2007). It is worth noting here that although more conclusions about surface modification can be made from the contact angle measurements over flat film without the roughness factor, the resulting surface morphology and chemical composition of films and electrospun fibers may vary due to differences in the processing techniques even if they are prepared from identical solutions (Dufficy, Geiger, Bonino, & Khan, 2015; Rafael S. Kurusu & Demarquette, 2015).

One of the problems with the “grafting-to” approach is that every new large macromolecules must diffuse through the polymer brush to able to attach to the surface, facing steric repulsion. Therefore, surfaces treated with this method tend to present low grafting density and low film thickness, which in turn may be desirable to preserve the mat morphology, for instance. The polymerization can also be performed *in situ* before grafting but one of the drawbacks in this case is that not every monomer molecule will be bonded to form polymers, which adds a washing step to the surface treatment in order to remove the unbounded molecules (K. Park et al., 2007). The possibility of controlling the surface chemistry and thickness of the covalently bonded layer is one the main advantages of the grafting-from method, which in turn can increase fiber diameter and compromise the open structure of electrospun mats. The penetration of the treatment on deeper layers of the mat is also a drawback in all grafting methods.

#### **1.3.1.4 Coating**

Coating involves a deposition on the fibers surface and therefore is different from the techniques presented above where the substrate needs to undergo degradation or other chemical reaction to achieve the desired functionality. The final wettability will depend on the chemical species involved, the penetration of the coating in deeper layers of the mat, and the homogeneity of the treatment. Simple physical adsorption can be achieved by intermolecular bonds such as van de Waals forces or hydrogen bond, electrostatic interactions or hydrophobic interactions (Yoo et al., 2009). Recent studies that used coating to change the wettability of electrospun mats are presented in Table 1.4.

Table 1.4 – Surface modification by coating or adsorption

Polymer	Coating / modification	Wettability Characterization	Application	ref
PHBV	Calcium hydroxide solution and simulated body fluid / HAp particles on the surface	Contact angle: untreated (109.9±1.8°) and treated (wicking)	Tissue engineering	(Ito et al., 2005)
PCL	iCVD to polymerize PFEMA and coat the surface with PPFEMA	Contact angle: untreated PCL (119° to 139°, depending on mat morphology), coated PCL (151° to 175°, depending on mat morphology)	Superhydrophobic surfaces	(Minglin Ma, Mao, Gupta, Gleason, & Rutledge, 2005)
CA	Two types of sol-gel with TEOS: with and without DTMS	Contact angle: untreated CA (wicking), coated with DTMS (>150°C and water-roll angles between 10-30°), coated without DTMS (wicking)	Superhydrophobic surfaces	(Ding et al., 2006)
CA	Layer-by-layer with cationic TiO <sub>2</sub> solution and anionic PAA solution followed by immersion in FAS solution	Contact angle: untreated CA (wicking), treated with FAS with 5 or 10 bilayers of TiO <sub>2</sub> /PAA (>150° with water-roll angle < 10°), treated with FAS with 20 or 30 bilayers of TiO <sub>2</sub> /PAA (≈140° with water-roll angle > 40°)	Superhydrophobic surfaces	(Tasuku, Bin, Yuji, & Seimei, 2007)
PLLA	Poly-L-lysine solution	Contact angle: untreated (63±10.5°) and treated (68±2.6°) (Aligned fibers)	Tissue engineering	(Corey et al., 2008)
PVA and PVA/ZnO composites	FAS solution	Contact angle: untreated PVA (wicking) and coated PVA (wicking), untreated PVA/ZnO (105°) and coated PVA/ZnO (132°), untreated calcined ZnO (wicking) and coated ZnO (>150°)	Superhydrophobic surfaces	(Ding, Ogawa, Kim, Fujimoto, & Shiratori, 2008)
PCL	Simulated body fluid / calcium phosphate on the surface	Contact angle: untreated PCL (113±5°), treated (wicking) / Wicking height: untreated PCL (0), treated (≈2.7cm)	Tissue engineering	(Yang et al., 2008)
PCL	Wool protein solution	Contact angle: untreated PCL (118°) and coated PCL (58° to wicking in < 10s)	Wound healing	(X. Liu et al., 2010)

Table 1.4 (continuation) - Surface modification by coating or adsorption

Polymer	Coating / modification	Wettability Characterization	Application	ref
PMMA/O-MMT composites	Sputter-coating with Ti target to form a TiO <sub>2</sub> film	Contact angle: untreated mats (126.5°) and treated mats (increased hydrophilicity, only pictures)	Photocatalytic membrane	(Q. Wang, Wang, Li, Cai, & Wei, 2011)
PU and PU-g-PANi	PTFE solution	Contact angle: static/hysteresis for coated PU ( $\approx 125^\circ / > 90^\circ$ ) and coated PU-g-PANi ( $\approx 160^\circ / \approx 10^\circ$ )	Anti-wetting and breathable membrane	(S. J. Cho, Nam, Ryu, & Lim, 2013)
PLA and PLA/ $\beta$ -TCP	PEO solution	Contact angle: untreated PLA and PLA/ $\beta$ -TCP ( $101.7 \pm 1.3^\circ$ and $122.6 \pm 0.1^\circ$ , respectively) and coated PLA and PLA/ $\beta$ -TCP ( $64.5 \pm 0.7^\circ$ to wicking and $50.7 \pm 0.2^\circ$ to wicking, respectively with no absorption time mentioned)	Tissue engineering	(Hu, Lee, Chen, Yang, & Yang, 2013)
PS solid (PS-s) and porous fibers (PS-p), PAN	Coated with PDOPA solution for 15 or 90 minutes. PDOPA was polymerized <i>in situ</i>	Contact angle: untreated and coated PAN ( $\approx 30^\circ$ to wicking in 4s), untreated PS-s and PS-p ( $106^\circ$ and $103^\circ$ , respectively), PS-s and PS-p coated for 15 minutes ( $102^\circ$ and $90^\circ$ to wicking in 4 s, respectively), PS-s and PS-p coated for 90 minutes ( $44^\circ$ and $40^\circ$ to wicking in 4s, respectively) / Moisture transport behavior (see text)	Liquid moisture transport membrane	(Dong et al., 2014)
PSu and PAN	Coated with PDOPA solution. PDOPA was polymerized <i>in situ</i>	Contact angle: untreated PSu ( $145.7^\circ$ ), coated PSu (wicking), untreated and coated PAN (wicking)	Filtration	(Huang et al., 2014)
PVA	Coated with polyhexamethyldisiloxane using CVD in either low pressure plasma or atmospheric pressure multi-jets plasma (hexamethyldisiloxane/Ar)	Contact angle: untreated PVA (wicking, soluble in water) coated in low pressure plasma ( $119^\circ$ to $133^\circ$ , depending on power); coated in atmospheric pressure multi-jets plasma ( $138^\circ$ to $148^\circ$ )	Surface modification	(Kedroňová et al., 2015)

Table 1.4 (continuation) - Surface modification by coating or adsorption

Polymer	Coating / modification	Wettability Characterization	Application	ref
PS	Vapor coating with PFDTS on plasma-treated mats	Contact angle: untreated PS ( $139\pm 2.7^\circ$ to $161\pm 2.6^\circ$ , according to fiber morphology) and coated PS (static contact angle from $163\pm 1.5^\circ$ to $172\pm 2^\circ$ , sliding angle from $3^\circ$ to $9^\circ$ , according to fiber morphology)	Surface modification	(Yuan et al., 2016)

Coating is another surface modification method that is used to mimic natural tissues by increasing hydrophilicity and biocompatibility in biomedical applications. In a study to produce scaffolds for bone tissue engineering, PHBV was prepared by electrospinning, immersed in a calcium hydroxide solution and after that soaked in simulated body fluid to produce PHBV/HAp composites. The hydrophobic untreated PHBV scaffolds became hydrophilic after the treatment and presented higher biodegradation rate but no remarkable change in cell adhesion (Ito et al., 2005). In another study to improve biocompatibility, PLA and PLA/ $\beta$ -TCP mats were prepared by electrospinning and dip-coated with a PEO solution. As expected, the untreated PLA and PLA/ $\beta$ -TCP presented high values of contact angle ( $101.7^\circ$  and  $122.6^\circ$ , respectively) while the coated mats presented values of contact angle lower than  $90^\circ$  that decreased over time until the droplet was absorbed into the mats. Cell experiments revealed that the hydrophilic membranes were not cytotoxic and presented better biocompatibility (Hu et al., 2013). In some cases coating may modify the typical interconnected porous structure found in electrospun mats and consequently the wettability will also change. If the pores of the mats are closed after coating, the surface may present contact angle results similar to films with less influence of the roughness. In a study in which PCL and PVA electrospun mats were dip-coated in wool protein solution to produce a scaffold for wound healing, the coating solution closed some pores in the first layers of fibers but in this case the mats still presented wicking (X. Liu et al., 2010).

The penetration of the coating and the wettability of the mat can be accessed indirectly by the ability of the mat to transport liquid from moisture, and in this case the interconnected porous structure has to be preserved after the treatment. If the coating treatment is homogeneous, liquid from moisture captured on the top surface of the mat should be able to pass through the membrane and reach the bottom surface of the mat. Figure 1.17 shows the contact angle and moisture transport results for electrospun PS mats coated with PDOPA solution (*in situ* polymerization of DOPA) for 15 or 90 minutes. The treatment was effective to hydrophilize the PS mats, as shown in Figure 1.17b and Figure 1.17c. Liquid transport results show that

uncoated PS mats could not transport any moisture and all the water remained on the hydrophobic top surface (Figure 1.17di). Mats coated for 15 minutes started to show transport ability while the mats coated for 90 minutes (Figure 1.17diii) showed greatly improved moisture transport capacity (Dong et al., 2014).

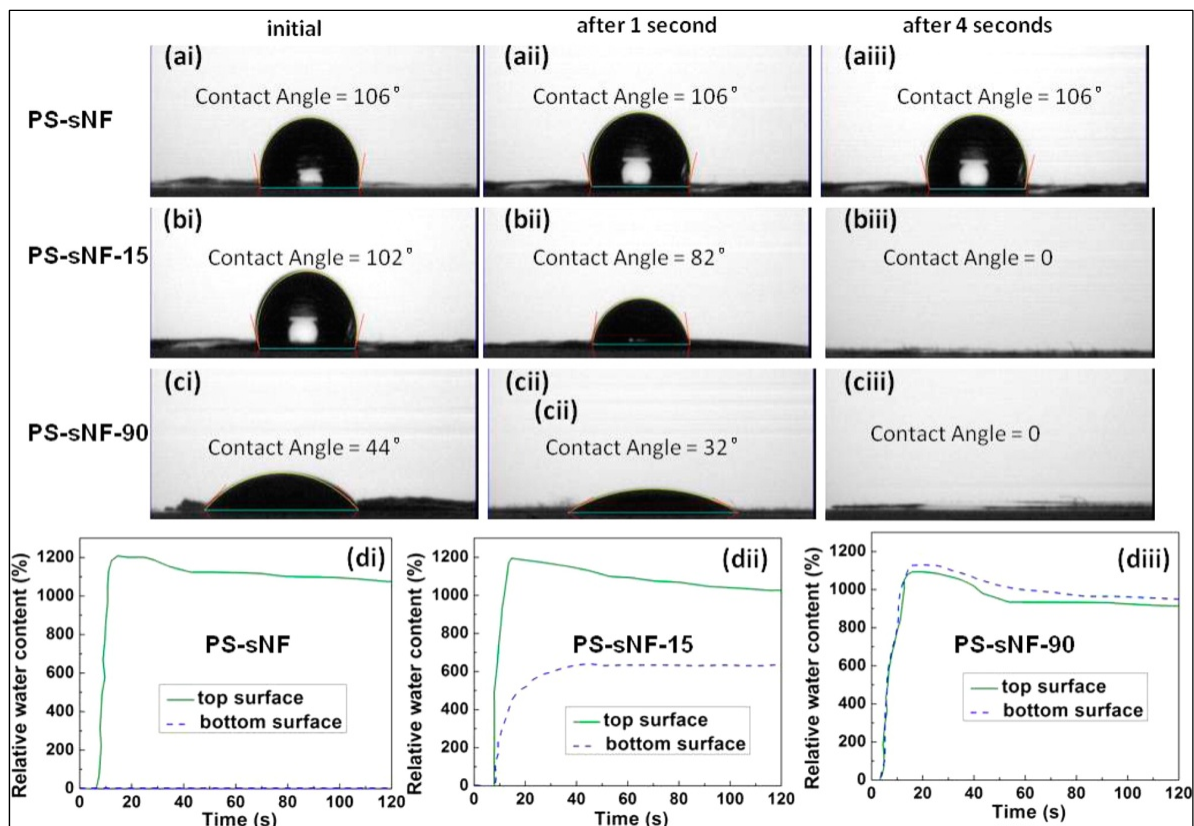


Figure 1.17 – Wettability of PS nanofibrous mats with solid fibers (PS-sNF) as a function of coating time in PDOPA solution: (1) Contact angle evolution for (a) uncoated mats, (b) PS mats coated for 15 minutes (PS-sNF-15), (c) PS mats coated for 90 minutes; (2) Moisture transport behavior for the same compositions, showing the water content on the top surface of the mat where the liquid is sprayed and on the bottom surface to evaluate the transport ability (Dong et al., 2014).

The combination of two coating treatments can also lead to the desired mat wettability. In an attempt to produce a superhydrophobic surface, CA mats were first coated by layer-by-layer,

a technique based on the alternating deposition of oppositely charged materials, and then immersed in a FAS solution. The layer-by-layer coating consisted of a bi-layer coating cycle, repeated different times, by immersion in a cationic  $\text{TiO}_2$  solution and then in an anionic PAA solution. After the second coating in the FAS solution, the bi-layer-coated samples presented more fluorine on the surface than the pure CA treated directly with FAS. Water contact angle over  $150^\circ$  and water-roll angle under  $10^\circ$  were reported for the mats with fewer  $\text{TiO}_2$ /PAA layers that presented higher roughness on the surface of the fibers (Tasuku et al., 2007).

There are also coating methods that are not based on solutions. Sputter coating with  $\text{TiO}_2$  was recently used to increase hydrophilicity and photocatalytic activity of PMMA/O-MMT composites of PMMA. Pure PMMA/O-MMT composite fibers presented rough surfaces and a contact angle of about  $126^\circ$ . The sputter-coated fibers presented a much larger diameter due to the flattening of fibers caused by the impact of  $\text{TiO}_2$  (Figure 1.18a to Figure 1.18d). Increasing sputter power produced holes in the fibers. The contact angle seemed to decrease with sputter power reaching values fewer than  $90^\circ$ . It was unclear whether the absence of wicking was caused by the altered surface morphology of the treated mats or if it was just not observed with time. The composite mats with improved hydrophilicity presented also improved photocatalytic properties (Q. Wang et al., 2011).

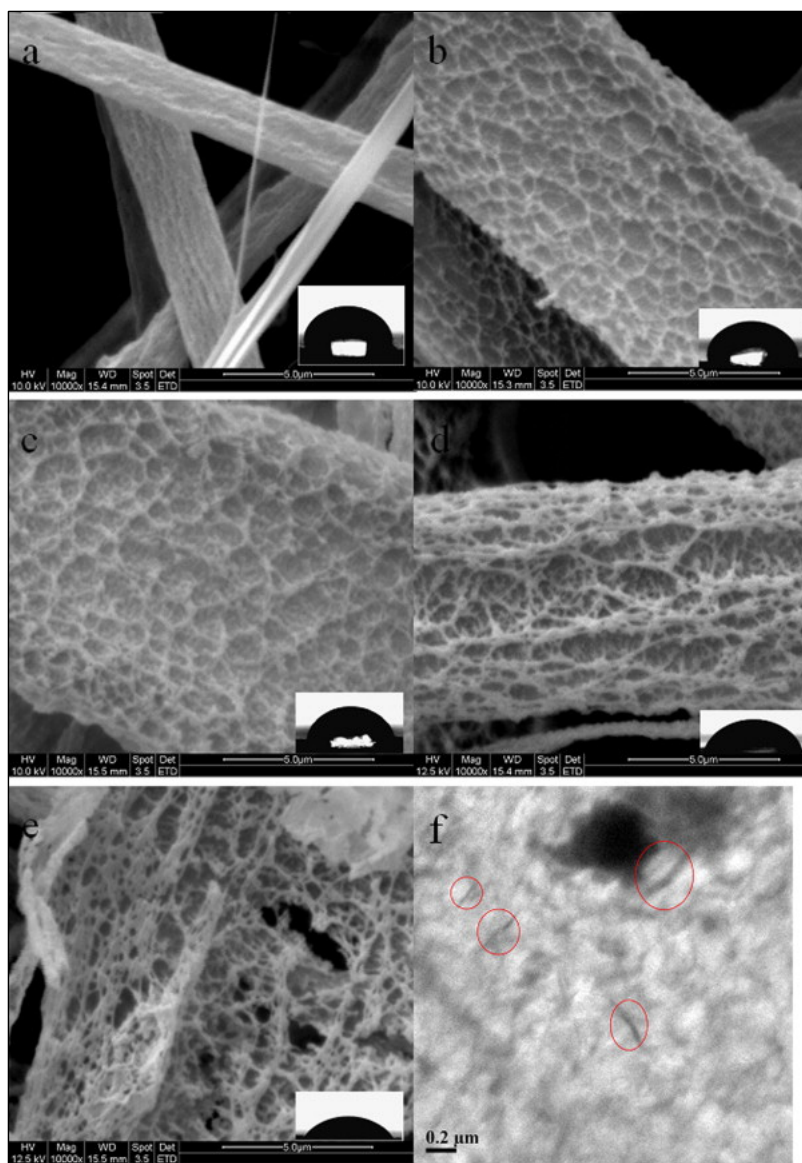


Figure 1.18 – SEM images and respective contact angle of PMMA/O-MMT composite fibers (a) untreated and sputter-coated with  $\text{TiO}_2$  with (b) 80 W, (c) 100 W, (d) 120 W and (e) 200 W of sputter power. TEM image of (a) showing nanoclay domains (Q. Wang et al., 2011).

iCVD is another coating technique that has been used to alter the surface properties of electrospun mats. The technique involves the thermal decomposition of an initiator on

resistively heated filaments followed by free-radical polymerization of a monomer at the substrate surface. The resulting polymer will form a thin coating adsorbed on the surface (Gleason, 2015). This technique was used to polymerize PFEMA into PPFEMA to coat the surface of PCL electrospun fibers (M. Ma, Y. Mao, et al., 2005). Although pure PCL mats were already hydrophobic (static contact angle of  $119^\circ$  to  $139^\circ$ , depending on mat morphology), the PPFEMA-coated mats presented static contact angle values higher than  $150^\circ$ . The combination of the surface roughness of electrospun mats with beads-on-string morphology with the low surface energy of the fluorinated acrylic polymer (PPFEMA) resulted in water contact angles as high as  $175^\circ$  and also in oleophobicity (M. Ma, Y. Mao, et al., 2005).

The examples above show that there are many possible variations to coat a surface from simple dip-coating to more complex methods such as iCVD. The outcome will depend on the affinity between coating and substrate and if the adsorption is not strong enough, the coating can be easily leached depending on the application. Another possible drawback of using coating as a surface treatment method for porous structures such as electrospun mats is that the solution must wet the substrate and have the appropriate viscosity to penetrate into deep fiber layers. Using a liquid with low surface tension like ethanol increases the wetting ability of the solution (Hu et al., 2013).

### **1.3.2 One-step surface modification**

#### **1.3.2.1 Nanoparticles**

The incorporation of nanoparticles to the polymer solution before electrospinning represents a practical alternative to alter the wettability of the fibers, provided that the particles are homogeneously located at the surface. Table 1.5 presents a summary of the recent literature on the effect of nanoparticles on the wettability of electrospun mats.

Table 1.5 – Nanoparticles to change surface properties of electrospun mats

Polymer	Nanoparticle	Wettability Characterization	Application	ref
PMMA	Fluorodecyl POSS	Contact angle: advancing/receding for pure PMMA ( $\approx 130^\circ/\approx 40^\circ$ ) and PMMA/POSS with POSS mass fraction higher than 0.1 ( $>150^\circ/>150^\circ$ )	Oil-water separation	(Tuteja et al., 2007)
PVA	ZnO	Contact angle: pure PVA (wicking), PVA/ZnO ( $105^\circ$ ) and calcined ZnO (wicking)	Superhydrophobic surfaces	(Ding et al., 2008)
TPU	Tourmaline	Contact angle: neat TPU ( $125.2^\circ$ ) and TPU with 1, 3 and 5 wt% of Tourmaline ( $69.5^\circ$ , $31.1^\circ$ and $13^\circ$ , respectively)	Antibacterial membrane	(Tijing et al., 2012)
PA 6	HAp	Contact angle: neat PA6 ( $\approx 120^\circ$ ) and PA6 with 1, 3, 5 and 10 wt% of HAp ( $\approx 120^\circ$ , $\approx 100^\circ$ , $\approx 70^\circ$ and wicking, respectively)	Tissue engineering	(Abdal-hay, Pant, & Lim, 2013; Abdal-hay, Tijing, & Lim, 2013)
PU, PU/CS and PU/HA	Ag	Contact angle: neat PU, PU/CS and PU/HA ( $95^\circ$ , $\approx 65^\circ$ and $\approx 45^\circ$ , respectively), PU, PU/CS and PU/HA with 0.5% of Ag ( $\approx 85^\circ$ , $\approx 95^\circ$ and $\approx 60^\circ$ , respectively), and PU, PU/CS and PU/HA with 1% of Ag ( $\approx 100^\circ$ , $\approx 70^\circ$ and $\approx 80^\circ$ , respectively)	Biomedical devices	(Filip et al., 2014)
PVDFhfp and PVDFhfp/PEG with 16.6 wt% of PEG of different $M_w$	TiO <sub>2</sub>	Contact angle: neat PVDFhft ( $145^\circ$ ), PVDFhfp/TiO <sub>2</sub> ( $131^\circ$ ), PVDFhfp/PEG( $M_w= 550 \text{ g.mol}^{-1}$ ) with and without TiO <sub>2</sub> ( $120^\circ$ and $131^\circ$ , respectively), PVDFhfp/PEG( $M_w= 20\text{K}$ or $100\text{K g.mol}^{-1}$ ) with and without TiO <sub>2</sub> (wicking)	Surface modification	(Fortunato, Guex, Popa, Rossi, & Hufenus, 2014)
Nafion	Silica	Contact angle: Silica/nafion membranes ( $120\text{-}130^\circ$ , depending on nafion concentration)	Oil-water separation	(J. Li et al., 2014)

Table 1.5 (continuation) - Nanoparticles to change surface properties of electrospun mats

Polymer	Nanoparticle	Wettability Characterization	Application	ref
PAN	Fumed Silica modified with hydrophobic (R805) or hydrophilic (A150) functionalities	Contact angle: neat PAN and PAN/A150 mats (wicking) and PAN/R805 with 0.5 wt% ( $>120^\circ$ to wicking in 30 minutes), 1.3 and 2.2 wt% ( $>130^\circ$ to $\approx 120^\circ$ in 30 minutes) of R805 / Wicking behavior could be tuned according to R805 content.	Surface modification	(Dufficy et al., 2015)
PU/FPU blends	CNT	Contact angle: neat PU/FPU ( $146\pm 2^\circ$ ) and composites with 0.25, 0.5, 0.75 and 1% of CNT ( $147\pm 3^\circ$ , $151\pm 2^\circ$ , $155\pm 2^\circ$ , $155\pm 3^\circ$ , respectively) / Waterproof ability and breathability: increased with CNT content	Waterproof and breathable membrane	(Y. Li, Zhu, Yu, & Ding, 2015)
PU	Silica modified with dodecyltrichlorosilane	Contact angle: neat PU ( $\approx 20^\circ$ ) and composites with 1, 3 and 5 % of modified silica ( $\approx 75^\circ$ , $\approx 85^\circ$ and $>90^\circ$ , respectively)	Surface modification	(S. H. Park, Ryu, & Kim, 2015)
PVDF	Graphene oxide	Decrease in static contact angle from around $70^\circ$ for pure PVDF to around $40^\circ$ for the PVDF/GO with 0.4 wt% of GO	Water treatment membrane	(Jang, Yun, Jeon, & Byun, 2015)
PLA	CNC and CNC-g-PEG	Contact angle: neat PLA ( $126.3^\circ$ ), PLA with 1 and 5% of CNC ( $124.9^\circ$ and $125.4^\circ$ , respectively) and PLA with 1, 5, and 10% of CNC-g-PEG ( $124.0^\circ$ , $126.1^\circ$ and $125.8^\circ$ , respectively)	Tissue engineering	(C. Zhang et al., 2015)
PLA	GO and GO-g-PEG	Contact angle: neat PLA ( $129.2\pm 0.9^\circ$ ), PLA with 1 and 2% of GO ( $129.0\pm 1.0^\circ$ and $129.5\pm 0.5^\circ$ , respectively) and PLA with 1, 2, and 5% of GO-g-PEG ( $125.5\pm 0.8^\circ$ , $122.5\pm 0.5^\circ$ and $116.2\pm 0.7^\circ$ , respectively)	Tissue engineering	(C. Zhang et al., 2016)

The homogeneity of the treatment will depend on the final dispersion of nanoparticles after solvent evaporation. The location of the nanoparticles will depend on their compatibility with the matrix, which is related to the surface energy of the components involved. Also, the incorporation of nanoparticles normally increases the dielectric constant of the solution and its ability to be electrospun and produce thinner fibers. If they are not well-dispersed, the mat can present nonuniform fiber morphology and surface treatment. In a study to produce antibacterial membranes, thermoplastic polyurethane (TPU) and tourmaline nanocomposite mats were prepared by dispersing the nanoparticles in a solution by ultrasonication and mixing with a TPU solution prior to electrospinning. Particle agglomeration was observed in the composite with higher tourmaline content (5 wt%) together with spiderweb-like nanofibers of much smaller diameter between thicker fibers (Figure 1.19a). The contact angle of neat TPU mats (around 125°) decreased steadily with the addition of nanoparticles, reaching 13° with 5 wt%. Although the uniformity of wetting properties was not mentioned, the authors observed that the composite mats submerge into water, revealing wicking (Tijing et al., 2012). Similar results were reported for electrospun nanocomposites of PA 6/HAp but in this case the dual-morphology of nanofibers and thinner spiderweb-like fibers was obtained with nanoparticles content as low as 1 wt%. The mat with the highest HAp amount (10 wt%) presented, in addition to the dual-morphology, some HAp particles on the surface of the fibers (Figure 1.19b). This mat was the only one that presented wicking (Abdal-hay, Pant, et al., 2013).

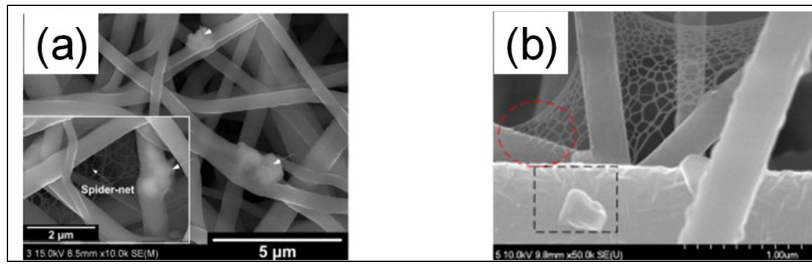


Figure 1.19 – Dual-morphology with thicker and spiderweb-like thinner nanofibers found in electrospun nanocomposites of (a) TPU/Tourmaline (95/05 wt%) (Tijing et al., 2012) (Reproduced with permission from Elsevier Ltd, UK) and (b) PA6/HAp (90/10 wt%) (Abdal-hay, Pant, et al., 2013).

The surface energy of the nanocomposite components, polymer and nanoparticles, is an important factor that can be used to tailor the location of the nanoparticles. As a general rule, hydrophilic materials have higher surface energy while hydrophobic materials have lower surface energy. If the surface energy of the particles is higher than the surface energy of the polymer, they will tend to be buried inside the polymer matrix to reduce the energy of the system, in thermodynamic equilibrium. A recent study showed that the incorporation of high surface energy hydrophilic nanoparticles was not effective to achieve hydrophilization of electrospun mats. PLA was mixed with CNC-g-PEG (C. Zhang et al., 2015) and GO-g-PEG (C. Zhang et al., 2016) nanoparticles acting as a reinforcement for tissue engineering scaffolds. The effect on the wettability of PLA, however, was negligible as the PLA composites mats with higher content of nanoparticles (10 wt% of CNC-g-PEG or 5 wt% of GO-g-PEG) presented contact angle values similar to pure PLA (C. Zhang et al., 2015; C. Zhang et al., 2016).

In the opposite case, particles with relative low surface energy will tend to segregate to the air interface and therefore can be more effective to change the surface properties of the fibers. Composite mats of PMMA with fluorodecyl POSS prepared by electrospinning showed the advancing and receding contact angle values above 150° resulting in both superhydrophobicity and superoleophobicity for oil-water separation. Water repellency was achieved due to the segregation of the low surface energy particles and the beads-on-string

mat morphology (Tuteja et al., 2007). In another study, composite fibers of PU/FPU with carbon nanotubes also presented advancing contact angle values higher than  $150^\circ$  and increased resistance to hydrostatic pressure (Y. Li et al., 2015).

However, the rapid processing time during electrospinning can keep the blend structure out of the equilibrium state. A recent study investigated model systems of PAN fibers mixed with fumed silica modified with either hydrophobic (R805) or hydrophilic (A150) functionalities. XPS results revealed slightly higher segregation of the hydrophilic-functionalized fumed silica to the surface, which suggested that the surface energy effects were hindered since it was expected that hydrophobic components with lower surface energy would segregate more to the surface. Pure PAN and PAN/A150 mats were hydrophilic but the composite mat showed faster water droplet absorption, faster wicking and greater water uptake capacity (Figure 1.20). The wicking behavior of PAN/R805 composite mats could be tuned by simply changing the R805 concentration due to different levels of surface coverage by the hydrophobic additive (Figure 1.20) (Dufficy et al., 2015).

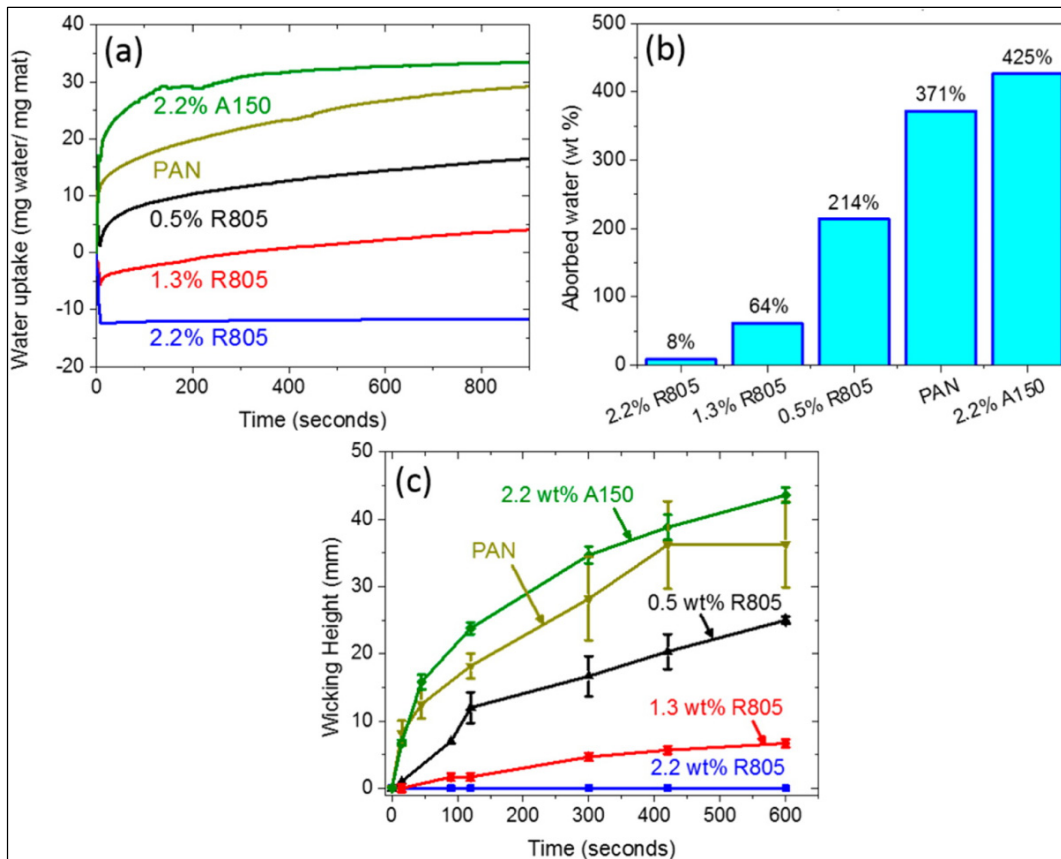


Figure 1.20 – Wicking behavior of PAN/fumed silica composite mats as a function of additive (A150 or R805) concentration: (a) water uptake as a function of time; (b) total absorbed water after wicking; (c) wicking height as a function of time (Dufficy et al., 2015).

Although the incorporation of nanoparticles to the electrospinning solution is an interesting and practical one-step method to change the surface properties of the fibers before deposition, many aspects have to be taken into account to produce an effective treatment such as the nanoparticles dispersion in the solution and their ability to segregate to the surface during electrospinning. Nanoparticles can also help to increase the surface roughness of the fibers and thus amplify the wettability of electrospun nanocomposites. To understand these phenomena, it is critical to consider the role of surface energy in multiphase systems such as nanocomposites or polymer blends.

### 1.3.2.2 Blending

A polymer blend is a mixture of two or more polymers that can be either miscible (at the molecular level) resulting in a single phase material or immiscible, forming phase-separated structures. Compatible blends are a subcategory of immiscible blends that are commercially attractive and have stable morphologies with enhanced properties (Utracki & Favis, 1989). Blending has been historically used as a method to improve bulk properties of polymers. A typical example is the incorporation of elastomers in thermoplastic matrices to increase toughness (Rafael Salles Kurusu, Demarquette, Gauthier, & Chenal, 2014). However, blending can also be used to change the surface properties of polymers (Kolahchi, 2014), which is crucial in structures with high surface area such as electrospun mats. The final properties will be defined by the processing technique and a possible preferential segregation of one of the polymers to the surface, which will define the surface chemical composition and morphology. Regarding the wettability of polymer surfaces, there are usually two approaches to achieve surface modification by blending: (i) incorporating hydrophilic or hydrophobic homopolymers or (ii) incorporating amphiphilic copolymers. These blends tend to be immiscible due to differences in chemical structure and therefore surface energy that lead high interfacial tension between the polymers. Figure 1.21 presents some possible morphologies obtained by blending two immiscible polymers. Regarding the surface properties, three possibilities come to mind: droplets or co-continuous structures reaching the surface, a surface mainly covered by the matrix or a surface covered by the modifying polymer. The recent use of blend to alter the wettability of electrospun mats is summarized in Table 1.6.

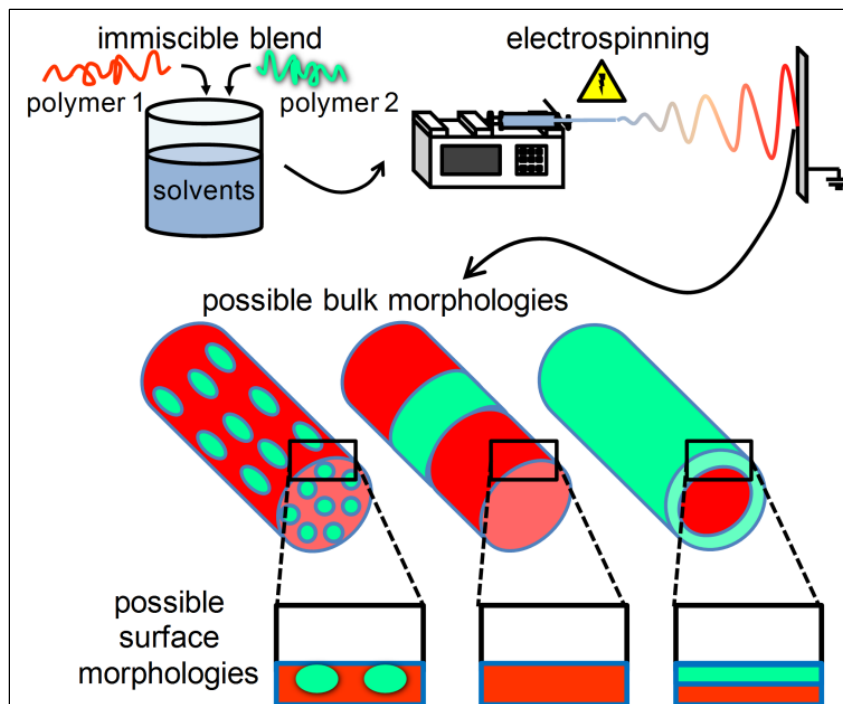


Figure 1.21 – Schematic of blending immiscible polymers by electrospinning and some of the possible bulk and surface morphologies.

Table 1.6 – Blending as a surface modification technique

Matrix	Blended with	Wettability Characterization	Application	ref
PLA	PLGA, PLA-PEG-PLA and lactide	Contact angle: pure PLGA (105°), PLGA/PLA-PEG-PLA/lactide (75/15/10 wt%) (46°)	Tissue Engineering	(K. Kim et al., 2003b)
PS	PS-PDMS	Contact angle: pure PS (138°); PS/PS-PDMS blends (163° with 15° of contact angle hysteresis)	Superhydrophobic surfaces	(M. Ma, R. M. Hill, et al., 2005)
PLGA	PEO-PPO-PEO (F108)	Contact angle: pure PLGA ( $\approx 120^\circ$ ), and PLGA/PEO-PPO-PEO blends (wicking, with absorption time varying according to PEO-PPO-PEO content)	Surface modification	(Vasita, Mani, Agrawal, & Katti, 2010)
PAA	PVA	Humidity sensitivity: pure PAA mats presented higher sensitivity than PAA/PVA blends	Humidity sensor	(Xianfeng et al., 2010)
PS	PNIPA	Contact angle: PS/PNIPA blend below 30°C (wicking), and above 45°C ( $>130^\circ$ )	Surface modification	(Muthiah, Hoppe, Boyle, & Sigmund, 2011)
PS	PVME	Contact angle: miscible blends up to 20 wt % of PVME ( $> 120^\circ$ ), with 30 wt% of PVME (wicking), phase-separated blends (wicking)	Bulk and surface modification	(Valiquette & Pellerin, 2011)
PVDF	Different surface modifying molecules (SMM-400, SMM-600 and SMM-1000) synthesized with PEG ( $M_w = 400, 600$ or $1000 \text{ g.mol}^{-1}$ )	Contact angle: pure PVDF ( $131.5 \pm 4.5^\circ$ ), PVDF/SMM-400 ( $139.8 \pm 4.7^\circ$ ), PVDF/SMM-600 ( $140.0 \pm 3.1^\circ$ ) and PVDF/SMM-1000 (wicking) / Water flux : Increased for PVDF/SMM-1000	Filtration	(Kaur et al., 2012)
PANi	PVB	Humidity sensitivity: improved humidity sensing performance with PVB sheath and PANi core	Humidity sensor	(Q. Lin, Li, & Yang, 2012)
PET	PVA	Contact angle: pure PET (131°), PET/PVA (20/1) (wicking)	Surface modification	(G. Li et al., 2013)

Table 1.6 (continuation) - Blending as a surface modification technique

Matrix	Blended with	Wettability Characterization	Application	ref
PLGA	PEO-PPO-PEO (F127)	Contact angle: pure PLGA (116°), PLGA/F127 (95/5 wt%)(106°) and PLGA/F127 (90/10 wt%) (81°) / Water uptake capacity after 60 minutes: pure PLGA (100±4%), PLGA/F127 (95/5 wt%)(459±191%) and PLGA/F127 (90/10 wt%) (1302±388%)	Tissue engineering	(Weijie, Anthony, James, & Sang Jin, 2013)
PCL	Chitin fibrils	Contact angle: PCL/chitin mats with 0, 5, 10, 15, 20, 25 and 30 wt% of chitin (117.8°, 123.4°, 126.1°, 125.8°, 122.0°, 83.9° and wicking, respectively)	Tissue engineering	(Ji, Liang, Shen, & Bowlin, 2014)
PCL	PEO	Contact angle: PCL/PEO blends at different ratios, 20/0, 18/0.6, 16/1.2, 14/1.8, 12/2.4, 10/3, 8/3.6, 6/4.2, 4/4.8, 2/5.4, 0/6 (117.9°, 98.1°, 84.6°, 28.8°, 19.9°, 23.0°, 33.1°, 37.0°, 34.7°, 40.3° and 16.4°, respectively)	Tissue engineering	(Y.-F. Li et al., 2014)
PVDF	PVP	Contact angle: PVDF/PVP blends at different ratios, 1/0, 3/1, 2/1, 1/1, 1/2, 1/3, 0/1 (136°, 134°, 127°, 125°, 75°, 73° and 18°, respectively)	Surface modification	(M. Wang et al., 2014)
PVDFhfp	PEG of different M <sub>w</sub>	Contact angle: neat PVDFhft (145°), PVDFhfp with 16.6 wt% of PEG with M <sub>w</sub> of 550, 1550 (131°, 138°, respectively) and 10K, 20K and 100K g.mol <sup>-1</sup> (wicking)	Surface modification	(Fortunato et al., 2014)
PLCL	PEO-PPO-PEO (F127)	Contact angle: pure PLCL (131°), PLCL/F127 (99/01 wt%) (85°), PLCL/F127 with higher F127 content (wicking)	Tissue engineering	(N.-h. Liu et al., 2014)
PAN and PU	FPU	Contact angle: mats composed of PAN/FPU and PU/FPU fibers with 0, 0.25, 0.5, 0.65 and 1 wt% of FPU (6°, 134°, 142°, 152° and 154°, respectively)	Filtration	(N. Wang et al., 2014)

Table 1.6 (continuation) - Blending as a surface modification technique

Matrix	Blended with	Wettability Characterization	Application	ref
SEBS	PEO-PPO-PEO (F127)	Contact angle: pure SEBS and SEBS/F127 blends with 5 and 10 wt% of F127 ( $\approx 140^\circ$ ), SEBS/F127 blends with 15 (wicking at different times) and 20 wt% of F127 (wicking in $\approx 2$ s)	Surface modification	(Rafael S. Kurusu & Demarquette, 2015)
PCL	SS	Contact angle: pure PCL ( $128 \pm 8^\circ$ ) and PCL/SS with mass ratio of 9/1, 8/2, 7/3, 6/4 and 5/5 ( $106 \pm 12^\circ$ , $75 \pm 9^\circ$ , $42 \pm 4^\circ$ , wicking for the last two)	Tissue engineering	(L. Li et al., 2015)
PMIA	PU	Contact angle: pure PMIA/PU with weight ratios of 2/8, 4/6, 6/4, 8/2 ( $101^\circ$ , $\approx 90^\circ$ , $\approx 70^\circ$ and $48.9^\circ$ , respectively)	Batteries	(Xiao, Zhai, Yu, & Ding, 2015)
SEBS	PEO-PPO-PEO (F127, P123 and L61)	Contact angle: All SEBS/P123 and SEBS/L61 mats (wicking) / High-speed imaging and Wicking time: varying droplet absorption time according to segregation and PEO-PPO-PEO type	Surface modification	(Rafael S. Kurusu & Demarquette, 2016)
PLA, PLA-g-poly(acrylPEG)	PEG ( $M_w=400$ and $2000$ g.mol <sup>-1</sup> )	Contact angle: pure PLA, PLA-g-poly(acrylPEG) and PLA/PEG mats ( $\approx 125^\circ$ )	Antibacterial membranes	(Toncheva et al., 2016)

Systems that can form miscible and immiscible blends are therefore interesting in order to understand the role of surface chemical composition and morphology on the final wettability of the mats. PS/PVME, for instance, can be miscible or immiscible depending on the solvents used in fabrication. This system was studied in electrospinning where miscible PS/PVME blends were prepared with benzene and an organic salt (TBAB) to increase the conductivity of the solution, while the immiscible blends were prepared with chloroform. As shown in Figure 1.22, the miscible PS/PVME mats with 0-20 wt% of PVME presented increased hydrophobicity when compared to the respective films mainly due to the introduction of roughness. Miscible blends with 30 wt% of PVME became hydrophilic. The immiscible phase-separated fibers presented a distinct core-sheath morphology with a PS-rich core and a PVME-rich sheath that resulted in hydrophilization in all range of compositions (Valiquette & Pellerin, 2011).

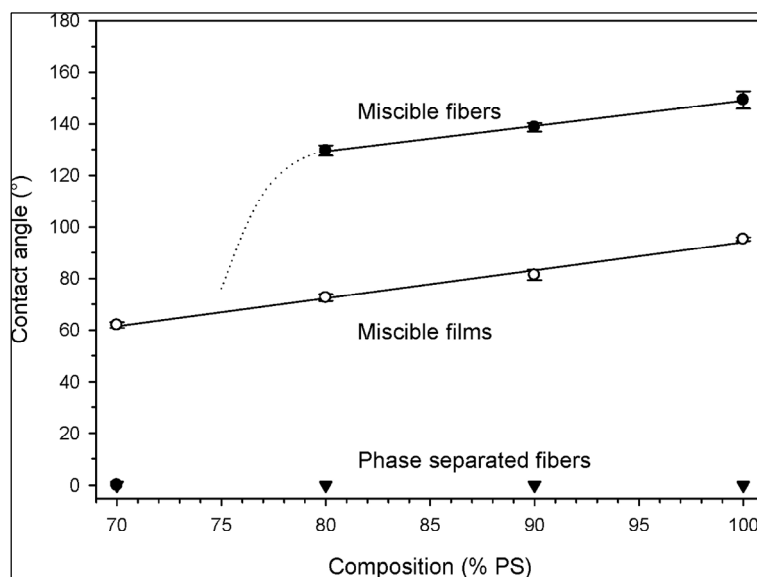


Figure 1.22 – Contact angle results for PS/PVME fibers, miscible and immiscible, and miscible films (Valiquette & Pellerin, 2011).

As noted for nanoparticles, the surface energy of the polymers that form the blend is a critical factor in controlling the surface morphology and consequently the wettability of the mat. Again, polymers with relative low surface energy will tend to segregate to the surface while polymers with relative high surface energy will tend to stay buried in the matrix, provided that the thermodynamic equilibrium can be reached. Hydrophobic PLA was recently blended with hydrophilic PEG, but the resulting mats remained hydrophobic with contact angle values similar to pure PLA ( $\approx 125^\circ$ ) (Toncheva et al., 2016). The molecular weight of the surface modifying polymer is also an important factor to be considered. Hydrophobic PVDFhfp with low surface energy was blended with different types of hydrophilic with high surface energy PEG. Contact angle results revealed that the blends (16.6 wt% of PEG) with low molecular weight PEGs remained hydrophobic while the blends with high molecular weight PEGs were hydrophilized and presented wicking. Other studies also investigated hydrophilization by blending with hydrophilic polymers. PVA was used to hydrophilize PET (G. Li et al., 2013) and n-chitin was used to make PCL mats hydrophilic (Ji et al., 2014). Moreover, the introduction of the second polymer to a solution can also alter the electrospinnability by altering properties like conductivity and viscosity. Figure 1.23a shows that pure PET fibers presented the typical beads-on-string morphology but the blend PET/PVA (20/1) showed uniform fibers (Figure 1.23b). In this case, high surface energy PVA was effective to hydrophilize hydrophobic PET (contact angle of  $131^\circ$ ) (G. Li et al., 2013). Figure 1.23 shows that the incorporation of 5 wt% of n-chitin to PCL mats produced a mat with a drastically decrease in diameter (Figure 1.23c and Figure 1.23d), but in this case hydrophilization was only achieved with 30 wt% of n-chitin (Ji et al., 2014).

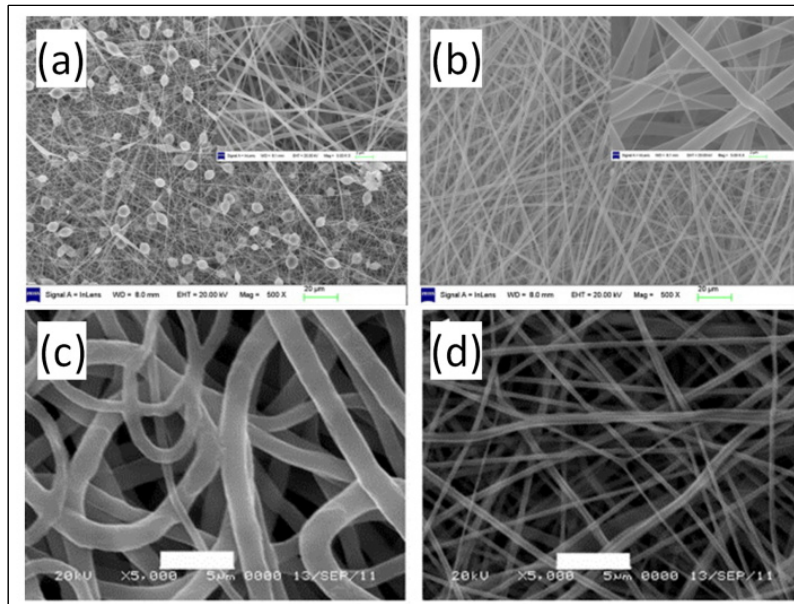


Figure 1.23 – Effect of blending on the mat morphology: (a) Pure PET and (b) PET/PVA (20/1 proportion) blend (G. Li et al., 2013) (Reproduced with permission from Elsevier Ltd, UK); (c) Pure PCL and (d) PCL/n-chitin (95:05) blend (Ji et al., 2014).

Amphiphilic block copolymers PEO-PPO-PEO, known commercially as Pluronics, have also been investigated as surface modifying polymers used to achieve hydrophilization. The idea in this case is that the low surface energy PPO block will drive the segregation to the air surface and drag the hydrophilic PEO blocks. Once on the surface, the PEO blocks will extend when in contact with an aqueous medium (Y.-q. Wang et al., 2005). PLGA was blended with PEO-PPO-PEO (Pluronic F108) in solution, and the resulting mats were hydrophilic even with small amounts of PEO-PPO-PEO. Surface enrichment was confirmed by chemical analysis and no phase separation was observed for the mats with lower PEO-PPO-PEO concentration (Vasita et al., 2010). Biocompatible and biodegradable PLCL was also blended with PEO-PPO-PEO (Pluronic F127) to adjust the scaffolds wettability. The contact angle of pure PLCL ( $131^\circ$ ) decreased to  $85^\circ$  with 1 wt% PEO-PPO-PEO and all the mats tested with higher PEO-PPO-PEO content presented wicking and final contact angle of zero (N.-h. Liu et al., 2014). Recently, PEO-PPO-PEO (F127) was also blended with hydrophobic thermoplastic elastomer SEBS and the results indicated that a specific blend

morphology contributed to produce homogenous superhydrophilic electrospun mats with the same water droplet absorption time for the blends with 20 wt% of the amphiphilic polymer (Rafael S. Kurusu & Demarquette, 2015). SEBS was later blended with three different types of PEO-PPO-PEO (F127, P123 and L61) with different molecular weight and PEO content to investigate the effect of these properties on the wetting behavior of electrospun mats. The smaller molecules with higher content of low energy PPO segregated more to the surface even reaching saturation (Figure 1.24). The wicking ratio could be tuned according to the PEO-PPO-PEO type and concentration. The liquid polymer, L61 with molecular weight of  $2\ 000\ \text{g}\cdot\text{mol}^{-1}$ , was easily leached when washed with water. SEBS/L61 blends presented non-durable hydrophilicity, which could be interesting for release applications (Rafael S. Kurusu & Demarquette, 2016). The control of segregation of the second component is one the most important factors to achieve surface modification by blending, be in the form of droplets or other type of phase-separated structures or free molecules. In the case of PEO-PPO-PEO, the segregation can continue over time for a long time even after the SEBS fibers are solidified. This movement is driven by the thermodynamic equilibrium morphology of the amphiphilic molecules with surfactant properties to be placed at the interface matrix/air. Therefore the contribution to surface modification when blending with amphiphilic molecules comes not only from the phase-separated structures that reached the surface during electrospinning, but also from free molecules that have the tendency to form a surfactant layer even in the solution before processing and continue to move over time depending on matrix characteristics like glass transition temperature and consequently the free volume to allow further segregation (see Chapter 5).

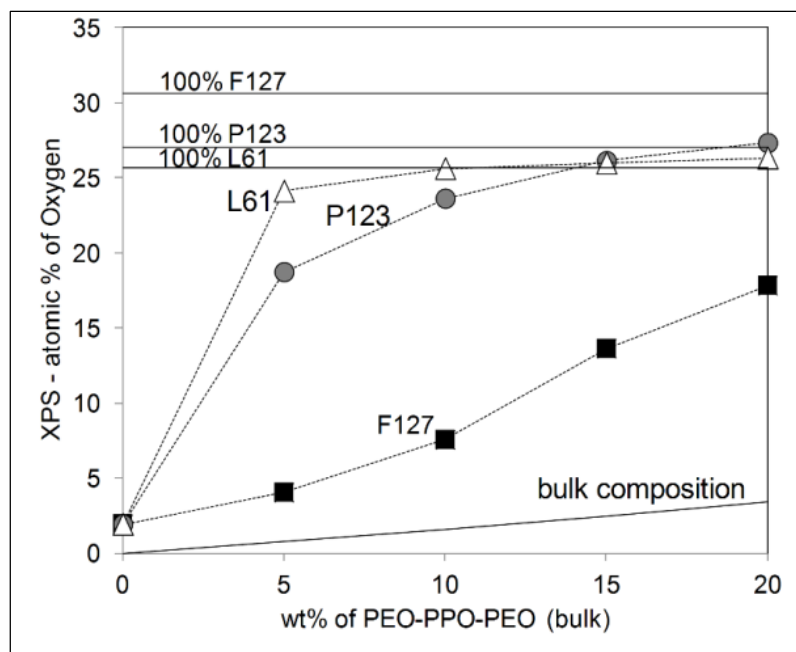


Figure 1.24 – Amount of oxygen at the surface of SEBS/PEO-PPO-PEO electrospun fibers prepared with different PEO-PPO-PEO (F127, P123, and L61). From bottom to top, the solid lines show the theoretical amount of oxygen according to the bulk composition, pure L61, pure P123 and pure F127 (Rafael S. Kurusu & Demarquette, 2016).

Blends with copolymers were also investigated to produce superhydrophobic mats. PS was blended with a PS-*b*-PDMS diblock copolymer and XPS results revealed surface enrichment with PDMS. Since the blend mat presented a much higher contact angle ( $163^\circ$ ) than pure PS ( $138^\circ$ ), as well as contact angle hysteresis of  $15^\circ$ , it was concluded that the superhydrophobicity was a result of both the surface roughness typical of electrospun mats and the segregation of PDMS to the surface (M. Ma, R. M. Hill, et al., 2005).

To summarize, the final chemical composition and morphology of the blend will define the wettability of the mat. The surface energy of the components and the kinetic conditions during electrospinning will affect the process outcome. The complexity of the system is a drawback, considering the most common case of two immiscible polymers in a solution with two solvents, which is recurrent to produce an electrospinnable solution.

#### **1.4 Future prospects and conclusions**

This review presented the main possible approaches to modify the surfaces of electrospun mats in order to change their wettability, which is critical for many applications. Hydrophilic mats are preferred for tissue engineering, for example, as the cells tend to have better attachment and proliferation on these type of surface. Hydrophobic or superhydrophobic mats are usually designed to block the passage of water, such as in oil-water separation membranes. The particular geometry of electrospun mats, composed of randomly aligned fibers with a usually a large volume of interconnected pores, makes them more susceptible to present extreme wetting behaviors from hydrophobic surfaces with high values of contact angle to fast-absorbing superhydrophilic mats. The simple static contact angle measurement must be taken as a starting point to characterize the wettability of the mats. It is possible to observe the reoccurrence of this switch mechanism in recent literature. In other cases, exceptions to this behavior are not always well explained, particularly for hydrophilic mats. Sometimes the contact angle was not measured over time – water absorption occurs sometimes after minutes. In other cases there only a few fiber layers and the mat is too thin, making it hard to rule out the influence from the substrate on which the fibers were deposited. In other exceptions, the mat presents, sometimes after surface modification, a different and more film-like morphology that can explain the contact angle results.

Surface modification methods performed after electrospinning such as plasma and wet-chemistry treatments, grafting and coating can be effective in providing a robust modification but in some cases present some drawbacks such as fiber degradation and lack of penetration. The incorporation of nanoparticles of other polymers in the solution before electrospinning can be an alternative to produce the desired surface properties in one-step, but the system becomes more complex and the location of the surface modifying agent has to be controlled as well. One of the objectives of this work was to show that all methods present advantages and disadvantages and the choice of the most suited method will also depend on the targeted application.



## CHAPTER 2

### ARTICLES ORGANIZATION

The literature review presented in Chapter 1 had the intention of understanding the current state of the art and the challenges associated with surface modification techniques to alter the wettability of electrospun mats. Within this context, the next three Chapters of this thesis present the specific scientific contributions to the field in the following order:

Chapter 3 presents the first article of this project, entitled “*Blending and Morphology Control To Turn Hydrophobic SEBS Electrospun Mats Superhydrophilic*”, which summarizes the study to achieve the first specific objective of this thesis, the evaluation of polymer blending with an amphiphilic copolymer (PEO-PPO-PEO) as a surface hydrophilization technique for electrospun SEBS mats. SEBS/PEO-PPO-PEO films and electrospun mats were prepared with different PEO-PPO-PEO concentrations. The mats were evaluated in terms of surface chemical composition, contact angle and morphology. The results led to the publication of the article in *Langmuir* in April 25, 2015

After the successful hydrophilization by blending presented in Chapter 3, the next step was to further explore and tune the wetting properties of electrospun SEBS/PEO-PPO-PEO mats prepared with three different types of PEO-PPO-PEO copolymers, with varying molecular weight and PEO content. For that, different techniques to analyze the wetting of hydrophilic mats were employed. To observe the dynamics of droplet spreading and impact, high-speed imaging was used. The wicking rate measured by the rise of water in mat strips of defined geometry was also evaluated. The resulting article, presented in Chapter 4 and entitled “*Wetting of Hydrophilic Electrospun Mats Produced by Blending SEBS with*

*PEO–PPO–PEO Copolymers of Different Molecular Weight*” was also published in *Langmuir* in January 19, 2016.

After experimental evidence showing that SEBS could be hydrophilized by blending with PEO-PPO-PEO copolymers and that its wettability could also be tuned, Chapter 5, entitled “*Surface morphology evolution in polymer blends by segregation of hydrophilic or amphiphilic molecules during and after electrospinning*” presents a study that goes more deep in the morphology and chemical composition evolution of SEBS-based blends. The first part of this Chapter presents a comparison between hydrophilic PEO with amphiphilic PEO-PPO-PEO as surface modifying agents for electrospun mats. The influence of having a low surface energy PPO mid-block on the surface segregation was evaluated in terms of surface chemical composition and wetting behavior. After that, surface energy measurements and interfacial tension calculations were also performed to help clarify the morphology evolution of those blends after electrospinning. The last part of this article compares the segregation of one of the amphiphilic copolymers in two different matrices, SEBS and pure PS. The results are currently under evaluation for publication and the submitted manuscript is presented in Chapter 5.

## CHAPTER 3

### **BLENDING AND MORPHOLOGY CONTROL TO TURN HIGHLY HYDROPHOBIC SEBS ELECTROSPUN MATS SUPERHYDROPHILIC**

Rafael S. Kurusu, Nicole R. Demarquette\*

\*Mechanical Engineering Department, École de technologie supérieure - ÉTS,  
1100 Notre-Dame Street West, Montréal, Québec – Canada H3C 1K3

This paper has been published in *Langmuir*, 2015, 31(19), pp 5495–5503

**ABSTRACT:** Thermoplastic elastomer SEBS, a triblock copolymer composed of styrene (S) and ethylene-co-butylene (EB) blocks, can be dissolved and processed by electrospinning to produce flexible non-woven mats that can be interesting for applications like filtration or separation membranes. Controlling surface properties such as hydrophobicity/hydrophilicity is critical to achieving a desired performance. In this study, highly hydrophobic electrospun SEBS mats were obtained, following which an amphiphilic molecule (Pluronic® F127) was solution-blended with SEBS prior to electrospinning, in a bid to produce a hydrophilic membrane. The result was a fast-spreading superhydrophilic mat with thinner fibers that preserved the flexibility of the SEBS. The morphologies of non-woven mats, flat films (prepared by dip-coating using identical solutions) and of the surface of individual fibers were characterized using different microscopy techniques (Optical, SEM and AFM). Chemical analysis by X-ray Photoelectron Spectroscopy (XPS) revealed a large F127 concentration in the outermost surface layer. In addition, an analysis of dip-coated flat films revealed that for 20 wt% of F127 there was a change in the blend morphology from dispersed F127-rich regions in the SEBS matrix to an interconnected phase homogeneously distributed across the film that resembled grain boundaries of micellar crystals. Our results indicated that this morphology change at 20 wt% of F127 also occurred to some extent in the electrospun fibers and this, combined with the large surface area of the mats, led to a drastic reduction in

the contact angle and fast water absorption, turning highly hydrophobic electrospun mats superhydrophilic.

### 3.1 Introduction

In a typical electrospinning experiment, a polymer solution inside a syringe is charged by connecting the syringe needle to a high voltage supply, and, in optimal conditions, a drop on the tip of the needle is deformed into a conic shape, and then a thin jet erupts and moves towards a grounded collector. Interactions between charges cause bending instabilities, reducing the diameter of the jet while the solvent evaporates. Finally, solid fibers are deposited on the collector (Bhardwaj & Kundu, 2010; Rutledge & Fridrikh, 2007). The result is a porous non-woven mat with randomly aligned fibers and a high superficial area. These mats can find many possible applications in tissue engineering, filtration, separation membranes, etc (Gopal et al., 2006; Hutmacher, 2000; Wu, Wang, Zhao, & Jiang, 2013). In all cases, the control of surface properties such as hydrophobicity/hydrophilicity is important to achieve a desired performance. As an example, in the event of an oil spill, a hydrophobic and oleophilic electrospun membrane can be used for filtration or adsorption in an oil-water system (M. W. Lee et al., 2013; J. Lin, Y. Shang, et al., 2012; Xue et al., 2014). Hydrophilic scaffolds can have non-fouling properties that are interesting for applications such as affinity membranes (Z. Ma, M. Kotaki, & S. Ramakrishna, 2005). Both superhydrophobicity and superhydrophilicity can be used as two different approaches to make self-cleaning mats (Ganesh, Nair, Raut, Walsh, & Ramakrishna, 2012; Srisitthiratkul, Yaipimai, & Intasanta, 2012), often inspired by nature's examples such as lotus or ragwort leaves, and the pitcher plant (Miyachi, Ding, & Shiratori, 2006; Nishimoto & Bhushan, 2013; Nuraje, Khan, Lei, Ceylan, & Asmatulu, 2013; Patankar, 2004).

Electrospun mats have rough surfaces that can amplify the natural hydrophobicity or hydrophilicity of a material (Ito et al., 2005; G. T. Lim, Puskas, Reneker, Jáklí, & Horton, 2011), by either enhancing the effect of chemical composition with greater surface area, or by producing a composite surface of polymer and trapped air or liquid, according to wetting

theories (José Bico, Marzolin, & Quéré, 1999; Callies & Quere, 2005; Nosonovsky, 2007). There are many examples of hydrophobization after electrospinning (M. Lee, Lee, & Park, 2013; M. W. Lee et al., 2013; G. T. Lim et al., 2011; M. Ma, R. M. Hill, et al., 2005). Combining micro (mat surface) and nanotexture (fiber surface) usually leads to high water contact angle values (M. Lee et al., 2013; G. T. Lim et al., 2011), and even naturally hydrophilic polymers can produce hydrophobic surfaces by electrospinning (M. Zhu, Zuo, Yu, Yang, & Chen, 2006). Although less frequently reported, hydrophilization can also be achieved after electrospinning with a naturally hydrophilic polymer such as Polycaprolactone (PCL) (C. H. Kim et al., 2006).

Another approach used to control the wetting properties of electrospun mats involves a post-treatment. Chemical vapor deposition (M. Ma, Y. Mao, et al., 2005) or silanization (Pisuchpen et al., 2011) can be used for hydrophobization. Hydrophilic mats can be also obtained after chemical vapor deposition or plasma treatment (Chandrasekaran et al., 2011; Jeon & Kim, 2014), solution coating (Ito et al., 2005; X. Liu et al., 2010), immersion precipitation (W. J. Cho et al., 2009), cross-linking (Cécile & Hsieh, 2010) and heat treatment (H. S. Lim et al., 2010). However, in these cases, there is a large increase in the cost and time needed to obtain the ideal surface condition.

Polymer blending can be a practical one-step alternative in producing superhydrophobic (M. Ma, R. M. Hill, et al., 2005), hydrophilic (K. Kim et al., 2003a; N.-h. Liu et al., 2014) and superhydrophilic mats (C. H. Kim et al., 2006; G. Li et al., 2013; N.-h. Liu et al., 2014; Valiquette & Pellerin, 2011; Vasita et al., 2010). In the case of surface hydrophilization, the strategies used involve either incorporating a hydrophilic polymer such as polyvinyl alcohol (PVA) (C. H. Kim et al., 2006; G. Li et al., 2013) and poly(vinyl methyl ether) (PVME) (Valiquette & Pellerin, 2011) or an amphiphilic polymer such as the copolymers of poly(ethylene oxide)-*b*-poly(propylene oxide)-*b*-poly(ethylene oxide) (PEO-PPO-PEO), known as Ploxamers, or commercially as Pluronic (N.-h. Liu et al., 2014; Vasita et al.,

2010). These polymers contain hydrophobic PPO as the mid-block and hydrophilic PEO as the end-blocks. The idea is that the hydrophobic segment will help anchor the molecule to the polymer matrix while hydrophilic segments will be active at the surface when in contact with water (J. H. Lee, Ju, & Kim, 2000; Y.-q. Wang et al., 2005). Vasita et al. obtained superhydrophilic mats of Poly(lactide-co-glycolide) (PLGA) by blending it with Pluronic F108. This effect was caused by an increased concentration of F108 at the surface, but the fiber morphology analysis revealed no phase separation between the two polymers at low concentrations (Vasita et al., 2010). Liu et al. also obtained superhydrophilic mats by blending poly ( $\epsilon$ -caprolactone-co-lactide) with Pluronic F127, used for tissue engineering applications (N.-h. Liu et al., 2014).

Despite these examples, there is still a lack of understanding of blend morphology as a key factor for the hydrophilization of electrospun fibers with Pluronics. Furthermore, Pluronics can self-assemble to form micelles in solution as a function of temperature and concentration (Alexandridis & Alan Hatton, 1995; Kell, 1996). These micelles can form agglomerates with different morphologies, and then lead to the formation of a crystalline phase due to micelle crowding (Ghofraniha, Tamborini, Oberdisse, Cipelletti, & Ramos, 2012; Tamborini, Ghofraniha, Oberdisse, Cipelletti, & Ramos, 2012).

In this work, linear triblock copolymer Styrene-*b*-ethylene-butylene-*b*-styrene (SEBS) was used to produce electrospun mats with different wetting behaviors. SEBS is interesting for electrospinning as it can be dissolved in different solvents, and the mechanical behavior of the resulting fibers is similar to that of elastomers. Pure SEBS and blends with different concentrations of PEO-PPO-PEO (Pluronic F127) were prepared in order to obtain a hydrophilic mat. Dip-coated flat films were prepared for comparison. Water contact angle measurements were carried out and explained based on the morphology of electrospun mats and films at the micron scale, chemical composition, segregation of the minor component to the surface and blend surface morphology at the sub-micron scale. To our knowledge, this is the first study on a phase-separated system with amphiphilic polymer (Pluronic) revealing the effect of blend morphology on the hydrophilicity of electrospun mats.

## 3.2 Experimental

Linear Triblock copolymer SEBS (G1652) with an average molecular weight of 79,000 g/mol and 30 wt% of styrene (S) blocks was kindly supplied by Kraton. Block copolymer PEO-PPO-PEO (Pluronic F127) with an average molecular weight of 12,600 g/mol and 73.2 wt% of ethylene glycol blocks was purchased from Sigma Aldrich. Chloroform and Toluene were purchased from Fisher Scientific.

A mixture of chloroform and toluene (80/20 wt%) (Rungswang et al., 2011a, 2011b) was used as the solvent and incorporated into a previously weighed dry mixture of SEBS/F127 at different ratios, with a constant total concentration polymer/solution of 15 wt%. The solutions were stirred vigorously for 15 minutes at room temperature until there was no sign of SEBS or F127 agglomeration. Following that, the solutions were either used for dip-coating or transferred to a syringe for electrospinning. Six compositions were studied: pure SEBS, SEBS/F127\_5 (95/05 wt%), SEBS/F127\_10 (90/10 wt%), SEBS/F127\_15 (85/15 wt%), SEBS/F127\_20 (80/20 wt%) and pure F127. Blends containing higher concentrations of F127 were also tested, but then the process became unstable and heterogeneous mats were obtained.

A Dip-Master 50 dip-coater (Chemat Technology) was used for dip-coating glass slides with a residence time of 3 seconds and speed of 10 mm/min. For the electrospinning experiments, each syringe was placed in a syringe pump (PHD Ultra 4400, Harvard Apparatus), and the needle was charged using a power source SL40\*150 (Spellman). A metallic plate covered with aluminum foil was used to collect the mats composed of randomly aligned fibers. The parameters used were: voltage of 15 kV, flow rate of 2 mL/h, distance to collector of 15 cm, 21G syringe needle, room temperature (24°C) and 30% of relative humidity.

Water contact angle (WCA) values were obtained using a VCA Optima (AST products, Inc.) and Milli-Q ultrapure water. A total of eight measurements were carried out in different regions of each sample.

Scanning electron microscopy (SEM) was performed with a S3600N microscope (Hitachi) in secondary electron mode with 5 kV of voltage. Prior to the analysis, the surfaces were coated with gold using a K550X sputter coater (Emitech). Films were also characterized by transmitted light microscopy with a BX51 optical microscope (Olympus). Atomic force microscopy (AFM) was performed with a FastScan Microscope (Bruker) with a Nanoscope V Controller in tapping mode, using medium oscillation damping with 300 KHz of resonance frequency. Electrospun fibers were deposited on glass slides, and then individual fibers were imaged by carefully bringing the AFM tip in contact with this fiber prior to scanning. An etched Si cantilever (model ACTA from APPNano Inc.) was employed. Four scans in different fibers were performed for each sample. ImageJ software was used for image analysis of the micrographs.

The chemical composition of the materials was analyzed by X-ray Photoelectron Spectroscopy (XPS) using an ESCALAB 3 MKII (VG) with a Mg K $\alpha$  source and 216 watts of power. The depth of analysis was 50-100 Angstroms and the surface area analyzed was 2mmx3mm for each sample.

Tensile tests of the electrospun mats were performed with an ElectroForce® 3100 test instrument (Bose) with a 22N load cell. Rectangular specimens measuring 16mmx0.5mm were cut from each mat and the thickness measured using a micrometer. Five specimens of two compositions (pure SEBS and SEBS/F127\_20) were tested. The distance between grips was kept at 4mm and the speed of testing was 40 mm/min. Due to equipment and configuration limitations, the maximum possible elongation at break was 300%.

### 3.3 Results and discussion

Figure 3.1 presents the water contact angle values and respective error bars for the electrospun mats as a function of F127 bulk concentration. Pure SEBS produced a highly hydrophobic mat with  $139^{\circ} \pm 2$  contact angle. The mats with 5 and 10 wt% F127 remained highly hydrophobic, just like pure SEBS, until complete evaporation of the droplet. When the amount of F127 reached 15 wt%, the contact angle measured remained around  $140^{\circ}$  instantly after the deposition, but then, the droplet impregnated the mat and the final angle was  $0^{\circ}$ , making it superhydrophilic. The time for this absorption varied between 10 seconds and 2 minutes depending on the region of the mat, which revealed heterogeneous surface properties for this composition. When the amount of F127 was further increased to 20 wt%, the mat became homogeneously superhydrophilic, with fast spreading of water in all regions tested. Figure 3.2 shows that the absorption for the SEBS/F127\_20 started at the moment the drop touched the mat ( $t=0s$  in Figure 3.2), and after released from the needle the spreading occurred in fractions of a second. Mat morphology was then investigated in order to understand this drastic drop in contact angle. It is worth noting that it was impossible to obtain electrospun fibers with pure F127. Even at high concentrations (50-60 wt%), electrospaying took place, possibly due to improper rheological properties considering the low molar mass of F127

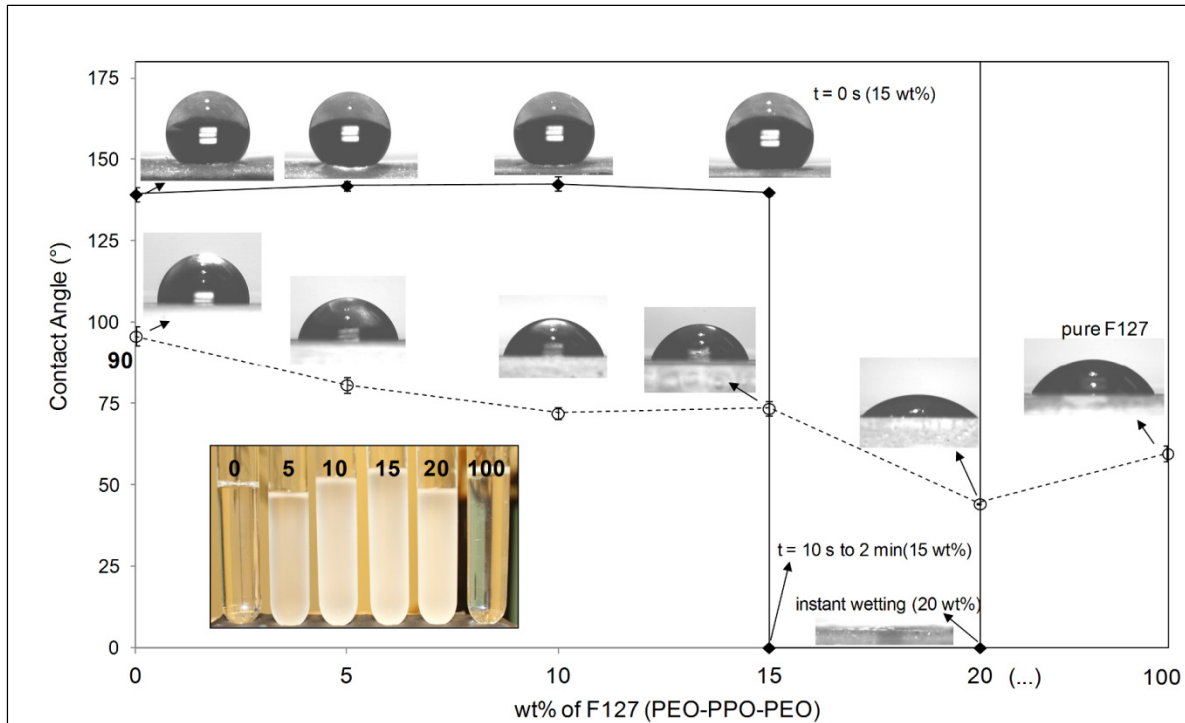


Figure 3.1 – Water contact angle for the electrospun mats (◆) and dip-coated films (⊖) as a function of F127 concentration in the SEBS/F127 blends. The insert shows the vials containing each solution.

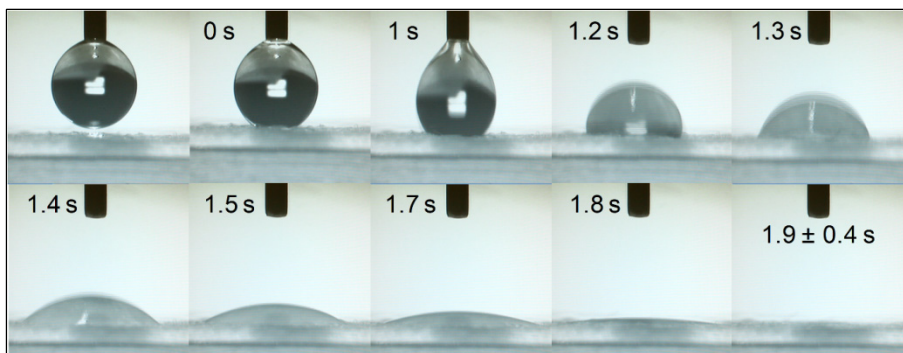


Figure 3.2 – Water droplet fast spreading for the superhydrophilic SEBS/F127<sub>20</sub> electrospun mat.

Figure 3.3 shows an overview of pure SEBS and SEBS/F127<sub>20</sub> mats. The most remarkable difference on mat morphology between pure SEBS and the blends is the reduction in fiber diameter, regardless of F127 percentage. The average fiber diameter for pure SEBS was

11.4±1.0 μm, and in the presence of 5, 10, 15 and 20 wt% of F127 was 5.2±0.3 μm, 4.9±0.5 μm, 4.4±0.4 μm and 4.9±0.6 μm, respectively. A rough estimate made by 2D image analysis showed that there was also a consequent pore size reduction following the same trend of fiber diameter. The simple incorporation of additives can change solution properties like viscosity (Rungswang et al., 2014) and influence fiber stretching during electrospinning. Similar results on SEBS fiber diameter reduction were reported by Rungswang et al. (Rungswang et al., 2014), but in this case with a different additive.

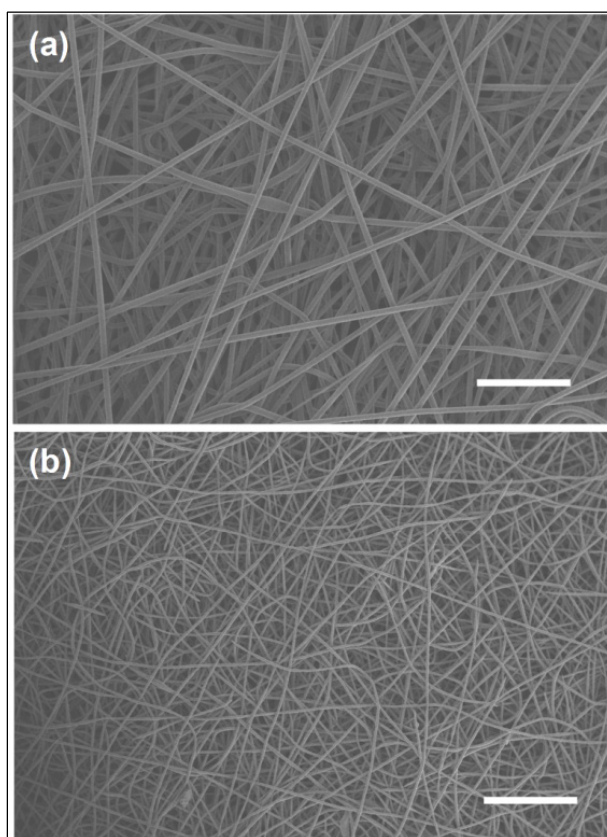


Figure 3.3 – Electrospun fibers observed by SEM with 100x magnification: (a) pure SEBS and (b) SEBS/F127\_20. Scale bars correspond to 200 μm.

Since all F127-containing electrospun mats (5, 10, 15 and 20 wt%) presented similar and homogeneous morphological features at the micron scale, there is no apparent correlation between mat morphology and water contact angle results. To understand the system SEBS/F127 without the typical rough surface of electrospun mats, identical solutions were dip-coated and tested. The results are also presented in Figure 3.1, showing that dip-coated pure SEBS had a contact angle of  $96\pm 3^\circ$ , while the electrospun mat had a contact angle of  $139\pm 2^\circ$ . Increasing the amount of F127 in the dip-coated blends led to an expected decrease in the contact angle values to  $81\pm 2^\circ$ ,  $72\pm 2^\circ$  and  $73\pm 2^\circ$  for SEBS/F127\_5, SEBS/F127\_10 and SEBS/F127\_15, respectively. There was a greater decrease in contact angle for the SEBS/F127\_20 flat film ( $44^\circ\pm 0.2$ ), and this value was remarkably smaller than that of pure F127 ( $60^\circ\pm 1$ ), i.e., the dip-coated film with 20 wt% of F127 was more hydrophilic than the film of pure F127. This can indicate that when the amount of F127 reached 20 wt% there was a higher concentration of hydrophilic segments (PEO blocks) at the surface. Similar minimum values for water contact angle (around  $44^\circ$ ) were reported for membranes containing Pluronic F127 blended in different polymer matrices, revealing a possible surface saturation (J. H. Lee et al., 2000; Y.-q. Wang et al., 2005).

As mentioned earlier, roughness can contribute to amplifying the hydrophilic or hydrophobic character of a given material by increasing the contact area with the droplet (Wenzel state) or by creating a composite structure of the material and trapped air (Cassie-Baxter state) (José Bico et al., 1999; Callies & Quere, 2005; Nosonovsky, 2007). The rough surface of electrospun SEBS is what accounts for the hydrophobic character of the mats with up to 10wt % of F127, compared to the dip-coated films. The large surface area and capillary action must also have contributed to the superhydrophilic effect of the blends with 15 and 20 wt% of F127, but the differences in water absorption time (inconstant for the SEBS/F127\_15 mats; constant and fast for SEBS/F127\_20 mats) cannot be fully explained by roughness alone. SEBS/F127\_15 must have a heterogeneous chemical composition or fiber morphology to explain the inconsistency in absorption times. Based solely on contact angle measurements, fast-spreading SEBS/F127\_20 seems to be homogeneous. XPS tests were therefore performed to understand the influence of the surface chemical composition.

Since Oxygen atoms are only present in the F127 molecules, a broad survey by XPS can provide information about the presence of this element at the surface of films and fibers. Based on the chemical structure and bulk composition, the amount (wt%) of F127 was calculated, and is presented in Figure 3.4a as a function of bulk composition. For the dip-coated films with a bulk composition of 5 and 10 wt% F127, the surface composition had around 70 wt% F127. The F127 surface concentration for the SEBS/F127\_15 film was almost 90 wt%, and practically 100 wt% for the SEBS/F127\_20 film. Electrospun mats also presented a significant F127 surface enrichment, but to a lesser extent compared to the dip-coated films. The bulk compositions of 5, 10, 15 and 20 wt% presented surface compositions of 23, 38, 58 and 70 wt%, respectively. Figure 3.4b shows a sequence of typical high resolution spectra of the electrospun mats as a function of F127 concentration from 5 wt% to 20 wt%. The increase in intensity for the ether carbon peak (-C-O-) at 286.6 eV confirmed the surface enrichment, given that this type of bond is only found in F127 molecules. For the dip-coated films, the trend was the same, but with a higher intensity for the ether carbon peak. However, in all cases, it is not possible to tell the difference between hydrophilic PEO segments and hydrophobic PPO segments, as both contain oxygen and the same types of C-C and C-O bonds.

F127 molecules have a tendency to segregate at the surface due to incompatibility with SEBS. PPO blocks anchor the F127 molecule to the hydrophobic surface of SEBS and brushlike PEO segments extend in contact with water (Shi et al., 2008; Y.-q. Wang et al., 2005). At first, PPO blocks with lower surface energy tend to segregate to the air surface while PEO blocks with higher surface energy are buried in the polymer matrix. Once the surface is in contact with an aqueous medium, hydrophilic PEO segments will extend and enrich the surface (Shi et al., 2008). Still, chemical composition alone does not fully explain the difference in wetting properties between SEBS/F127\_15 and SES/F127\_20. Therefore, blend morphology was investigated.

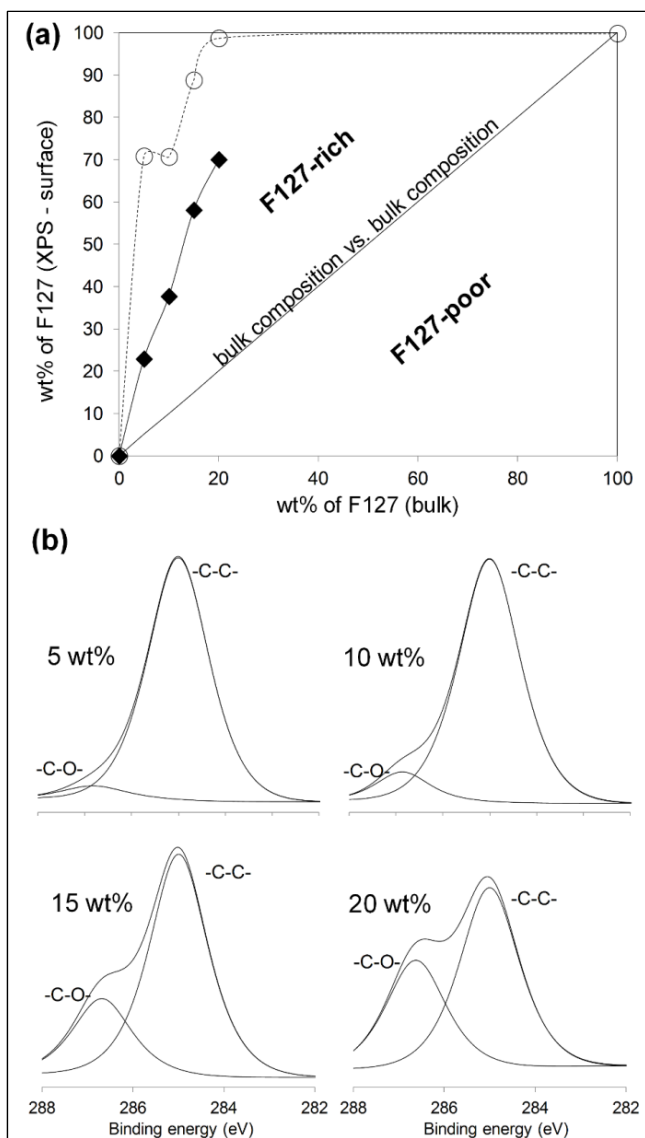


Figure 3.4 – XPS results: (a) Measured % of oxygen atoms converted in wt% of F127 vs. bulk wt% of F127 for the electrospun mats (◆) and dip-coated films (⊖); (b) High resolution XPS spectra for the electrospun SEBS/F127 mats with 5, 10, 15 and 20 wt% of F127.

Figure 3.5 presents the images obtained by transmitted light microscopy for the dip-coated films. There was always phase separation regardless of the concentration, confirmed by DSC results (not shown here). The blend with 5 wt% of F127 (Figure 3.5b) presented a typical dispersed phase in the SEBS matrix, with the droplet diameter ranging from 0.5 to 5  $\mu\text{m}$ .

With 10 wt% of F127 (Figure 3.5c), the film contained a combination of the previously observed dispersed phase and larger domains of different morphology, with the diameter ranging from 10 to 30  $\mu\text{m}$ . These domains are formed either by coalescence of smaller domains or by concentration fluctuations. SEBS/F127\_15 (Figure 3.5d) presented similar features, but with larger domains containing the distinct morphology. With 20 wt% of F127 (Figure 3.5e), there was a complete switch to an interconnected morphology, replacing the previous dispersed phase, with grain-like regions having a diameter of about 10  $\mu\text{m}$ , and surrounded by an interconnected phase that resembled grain boundaries with a thickness of approximately 1  $\mu\text{m}$  (Figure 3.5e). This unique morphology was observed evenly across the entire film. Pure F127 dip-coated film (Figure 3.5f) also presented a grain-like structure, but with smaller grains. At smaller magnifications (not shown here), pure F127 presented a spherulitic morphology. Figure 3.6 shows the surface topography of SEBS/F127\_20 (Figure 3.6a) and pure F127 (Figure 3.6b) flat films using SEM in secondary electrons mode. The blend presented a rougher surface compared to pure F127. Considering that the chemical composition is practically the same, this roughness increase may explain the lower contact angle values for the blend.

The change in morphology possibly occurred due to a particular self-organization of F127 micelles with SEBS at around 80/20 wt%. Micelle agglomeration in different structures occurs in solution due to increased concentration, and can lead to the formation of crystalline structures similar to those observed for SEBS/F127\_20 and pure F127 (Alexandridis & Alan Hatton, 1995; Ghofraniha et al., 2012; Kell, 1996; Tamborini et al., 2012). Depending on the size of the agglomerates, colloidal dispersions can scatter light, and are therefore usually turbid when viewed with the naked eye. The insert in Figure 3.1 shows that all the solutions containing SEBS and F127 presented the typical turbidity of colloidal dispersions. Clear solutions were observed for pure SEBS and pure F127. Since identical solutions were used in dip-coating and electrospinning, from the original concentration to the complete absence of solvent, it was expected that any change in colloidal agglomeration due to different

concentrations would affect the outcome of both techniques. The main difference lies in the order of magnitude of the structures formed during evaporation in each case. In dip-coating, the surface area in contact with air is much smaller, so that evaporation takes more time to occur. F127 molecules and micelles have mobility for a longer time period, increasing self-assembly and agglomeration in ordered structures. In electrospinning, jet stretching provides a greater contact area with air and facilitates evaporation (Rutledge & Fridrikh, 2007), leaving less time for self-organization. The fibers are solid before reaching the collector. Given that the fiber diameter is smaller than the grain-like structures observed in the flat films, the combined micelles of F127 and SEBS must have organized themselves in a different crystalline structure.

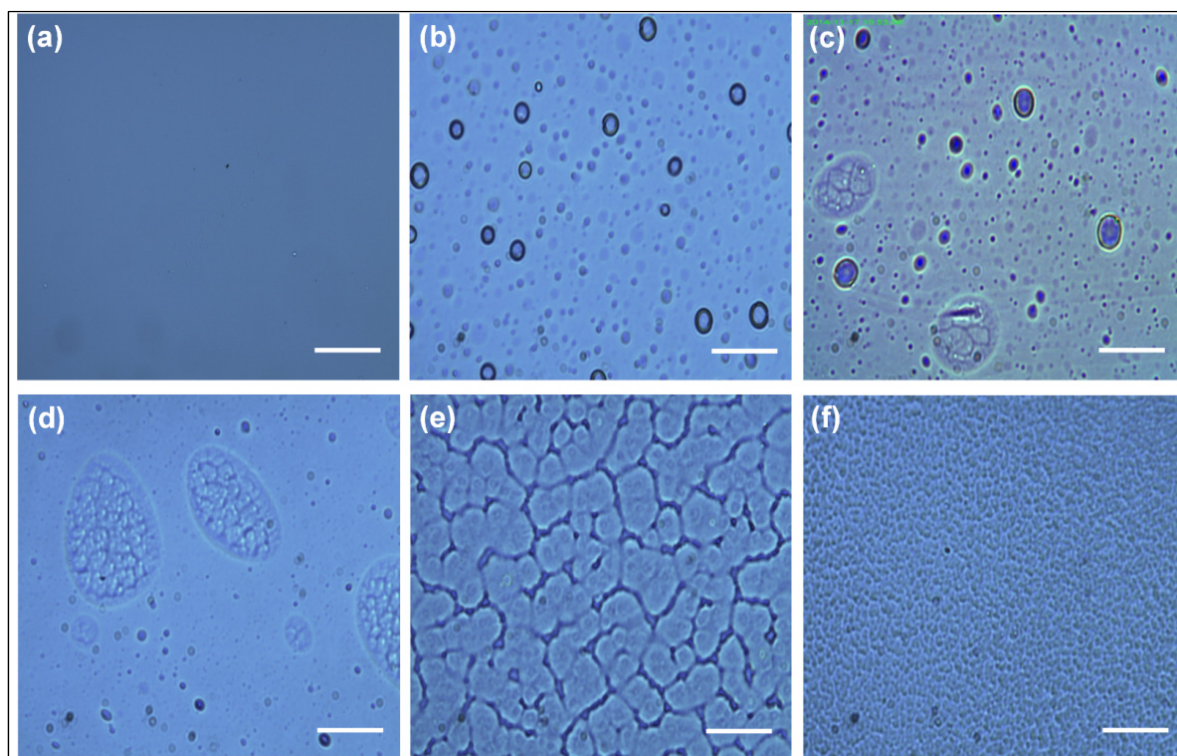


Figure 3.5 – Dip-coated films observed by transmitted light microscopy at 1000x magnification: (a) Pure SEBS, and increasing F127 concentration to (b) 5 wt% (c) 10 wt% (d), 15 wt% (e) 20 wt% (f) and pure F127. Scale bars correspond to 20  $\mu\text{m}$ .

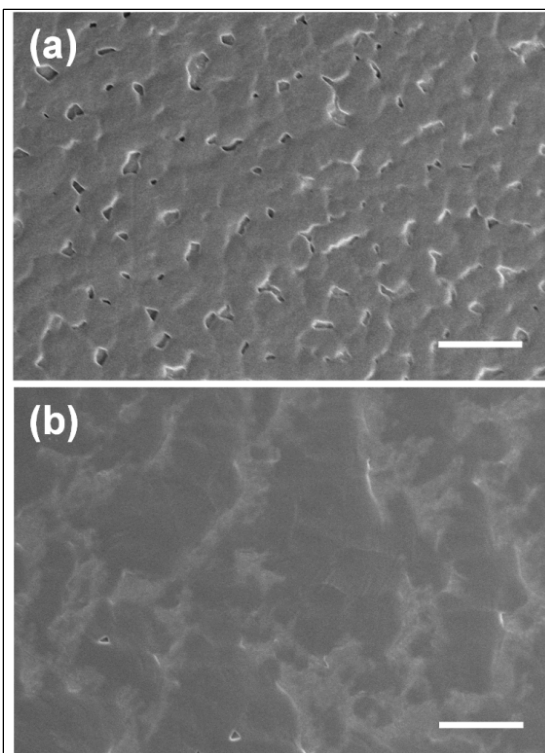


Figure 3.6 – Dip-coated films observed by SEM in secondary electrons mode and 1000x magnification for the (a) SEBS/F127\_20 blend, and (b) pure F127. Scale bars correspond to 20 µm.

Figure 3.7 shows the surface topography of the electrospun fibers observed by SEM. Despite the differences in diameter, it can be observed that pure SEBS (Figure 3.7a) and SEBS/F127\_15 (Figure 3.7b) fibers presented a much smoother surface as compared to SEBS/F127\_20 (Figure 3.7c). This is analogous to what was found for the dip-coated films, where the SEBS/F127\_20 blend had the interconnected morphology and a slightly rough surface (Figure 3.6a). However, it is important to highlight here that for the dip-coated films, the morphology features were in the micron scale, while for the electrospun fibers, the morphology was in the sub-micron scale ( $<1\mu\text{m}$ ). This difference in order of magnitude can contribute to bring a much more dramatic effect to the surface properties of electrospun mats.

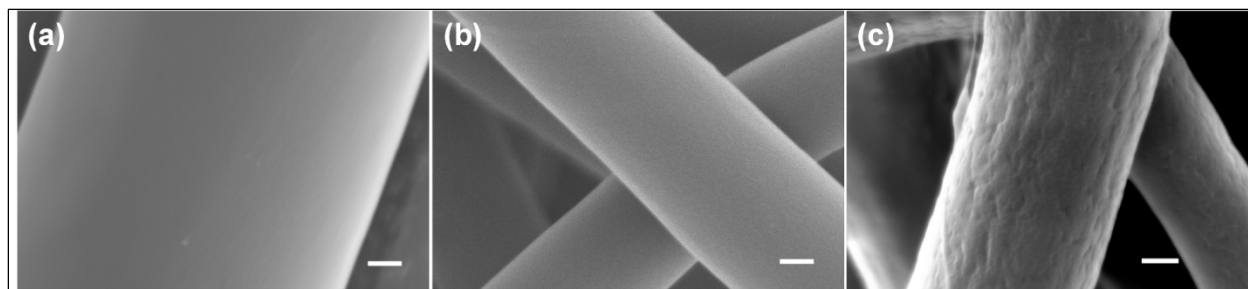


Figure 3.7 – SEM images of (a) Pure SEBS, (b) SEBS/F127\_15 and (c) SEBS/F127\_20 at 10.000x magnification. The scale bars correspond to 1  $\mu\text{m}$ .

Tapping mode AFM was used to analyze the surface of single fibers at higher magnification. This was possible because the diameter of the fibers was around at least 5  $\mu\text{m}$ . The experimental scheme and results for phase images are summarized in Figure 3.8. SEBS presented a typical block copolymer microstructure (Y. Wang, Hong, Liu, Ma, & Zhang, 2008) with cylindrical-lamellar morphology for the styrene blocks, which appear brighter (Figure 3.8a). Figure 3.8b and Figure 3.8c show two types of fiber surface morphology found for the SEBS/F127\_15 blend. In the first type (region 1 – Figure 3.8b), it was possible to observe a pure SEBS structure, but in this case with a larger presence of cylindrical block morphology with cylinders perpendicular to the surface. Besides SEBS, a second phase dispersed on the surface was observed, which represented the minor component F127. The other type of morphology (region 2) found on SEBS/F127\_15 samples is presented in Figure 3.8c, where it seemed that F127 practically covered the entire surface. There were also circular domains of about 20 nm in diameter. Similar Pluronic micelle diameter values have been already reported in literature (Alexandridis & Alan Hatton, 1995; Tamborini et al., 2012). These different degrees of F127 dispersion and concentration for this particular composition can explain the variations in time for the meshes to absorb water in the contact angle tests. With 20 wt% of F127 (Figure 3.8d), all the regions analyzed showed a complete cover of the surface without the presence of SEBS domains, but the morphology seemed different from the region 2 of SEBS/F127\_15, possibly due to a different organization of F127 micelles with SEBS.

This apparent homogeneous surface, combined with XPS, contact angle, and SEM (Figure 3.7) results, reinforces the theory that the morphology change observed in dip-coating also occurred during the electrospinning process. A combination of rough/porous structure, chemical composition and blend morphology led to a superhydrophilic electrospun mat. Figure 3.9 summarizes a possible simplified scheme for the wetting properties of the electrospun mats. The insert shows the hydrophilic PEO segments extended in the water. The differences in fiber surface cover resulted in the different absorption times for SEBS/F127\_15 and the homogeneously covered SEBS/F127\_20 produced constant fast absorption.

Lastly, tensile testing was performed to investigate the effect of hydrophilization on the mechanical properties of the meshes (Table 3.1). The superhydrophilic composition with 20 wt% of F127 was chosen and compared with pure SEBS. The mechanical performance is similar to pure SEBS, with an elongation at break greater than 300% (experimental limit). It is worth noting that these measurements for tensile properties are mainly qualitative, and were performed for the sake of comparison. The results show that there was no deterioration of mechanical properties upon the addition of 20 wt% of F127.

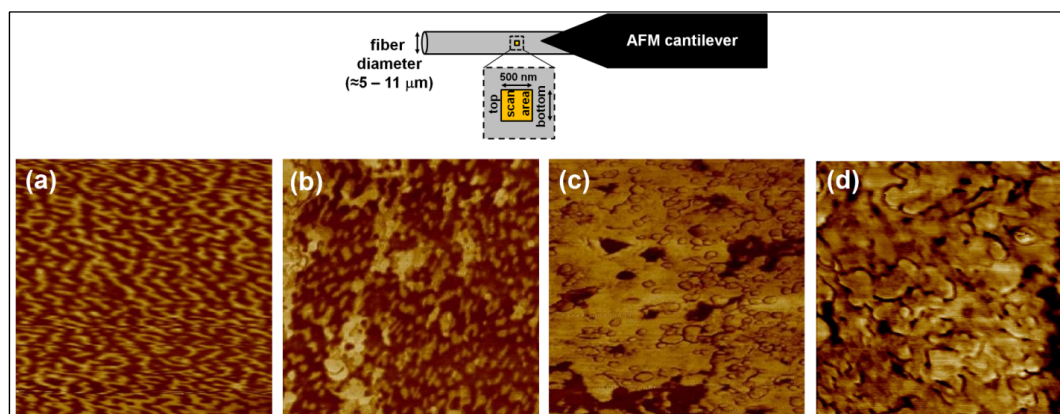


Figure 3.8 – AFM experimental scheme for electrospun fibers with a scan area of 500nmX500nm; (a-d) Phase images of (a) Pure SEBS, (b) region 1 of SEBS/F127\_15, (c) region 2 of SEBS/F127\_15, and (d) SEBS/F127\_20.

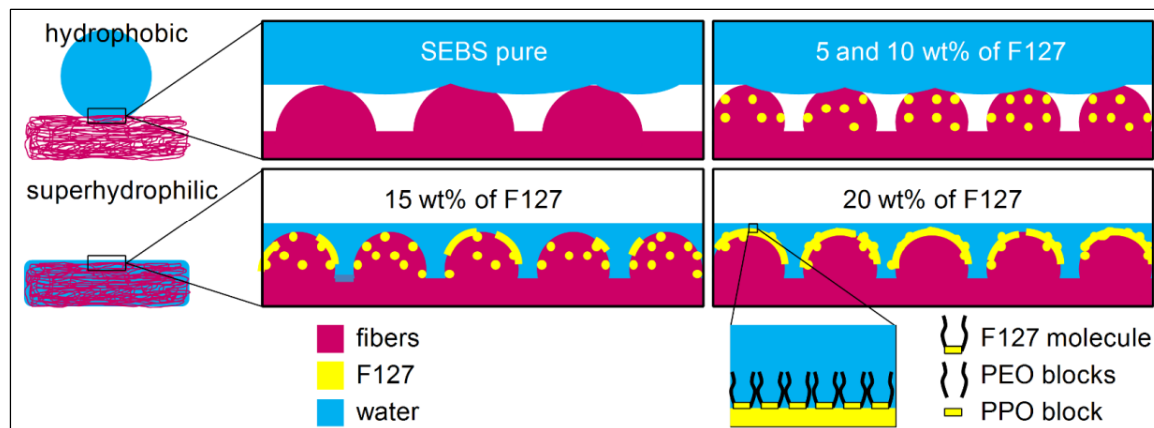


Figure 3.9 – Schematic simplified illustrations of a water drop in contact with electrospun mats for the hydrophobic and superhydrophilic compositions.

Table 3.1 - Mechanical properties of electrospun mats

Composition	Tensile Strength (MPa)	Elongation at break (%)
SEBS	$0.88 \pm 0,10$	> 300
SEBS/F127 (80/20)	$0.85 \pm 0,10$	> 300

### 3.4 Conclusions

Electrospun SEBS mats were highly hydrophobic and flexible. By blending SEBS with 20 wt% of amphiphilic polymer Pluronic F127, it was possible to obtain superhydrophilic mats and maintain mechanical flexibility. Surface chemical composition results revealed a major segregation of F127 to the surface of the fibers, but this could not fully explain the differences in wetting behavior observed among the mats.

Identical solutions were used to produce dip-coated films. The SEBS/F127 system went through a change in morphology when the concentration reached 20 wt% of F127, from a typical dispersed phase to a grain-like structure homogeneously distributed across the film. A particular micellar structure combining F127 and SEBS must have been formed for this composition. The results for electrospun fibers also suggested that the same switch in

morphology occurred, leading to a much more homogenous superhydrophilicity. Complex mixtures of copolymers and solvents may present unique morphologies in their phase diagrams, and therefore an analysis of these features can lead to a better choice of composition and processing conditions for a desired dispersion or property.

Unlike classical polymer processing techniques that produce blends with morphological features (e.g. size of the dispersed phase) in the range of micrometers, electrospinning fibers have diameters generally varying from hundreds of nanometers to a few micrometers, bringing the dispersion of two immiscible polymers to a different order of magnitude. The effect could enhance the property synergy between the two polymers.

### **3.5 Acknowledgements**

The authors wish to thank the Natural Sciences and Engineering Research Council of Canada (NSERC) and ÉTS Montreal for their financial support, and professors Sophie Lerouge, Sylvain Cloutier and Vladimir Brailovski from ÉTS Montreal for allowing us to perform contact angle and dip-coating experiments.



## CHAPTER 4

### WETTING OF HYDROPHILIC ELECTROSPUN MATS PRODUCED BY BLENDING SEBS WITH PEO-PPO-PEO COPOLYMERS OF DIFFERENT MOLECULAR WEIGHT

Rafael S. Kurusu, Nicole R. Demarquette\*

\*Mechanical Engineering Department, École de technologie supérieure - ÉTS, 1100 Notre-Dame Street West, Montréal, Québec – Canada H3C 1K3

This paper has been published in *Langmuir*, 2016, 32(7), pp 1846–1853

**ABSTRACT:** The interaction of electrospun mats with water is critical for many possible applications, and the water contact angle on the surface is the parameter usually measured to characterize wetting. Although useful for hydrophobic surfaces, this approach is limited for hydrophilic mats, where wicking has also to be considered. In this case, it is still unclear how the fiber surface chemical composition and morphology will affect the wetting behavior of electrospun mats. In this work, wetting was studied with different hydrophilic membranes produced by blending thermoplastic elastomer SEBS with amphiphilic PEO-PPO-PEO molecules. Three different types of PEO-PPO-PEO, with different molar masses, PEO content and physical form were used. The effect of these differences on the wetting behavior of the electrospun mats was evaluated by contact angle goniometry, wicking measurements and different imaging techniques. X-ray photoelectron spectroscopy was used to characterize the surface chemical composition. The smaller molecules quickly saturated the surface at low concentrations, making the mats hydrophilic. The sheath of PEO-PPO-PEO also resulted in fast absorption of water, when comparing the saturated and non-saturated surfaces. Longer PEO chain-ends seemed to hinder complete segregation and also led to a higher activation time when in contact with water. Liquid PEO-PPO-PEO was easily leached by water.

## 4.1 Introduction

High surface area is one of the main features of electrospun mats and therefore understanding and controlling their surface properties is critical. Water wetting, for example, will help defining the performance of mats for several possible applications where there is interaction with aqueous solutions, such as separation and filtration membranes or scaffolds for tissue engineering (Hutmacher, 2000; Wu et al., 2013; Xue et al., 2014).

Electrospun mats are generally classified as hydrophobic or hydrophilic. In the case of many polymers (De Schoenmaker, Van der Schueren, De Vrieze, Westbroek, & De Clerck, 2011; Hwa Hong & Jin Kang, 2006; Khatri, Wei, Kim, & Kim, 2012; H. Liu & Hsieh, 2002), the mats produced by electrospinning are hydrophobic and need to undergo a post-treatment in order to present hydrophilicity. This can be achieved by hydrolysis (Khatri et al., 2012; H. Liu & Hsieh, 2002), plasma (Savoji et al., 2015), immersion precipitation (W. J. Cho et al., 2009), etc., but this adds time and cost. Another approach is to use polymer blending to incorporate hydrophilic (G. Li et al., 2013) or amphiphilic (N.-h. Liu et al., 2014; Vasita et al., 2010) polymers in the hydrophobic matrix to alter the surface properties of the fibers. Previously (Rafael S. Kurusu & Demarquette, 2015), we have shown that mats of elastomeric poly(styrene)-*b*-poly(ethylene-butylene)-*b*-poly(styrene) (SEBS) could be hydrophilized by blending it with amphiphilic poly(ethylene oxide)-*b*-poly(propylene oxide)-*b*-poly(ethylene oxide) (PEO-PPO-PEO). Not only the chemical composition but also the blend morphology was important to produce a homogeneously hydrophilic mat. The low surface energy PPO midblock tends to segregate to the surface and drag the hydrophilic PEO groups. When in contact with an aqueous medium, the hydrophilic PEO segments will extend and the surface will become hydrophilic (Shi et al., 2008). There exist other examples in literature where PEO-PPO-PEO polymers have been successfully used to modify the wettability of the electrospun mats (N.-h. Liu et al., 2014; Vasita et al., 2010), but to our knowledge the characterization of wetting was based only in static contact angle measurements.

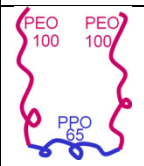
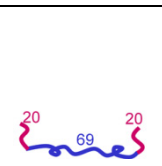
In the hydrophobic case, electrospun mats can be seen as a rough surface, and many papers in the literature have discussed the reasons and definitions for hydrophobicity based on contact angle measurements and wetting theories (Callies & Quere, 2005; Öner & McCarthy, 2000). In the hydrophilic case, however, electrospun mats cannot be seen only as a rough surface, but also as a porous material subject to absorption by capillary action (wicking). So to better understand the wetting behavior of hydrophilic electrospun mats, not only contact angle but also wicking measurements have to be analyzed. The latter have been used to determine the contact angle of electrospun mats indirectly (H. Liu & Hsieh, 2002), or to compare the wicking rate of spunbond and electrospun fibers (Hwa Hong & Jin Kang, 2006), mats of the same polymer with different fiber diameter (De Schoenmaker et al., 2011) or mats containing two types of fibers independently co-electrospun (Khatri et al., 2012). Another way used to characterize the dynamics of wetting is the observation of the spontaneous spreading or impact of droplets (Clarke, Blake, Carruthers, & Woodward, 2002; Seveno, Ledauphin, Martic, Voué, & De Coninck, 2002), which can also be important for applications in humid conditions or related to the deposition of aqueous fluids. However, it is still unclear how the fiber surface chemistry and morphology will affect wetting of electrospun mats.

Since there are many different grades of PEO-PPO-PEO copolymers commercially available, combining hydrophilization by blending with different types of PEO-PPO-PEO and analyzing contact angle, wicking rate, spreading and impact of water on the mats can give new information about the role of fiber surface composition and morphology on the wetting behavior of electrospun mats. In this work, SEBS/PEO-PPO-PEO mats were produced by electrospinning with three types of PEO-PPO-PEO molecules having different molar masses, PEO content and physical form (one is a solid polymer, the other a paste-like material and the last one a viscous liquid). The effect of these differences on the wetting behavior of the mats was evaluated by contact angle, wicking measurements and imaging techniques. Surface chemical composition and both mat and fiber morphology were also characterized.

## 4.2 Experimental

Linear triblock copolymer SEBS (G1652) with 79 000 g/mol of average molecular weight and 30 wt% of styrene blocks was kindly supplied by Kraton. PEO-PPO-PEO copolymers (Pluronic<sup>®</sup>) were purchased from Sigma Aldrich. Chloroform and toluene were purchased from Fisher Scientific. Three types of PEO-PPO-PEO copolymers were used: Pluronic<sup>®</sup> F127, Pluronic<sup>®</sup> P123 and Pluronic<sup>®</sup> L61, each with different molecular weight and PEO content. The main characteristics are presented in Table 4.1 with a visual comparison using an arbitrary scale of the difference in length and PEO content in each polymer with the respective number of EO and PO repeat units.

Table 4.1 - Main features of the PEO-PPO-PEO copolymers used in the present study

Polymer	F127	P123	L61
Molecular weight (g/mol)	12 600	5 800	2 000
wt% of PEO	73.2	30.0	10.0
Physical form	Flakes	Paste	Liquid
Comparative sketch			

The polymers were weighed and mixed with chloroform and toluene (80/20 wt%) using a magnetic stirrer for 15 minutes until a homogeneous solution was obtained. The final polymer concentration for all solutions was 15 wt%. Four compositions of SEBS/PEO-PPO-PEO with 5, 10, 15 and 20 wt% of each PEO-PPO-PEO were prepared and named as F127\_x, P123\_x and L61\_x, where x is the wt% of PEO-PPO-PEO.

Electrospinning was performed with 10 ml syringes, 21G needles, voltage of 15 kV, distance to collector of 15 cm and flow rate of 2 mL/h. All the tests were performed at room temperature and 30 % of relative humidity.

Water contact angle measurements were performed with a VCA Optima (AST products, Inc.) and Milli-Q<sup>®</sup> ultrapure water. Mat strips were attached to glass slides to maintain a horizontal surface. Each blend was tested five times in different regions of the mats.

For the wicking measurements, ultrapure water was dyed with methylene blue and poured in a beaker. Mat strips with 20 mm of height, 10 mm of width and 150-200  $\mu\text{m}$  of thickness were attached to a polyethylene tab containing a millimetric scale. The tab was lowered until the solution touched the mat and the water started to rise by capillary action. All the process was recorded with a Canon T4i at thirty frames per second. The time to reach each millimeter in the scale was then plotted in a height vs. time graph. Three samples of each composition were tested.

Optical microscopy was performed with an Olympus BX51 with magnification up to 1000 $\times$  to observe the fiber morphology and leaching. Scanning electron microscopy (SEM) was used to observe both the mat morphology (fiber diameter and shape) and fiber surface morphology. The experiments were performed with a S3600N microscope (Hitachi) at 5kV in secondary electrons mode. The samples were previously coated with platinum using a Q150T S (Quorum Technologies) sputter coater. High-speed images of wetting were obtained using a Fastcam SA1 Camera (Photron Ltd, Tokyo, Japan) working at 500 to 2000 frames per second depending on the absorption velocity of each sample. This technique was used to analyze the dynamics of spreading and impact of water drops on the mat surfaces. All images were analyzed using ImageJ and the plugin DiameterJ (Hotaling, Bharti, Kriel, & Simon Jr, 2015) for measurements.

The surface chemical composition of the samples was measured by X-ray Photoelectron Spectroscopy (XPS) using an ESCALAB 3 MKII with a Mg K $\alpha$  source and 216W (12 kV, 18 mA) of power. An area of 2 mm  $\times$  3 mm was analyzed for each sample, with a depth of analysis of 50 - 100  $\text{\AA}$ .

### 4.3 Results and discussion

Figure 4.1 shows the water contact angle results for each blend as a function of PEO-PPO-PEO bulk content for the three types of PEO-PPO-PEO (F127, P123 and L61). Pure SEBS mats were hydrophobic with contact angle of  $139 \pm 2^\circ$ . For the blends containing F127, the hydrophilization (absorption resulting in contact angle of  $0^\circ$ ) was achieved at 15 wt% of PEO-PPO-PEO, but only the composition with 20 wt% presented a homogeneous hydrophilicity in all regions of the mat. The addition of 5 wt% P123 or L61 was enough to hydrophilize the mats. Blends with only 1 wt% of P123 and L61 were later prepared, producing hydrophobic mats with contact angle closer to pure SEBS ( $\approx 140^\circ$ ).

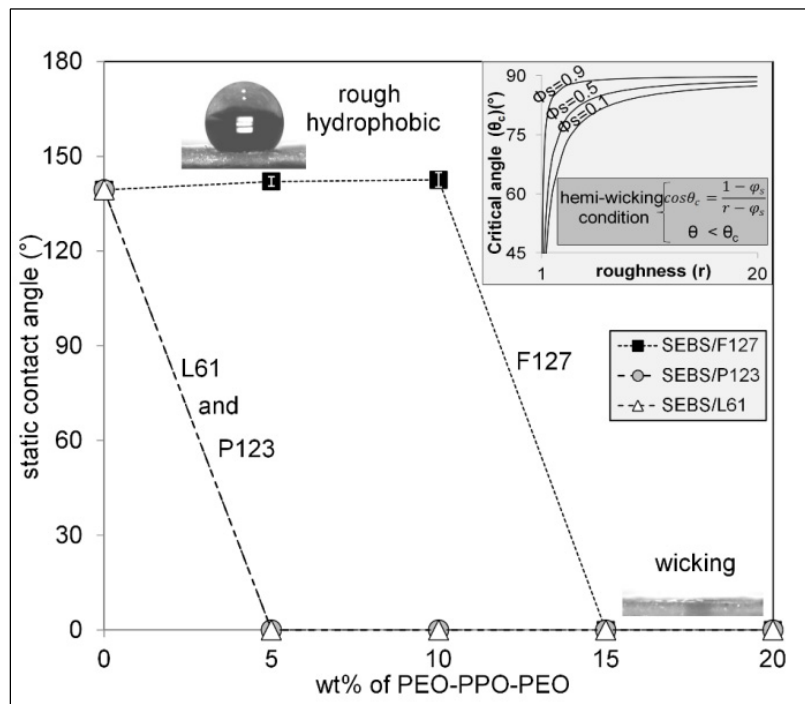


Figure 4.1 – Water contact angle results for all electrospun mats as a function of PEO-PPO-PEO content. The insert is a plot of the hemi-wicking condition (J. Bico et al., 2001), the critical contact angle  $\theta_c$  as a function of roughness  $r$  for different values of solid/liquid interface fraction ( $\phi_s$ ).

The condition for wicking in a perfect capillary is that the surface energy between the solid and the liquid ( $\gamma_{SL}$ ) must be smaller than the surface energy between the solid and the air/vapour ( $\gamma_{SV}$ ). Using the equilibrium contact angle  $\theta_E$  of the Young's equation ( $\gamma_{SV} - \gamma_{SL} = \gamma_{LV} \cos \theta_E$ ), which describes the balance of energies for a drop of liquid deposited in a perfectly flat surface, the condition for wicking may be written as (Ishino, Reyssat, Reyssat, Okumura, & Quéré, 2007)  $\theta_E < 90^\circ$  that gives  $\gamma_{SV} - \gamma_{SL} > 0$ .

Electrospun mats can be considered as non-perfect porous structures in which the solid/vapour interface will not be ideally replaced by a solid/liquid interface, leaving some dry islands. The condition for wicking or hemi-wicking can be described as (J. Bico et al., 2001):

$$\theta_E < \theta_c \text{ and } \cos \theta_c = \frac{1 - \varphi_s}{r - \varphi_s} \quad (4.1)$$

where  $r$  is the roughness (ratio of the real area to the projected area),  $\varphi_s$  is the fraction of the solid/liquid interface below the drop,  $\theta_E$  is again the equilibrium contact angle on an ideal flat surface with the same chemical composition of the rough surface and  $\theta_c$  is the critical contact angle that will define the start of the imbibition (J. Bico et al., 2001). For a perfect porous material ( $r \rightarrow \infty$  and therefore  $\cos \theta_c \rightarrow 0$ ), wicking will occur again for  $\theta_E < 90^\circ$  and, if this condition is fulfilled, the final apparent contact angle will be  $0^\circ$ . Considering that electrospun mats are porous materials with high values of roughness, the condition for imbibition is easily achieved, and for any value of  $\varphi_s$ ,  $\theta_c$  tends to be close to  $90^\circ$ , as shown in the insert in Figure 4.1. This explains the recurrent switch (ON/OFF) mechanism found for the contact angle of electrospun mats, from hydrophobic or superhydrophobic rough surfaces with high contact angle values to superhydrophilic absorbing porous structures with contact angle zero (Dufficy et al., 2015; C. H. Kim et al., 2006; G. Li et al., 2013; Valiquette & Pellerin, 2011; Vasita et al., 2010).

Mats that present values of contact angle smaller than  $90^\circ$  but higher than  $0^\circ$  can be a result of: non-uniform chemical composition, with hydrophobic regions unevenly mixed with hydrophilic regions; small mat thickness with insufficient pore volume to absorb the droplet; measurement at different times, as some mats present a slow wicking rate until the contact angle reaches zero. The contact angle right after the droplet deposition may be different from zero and then reach zero after a time interval (Vasita et al., 2010). In the case of this work, the absorption occurred rapidly after the drop deposition.

The contact angle measurement was useful to determine the effectiveness of the hydrophilization treatment chosen, i.e., blending with PEO-PPO-PEO molecules, but it did not allow a comparison between the different hydrophilic compositions. To investigate the dynamics of spreading and imbibition from the moment the drop touched the mat until it was completely absorbed, high-speed imaging was used (Figure 4.2). Four compositions were chosen for clarity and because they summarize the main trends observed. The evolution of the contact angle  $\theta$  of the droplet on the surface was observed as a function of time (Figure 4.2a). Upon contact, all mats presented contact angles around  $140^\circ$ , which is similar to the values obtained for pure SEBS and for the hydrophobic blends. Given the difference in time scale for the complete absorption, the curve for the F127\_20 mat was included as an insert. Contact angle values decreased with a higher rate until around 800 milliseconds (0.8 seconds) for the F127\_20 and around 50 milliseconds (0.05 seconds) for the P123\_20, L61\_5 and L61\_20. A second regime with a lower decrease rate took place after that, at around  $20-30^\circ$ , for all the mats. The contact angle continued to decline until complete absorption of the droplet at around 2000 milliseconds (2 seconds) for the F127\_20, 200 milliseconds for the P123\_20 and 80-90 milliseconds for the blends with L61, which presented similar behavior for all parameters. Besides the differences in order of magnitude the spreading behavior was analogous for the mats tested.

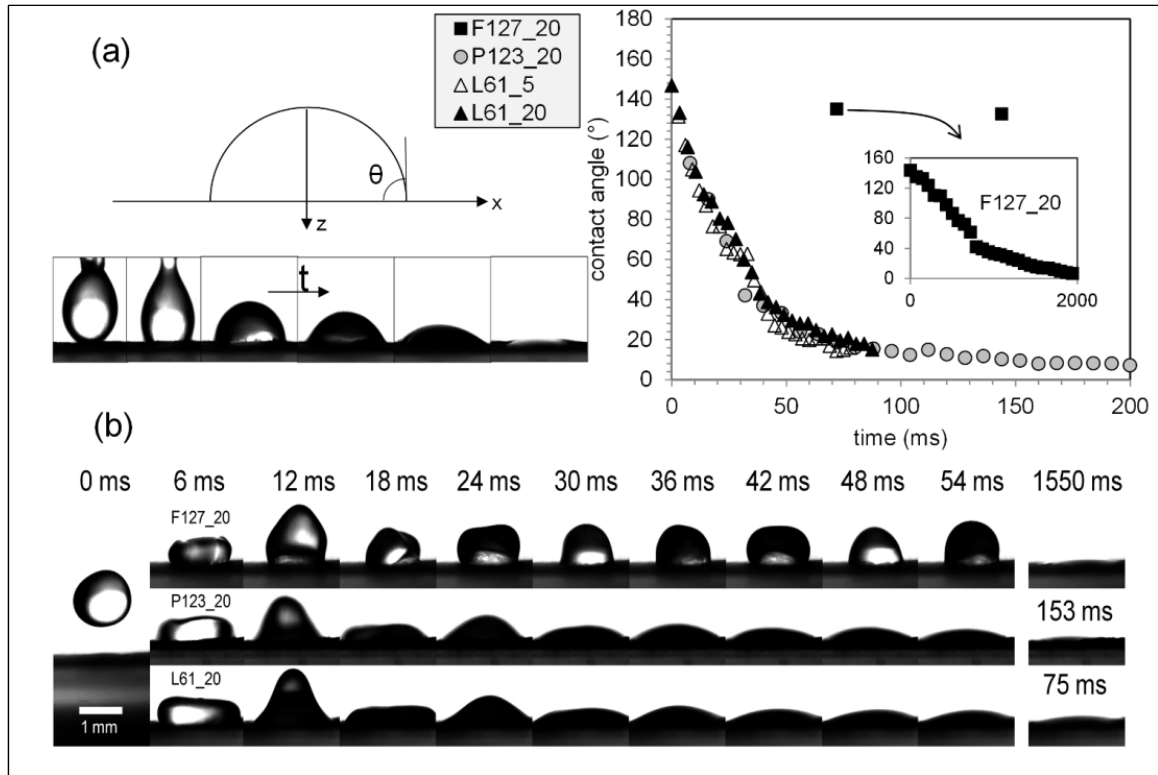


Figure 4.2 – (a) spreading and imbibition experiments methodology and results for the contact angle  $\theta$  as a function of time; (b) drop impact images showing the last frame before impact as the first image and the total time for absorption as the final image for F127\_20, P123\_20 and L61\_20 (top to bottom).

The differences in drop absorption between F127\_20, P123\_20 and L61\_20 were also observed in drop impact experiments (Figure 4.2b). For the F127\_20 mat, there was no apparent change in volume and contact angle in the early stages after the impact, and droplet moved up and down for a longer time without bouncing. In the case of P123\_20 and L61\_20, the droplet adhered and moved on the surfaces while it was rapidly absorbed. As concluded by the spreading experiments, there was a drastic difference between the behavior of F127\_20 and the P123\_20 and L61\_20. Also, the impact reduced the final absorption time by about 20 %. The pictures presented in Figure 4.2b also show that in all cases the drop adhered to the surface and no splashing was observed.

One way to predict the impact behavior of a liquid drop on a surface is to calculate the dimensionless Weber number ( $We = \rho r v^2 / \gamma$ ), where  $\rho$  is the liquid density,  $r$  the drop radius,  $v$  its impact velocity and  $\gamma$  the surface tension. A rough evaluation of the Weber number for the present work ( $\rho = 1000 \text{ kg.m}^{-3}$ ,  $r = 650 \text{ }\mu\text{m}$ ,  $v = 0.3 \text{ m.s}^{-1}$  and  $\gamma = 72 \text{ mN.m}^{-1}$ ) leads to  $We = 8.2$ , which is much lower than the splashing thresholds usually reported (Alexandridis & Alan Hatton, 1995; Reyssat, Pépin, Marty, Chen, & Quéré, 2006; Tsai, Pacheco, Pirat, Lefferts, & Lohse, 2009), even considering that the roughness can reduce this limit (Range & Feuillebois, 1998), explaining therefore the absence of splashing in our work. Furthermore, hydrophilic surfaces cause a much stronger viscous dissipation near the moving contact line that slows down the droplet spreading, in contrast to hydrophobic surfaces (Reyssat et al., 2006), which can also contribute to avoid splashing. However, it is worth noting that a small increase in the drop velocity drastically changes the impact behavior, and that even hydrophobic electrospun membranes can be penetrated by water if the velocity is high enough (Lembach et al., 2010; Sahu, Sinha-Ray, Yarin, & Pourdeyhimi, 2012). Lembach et al. (Lembach et al., 2010) also performed drop impact experiments on electrospun mats produced with a partially wettable polymer, and defined a splashing threshold for these mats. To reach this threshold with the mats used in the present work, a velocity of 2.7 m/s would be necessary (much higher than the one used in the present work).

Wicking experiments with mat strips were performed to evaluate another aspect of the wetting behavior (Courbin, Bird, Reyssat, & Stone, 2009) of electrospun materials. The results are presented in Figure 4.3a for the hydrophilic compositions from the moment the dyed water touched the mat until it reached the sample height of 20 mm, as shown by the pictures in Figure 4.3a. Although ultimately hydrophilic in terms of contact angle, the strips of the composition with 15 wt% of F127 presented heterogeneous water rise with time so that the results are not shown here. The dyed water had a preference for the more hydrophilic regions, which were randomly distributed in the mats. Controlling the exact location of hydrophobic and hydrophilic regions could lead to a tailored wicking behavior that could be interesting for applications involving fluid transport.

The wicking rate was clearly smaller for the mat with 20 wt% of F127, and the time to reach the maximum height was about 17 seconds. All the mats with P123 quickly absorbed water with a total time between 5 and 8 seconds. The wicking rate for the mats with L61 was even higher with total time between 4 and 6 seconds to reach the maximum height.

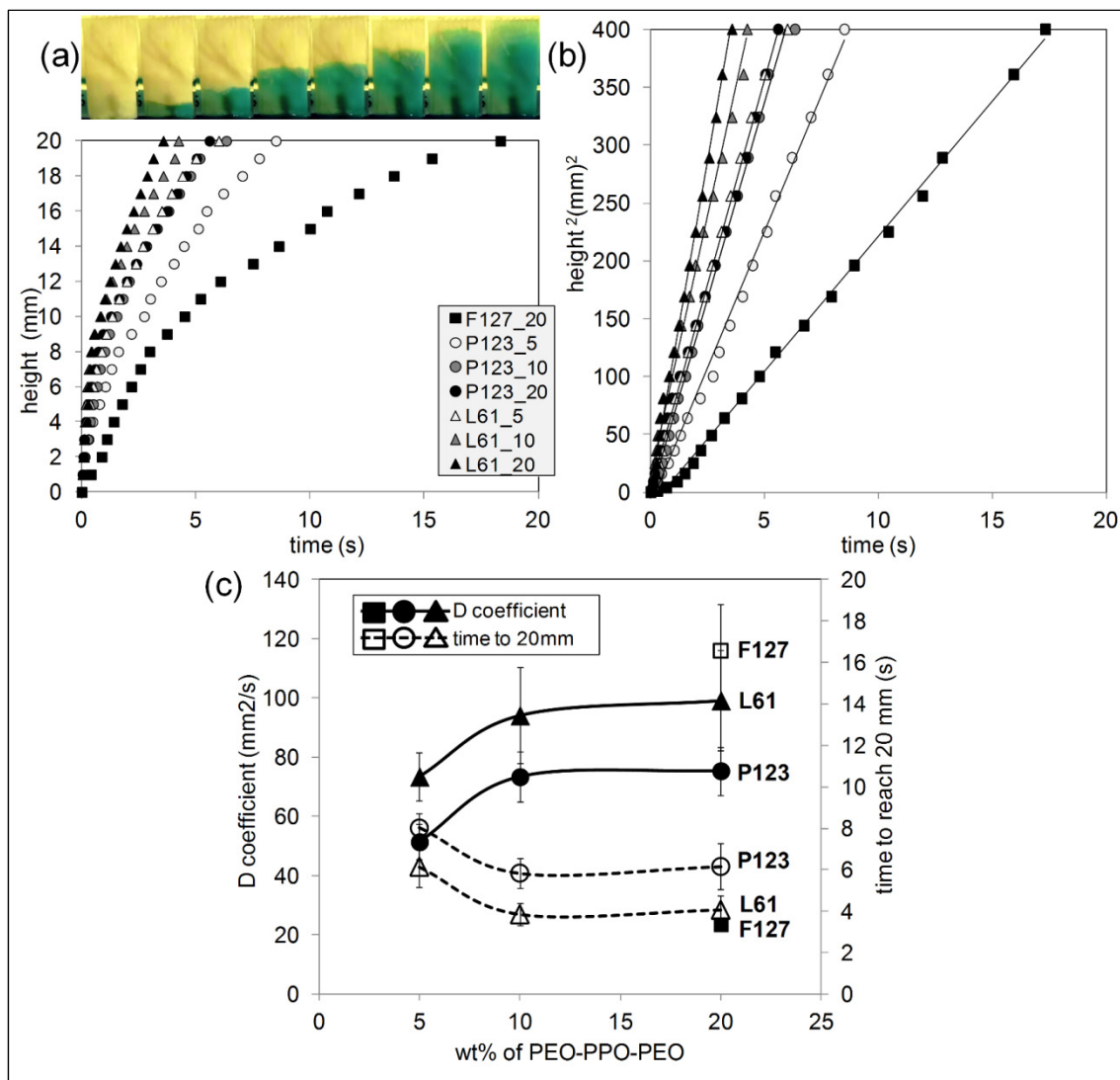


Figure 4.3 – Results for the wicking measurements: (a) example of the experiments pictures and the results for height as a function of time; (b) the square of height ( $h^2$ ) versus time; (c) Diffusion coefficient  $D$  and total time to reach the maximum height as a function of PEO-PPO-PEO content.

Porous materials like electrospun mats can exhibit classical wicking dynamics analogous to what was described by Washburn (Washburn, 1921) considering a porous structure as a series of  $n$  cylindrical capillaries with an equivalent radius of the capillary structure  $r$ . Neglecting the hydrostatic pressure, the relation between the height  $h$  and time  $t$  can be described as (Ferrero, 2003):

$$h^2 = \left( \frac{r \cdot \cos\theta_E}{2} \right) \cdot \left( \frac{\gamma}{\eta} \right) \cdot t \quad (4.2)$$

where  $\gamma$  and  $\eta$  correspond to the surface tension and viscosity of the liquid. The rise of liquid in a capillary then takes the form:

$$h^2 = D \cdot t \quad (4.3)$$

where  $D$  is a diffusion coefficient based on fluid properties and capillary geometry, and the square of the height varies linearly with time. Figure 4.3b shows that the equation fitted well to the wicking behavior of electrospun mats considering the whole experiment, as previously reported (De Schoenmaker et al., 2011; Hwa Hong & Jin Kang, 2006). The differences in wicking rate described before are easier to observe.

Figure 4.3c presents the  $D$  coefficient and time to reach the maximum height as a function of PEO-PPO-PEO content for all the compositions and samples tested. The time to reach the maximum height of 20 mm, a parameter used in many wicking standards, decreased with higher PEO-PPO-PEO content, but reached a plateau around 10 wt%. The  $D$  coefficient followed the inverse trend, increasing with PEO-PPO-PEO content, but also stabilizing after 10 wt%.

Since  $D = (r \cdot \cos\theta_E/2) \cdot (\gamma/\eta)$  and only water was used in the experiments (constant  $\gamma$  and  $\eta$ ), any difference in the wetting behavior comes from differences on the porous structure or the surface chemical composition.

The main structure parameters that will affect wicking in a simplified electrospun mat (Insert in Figure 4.4b) are the fiber diameter  $d$  and the distance between fibers  $f$ , which will influence pore (capillary) size. SEM images for some of the samples are presented in Figure 4.4a, showing that all compositions produced homogeneous fibers with the exception of P123\_20, which presented fibers with varying diameter, and L61\_20, which presented broken fibers. Fiber diameter decreased drastically with the incorporation of 5 wt% of all three types of PEO-PPO-PEO molecules, and remained stable until the maximum concentration of 20wt% (Figure 4.4b) The only exceptions are again P123\_20 and L61 20, which presented an increase in the average diameter (Figure 4.4b). The higher amount of PEO-PPO-PEO started to disrupt the electrospinning process in these two cases. Image analysis was performed to calculate the distance between fibers and the pore size of the mats, but the data (not presented here) revealed, as expected, a great variation since the mats are composed of randomly oriented fibers. However, it is known that mats containing fibers of smaller diameter have smaller pores (Lowery et al., 2010), so that one could expect smaller pores for the blends containing F127 and therefore smaller capillaries that would increase the wicking rate, but that was not observed. The total porosity value taken from immersion experiments in ethanol revealed similar values for all mats (around 75%). Therefore, based on this simple analysis, there is no apparent correlation between geometry and the wetting behavior of the mats.

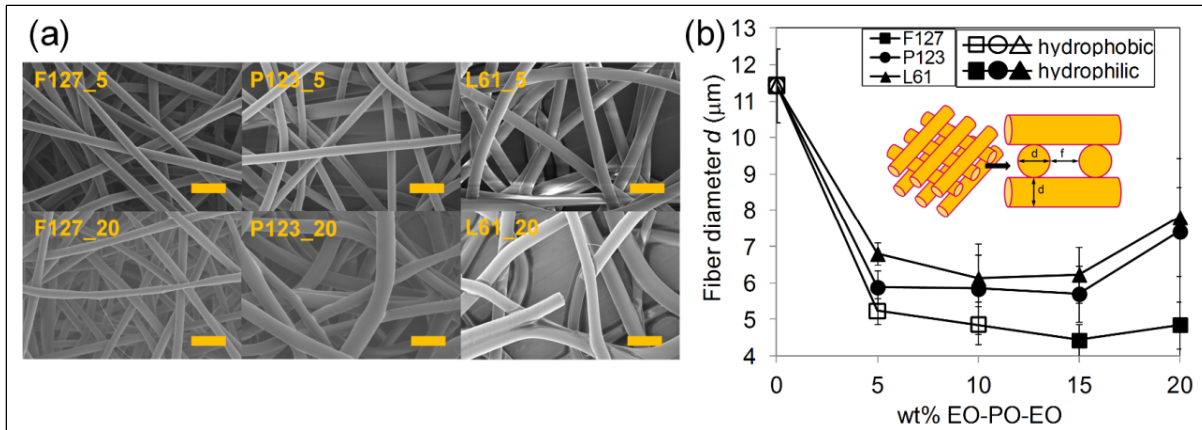


Figure 4.4 – (a) SEM micrographs of the samples containing 5 and 20 wt% of PEO-PPO-PEO (scale bar = 20  $\mu\text{m}$ ) and (b) the results of fiber diameter as a function of PEO-PPO-PEO content for all samples.

The chemical composition at the very top surface of the mats, measured by XPS, is presented in Figure 4.5. Since only the PEO-PPO-PEO molecules have oxygen, the atomic percentage of this element can tell whether the surface is enriched with this polymer or not. Figure 4.5a shows the XPS survey spectra for pure SEBS, the three blends containing 20 wt% of PEO-PPO-PEO and a film of pure PEO-PPO-PEO (P123). The small oxygen peak in the spectrum of pure SEBS, combined with a small silicon peak, appeared possibly due to a small amount of silicone oils that can be found in some commercial polymers. The spectra for P123\_20, L61\_20 and pure PEO-PPO-PEO (P123) presented similar proportion between carbon and oxygen peaks, although the sample for pure PEO-PPO-PEO was a film, since it is not electrospinnable. The curves in Figure 4.5b show the atomic percentage of oxygen for each composition. From bottom to top, the straight lines without markers show the theoretical amount of oxygen expected according to the bulk compositions and the theoretical amount of oxygen in pure L61, P123 and F127, respectively. All compositions presented surface enrichment with PEO-PPO-PEO, which confirms that there was segregation of these molecules. For the blends with F127 there was a gradual increase in the amount of oxygen according to the composition. Blends with P123 showed an instant high amount of oxygen at 5 wt% of P123, similar to the blend with 20 wt% of F127. From 10 until 20 wt% of P123, the surface is practically saturated (91 to 100 wt%) with PEO-PPO-PEO molecules. When L61

was used as the second phase, all compositions tested presented completely coverage with the amphiphilic molecule.

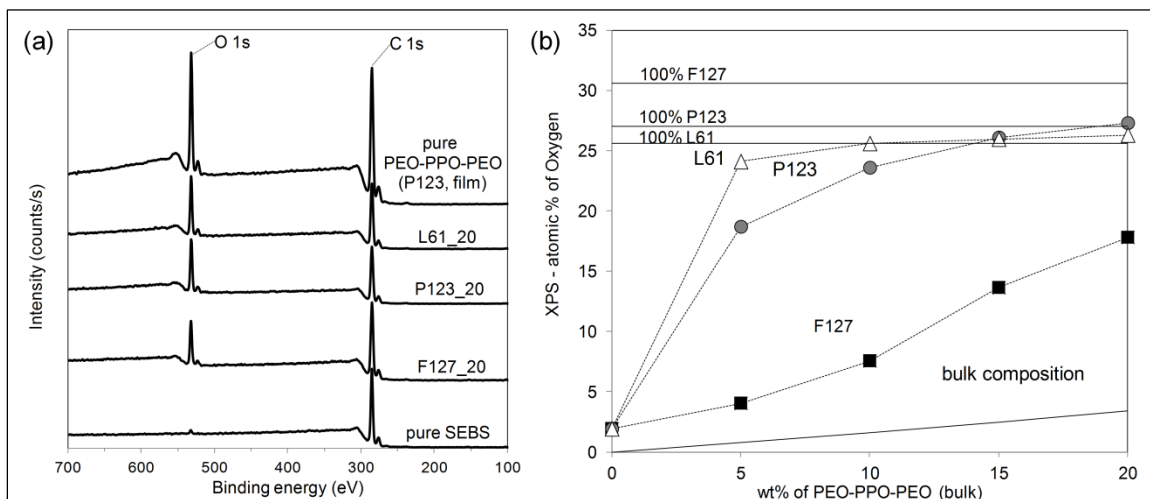


Figure 4.5 – (a) X-ray photoelectron spectroscopy (XPS) survey spectra for pure SEBS, F127\_20, P123\_20, L61\_20 and pure PEO-PPO-PEO; (b) XPS results of the atomic percentage of oxygen as a function of blend bulk composition. The straight lines are theoretical values based on the chemical structure of each molecule.

The results show that the amount of PEO-PPO-PEO needed to achieve surface coverage and the consequent changes in surface properties is smaller for the molecules with lower molecular weight. Surface hydrophilization depends on the extension of PEO chain ends of each molecule when the surface is in contact with water. The length of PEO chain ends of the three PEO-PPO-PEO molecules chosen for this study varies greatly: F127 (PEO<sub>100</sub>-PPO<sub>65</sub>-PEO<sub>100</sub>) has approximately 100 EO units in each side of the molecule, while P123 (PEO<sub>20</sub>-PPO<sub>69</sub>-PEO<sub>20</sub>) and L61 (PEO<sub>2</sub>-PPO<sub>30</sub>-PEO<sub>2</sub>) have in average 20 and 2 units of EO in each PEO block, respectively (Kabanov, Batrakova, & Alakhov, 2002). The blends F127\_20 and P123\_5 have similar chemical compositions, but remarkably different wicking behavior, which indicate that the shorter PEO chains are activated faster in P123. An analogous behavior is observed when comparing the blends with saturated surfaces. The compositions

with L61 molecules showed a faster wicking than the membranes containing P123 molecules (Figure 4.3). A plot of the time to reach the maximum height in the wicking experiments as a function of PEO length in each chain end (Figure 4.6) shows that wicking rate increased with decreasing PEO length. Furthermore, for each molecule of F127 with two PEO chain-ends, there are approximately two times more P123 molecules and six times more L61 molecules, considering the same mass of polymer used.

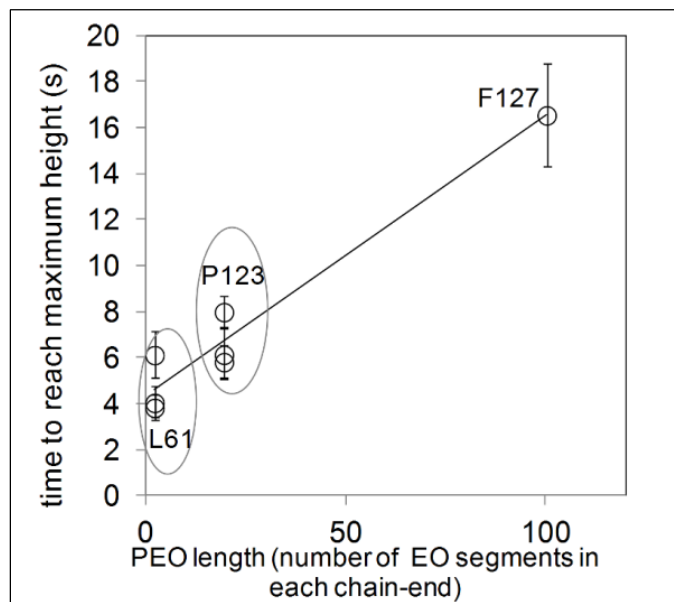


Figure 4.6 – Wicking results as a function of the number of EO segments in each side of the PEO-PPO-PEO molecules.

Besides the idea of a longer time to extend and hydrophilize the surface, another possible explanation is that the longer PEO chain-ends, like in F127, hindered the segregation of the molecule. Both arguments are plausible when comparing F127\_20 and P123\_5, blends with similar surface chemical composition and PPO-block length. The wicking rate was higher for P123\_5, indicating faster activation, but the amount of PEO-PPO-PEO (bulk composition) in this blend is much smaller than in F127\_20, indicating faster segregation.

Results above showed that SEBS electrospun fibers blended with PEO-PPO-PEO molecules presented graded morphology with a PEO-PPO-PEO-rich surface, resulting in mat hydrophilization. Smaller PEO-PPO-PEO molecules seem to be more effective to generate faster water absorption even though the order of molecular hydrophilicity (proportion of PEO) is F127>P123>L61.

Once the surface is saturated, the compositions with higher concentrations will tend to have a thicker surface layer of PEO-PPO-PEO, which can contribute to fast interaction with water. But this thicker layer can also be more easily removed or leached by water. In the particular case of SEBS/L61 fibers, a liquid residue was observed whenever the mats were placed on a glass slide. Leaching of L61\_20 fibers by water was then observed by optical microscopy (Figure 4.7a). When the flow of water passed (arrow in Figure 4.7a), L61 molecules were removed from the fibers surface and formed bubbles in fractions of a second. The wetting behavior of the SEBS/L61 blends with higher concentrations of L61 was mainly a result of a liquid surface exuded from the SEBS matrix. The SEM image of the L61\_20 fibers (Figure 4.7b) also revealed a residue on the substrate after fiber deposition, in addition to broken fibers. Higher concentrations of the smaller molecules of L61 reduced the stability of the jet during electrospinning, leading to fiber breakage in some points due to the electrical forces and bending instabilities.

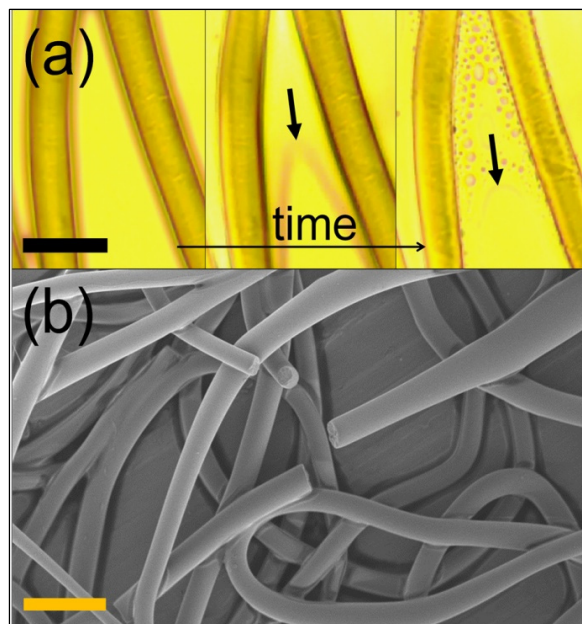


Figure 4.7 – L61\_20 fibers: (a) L61 leaching observed by optical microscopy, in which the arrows indicate the water front advancing direction (scale bar = 10  $\mu\text{m}$ ); (b) SEM image of the same composition showing broken fibers (scale bar = 30  $\mu\text{m}$ ).

Leaching could not be observed for the other compositions with only optical microscopy and static contact angle measurements. Leaching is a problem for applications that demand long-term hydrophilicity, but it can be interesting for other applications where the release of molecules is targeted. A more systematic and detailed study is needed to understand how to control a specific leaching behavior of PEO-PPO-PEO molecules for a given application.

#### 4.4 Conclusions

Electrospun SEBS fibers were successfully hydrophilized by solution blending with amphiphilic PEO-PPO-PEO molecules. During electrospinning and until solvent evaporation these molecules segregated to the surface and completely altered the wetting behavior of the mats. This was confirmed by the chemical composition at the very top surface.

Although superhydrophilic considering only contact angle measurements, a drastic difference in absorption time was noticed. Wicking tests quantified this difference revealing that the PEO-PPO-PEO molecules with smaller molecular weight were more effective, enabling hydrophilization with smaller amount of material incorporated in the SEBS matrix. Moreover, smaller PEO chain-ends seemed to respond more rapidly when in contact with water, resulting in faster wicking. High-speed imaging also reinforced the results.

Liquid PEO-PPO-PEO (L61) is clearly leached from the fibers surface when in contact with water, while the other types of PEO-PPO-PEO molecules (P123 and F127) seemed to produce more robust hydrophilization.

#### **4.5 Acknowledgements**

The authors wish to thank the Natural Sciences and Engineering Research Council of Canada (NSERC), *Fond de recherche du Québec* (FRQ) and *École de Technologie Supérieure* (ÉTS) for financial support and Navid Sharifi and Professor Ali Dolatabadi from Concordia University for the help with high-speed imaging.



## CHAPTER 5

### **SURFACE PROPERTIES EVOLUTION IN ELECTROSPUN POLYMER BLENDS BY SEGREGATION OF HYDROPHILIC OR AMPHIPHILIC MOLECULES**

Rafael S. Kurusu, Nicole R. Demarquette\*

Mechanical Engineering Department, École de technologie supérieure - ÉTS, 1100 Notre-Dame Street West, Montréal, Québec – Canada H3C 1K3

This paper has been submitted to the *European Polymer Journal* on 28/11/2016

**ABSTRACT:** Polymer blending can be used as a one-step surface modification technique to alter the wettability of electrospun mats. In this work, blends of hydrophobic thermoplastic elastomer SEBS with hydrophilic PEO or amphiphilic PEO-PPO-PEO were prepared and the resulting surface properties investigated. The presence of the low surface energy PPO block drove the segregation of the amphiphilic polymer and hydrophilization was achieved in aqueous medium. Surprisingly, surface segregation continued at room temperature during weeks after processing. The expected equilibrium morphology is discussed to explain the aging results. In addition, the effect of different matrices on the mobility of the amphiphilic molecules was analyzed by comparing the segregation of PEO-PPO-PEO in rubbery SEBS and rigid PS. The low glass transition temperature of SEBS increased the free volume at room temperature and facilitated the segregation.

#### **5.1 Introduction**

Surface modification of polymers is especially interesting for structures with high surface area-to-volume ratio such as electrospun mats, allowing the adjustment of surface properties without compromising the bulk properties. Hydrophilization is one the possible desired outcomes of surface modification, important for applications in which interaction with an

aqueous medium is expected. Examples include hydrophilic tissue engineering scaffolds with enhanced cell attachment and proliferation (Z. Ma, M. Kotaki, T. Yong, et al., 2005), or antifouling hydrophilic surfaces composed of polyethylene oxide (PEO) groups at the surface that can prevent protein adsorption (H. S. Kim et al., 2013).

Many post-electrospinning treatments such as coating or plasma are used for this purpose, not only adding cost and time but sometimes failing to produce a homogeneous treatment on deeper fiber layers (Savoji et al., 2015). Alternatively, the addition of nanoparticles or second polymer (by blending) to the electrospinning solution can alter the surface properties of the fibers before the deposition and therefore result in a more homogeneous surface treatment throughout the nonwoven mat produced. Blending, in particular, established as a way to change bulk properties, can also be used as a surface modification technique considering that the blend morphology at the surface can be different from the bulk (Geoghegan & Krausch, 2003).

To achieve hydrophilization by blending two alternatives are possible: mixing the hydrophobic matrix with either a hydrophilic or an amphiphilic polymer (Toncheva et al., 2016). Examples of the former include blends with poly(vinyl alcohol) (PVA) (B. Duan et al., 2006; C. H. Kim et al., 2006; G. Li et al., 2013; W. Zhang et al., 2007), poly(vinyl methyl ether) (PVME) (Valiquette & Pellerin, 2011) or poly(glycolic acid) (PGA) (Aghdam et al., 2012), while examples of the latter can be found in recent studies about the hydrophilization of different hydrophobic polymers with the amphiphilic block copolymer poly(ethylene oxide)-b-poly(propylene oxide)-b-poly(ethylene oxide) (PEO-PPO-PEO) with great surface segregation (Rafael S. Kurusu & Demarquette, 2015, 2016; Vasita et al., 2010).

However, it is still unclear how the morphology of these electrospun blends evolves and if the surface modification is achieved only through the segregation of phase-separated structures, like droplets, or also by isolated molecules. Some immiscible blends can present a complete wetting layer as the equilibrium morphology, for example, while the surface of miscible blends can be enriched with the modifying molecules. Energy effects play a major

role on surface segregation during blending: the component with low surface energy will tend to segregate to the solid/air surface while higher surface energy components will tend to be immersed in the matrix (Morita, Kawakatsu, & Doi, 2001; Rezaei Kolahchi, Ajjji, & Carreau, 2014). From this perspective, hydrophilic polymers like polyethylene oxide (PEO) are not a good choice due to their high surface energy that hinders segregation. Annealing in an aqueous environment can help the segregation of hydrophilic polymers (Rodriguez-Hernandez, Ibarboure, & Papon, 2011). In the case of amphiphilic molecules like PEO-PPO-PEO block copolymers, the idea is that the lower surface energy block (PPO) will segregate to the air surface and drag the hydrophilic blocks (PEO), which will hydrophilize the surface once a contact with an aqueous medium is established (J. H. Lee et al., 2000; Y.-q. Wang et al., 2005; L.-P. Zhu et al., 2008). Still, some studies revealed that entropic factors related to the molecular weight of the blended polymers may overcome energy factors and favour the segregation of higher energy components to the surface (Rezaei Kolahchi, Ajjji, & Carreau, 2015; Tanaka, Takahara, & Kajiyama, 1998).

In electrospinning, the rapid processing can “freeze” the microstructure in a state out of its thermodynamic equilibrium. A thermal treatment like annealing can resume the blend morphology evolution towards the equilibrium and, like mentioned above, a wetting layer or a more enriched surface may be formed after processing. The concept is that treating the matrix above its glass transition temperature will increase its free volume and the mobility of the second phase with lower surface energy, which may continue to segregate to the surface (Campoy-Quiles et al., 2008; Geoghegan & Krausch, 2003). Another possibility is that the post-processing segregation can occur even at room temperature through longer periods of time. Migration over months of small molecular weight polyethylene glycol (PEG) molecules inside a polyethylene terephthalate (PET) matrix have been reported recently (Rezaei Kolahchi et al., 2015). There are also questions regarding the role of the polymer matrix properties on this post-processing segregation. It is known that films with elastomeric matrices like the copolymer of Styrene-*b*-ethylene-butylene-*b*-styrene (SEBS) presented

enhanced segregation of surface modifying molecules (Sundaram et al., 2011), but no study investigating this effect over time in electrospun mats has been reported so far.

This work aims to understand the morphology evolution of electrospun SEBS blends using both PEO-PPO-PEO and pure PEO as surface modifying polymers. The surface energy and architecture of each molecule are used to explain the final surface morphology, composition and wettability right after electrospinning and after aging at room temperature. A comparison between SEBS and pure PS in respect to their ability to allow segregation is also presented.

## 5.2 Experimental

Thermoplastic elastomer SEBS (grade G1652,  $M_w = 79\,000\text{ g.mol}^{-1}$ ) with 30 wt% of Styrene (S) blocks was kindly supplied by Kraton. Pure polystyrene ( $M_w = 238\,000\text{ g.mol}^{-1}$ ), two types of amphiphilic PEO-PPO-PEO, F127 ( $M_w=12\,600\text{ g.mol}^{-1}$ ) with 73.2 wt% of EO blocks and P123 ( $M_w = 5\,800\text{ g.mol}^{-1}$ ) with 30 wt% of EO blocks, and pure PEO ( $M_w = 12\,000\text{ g.mol}^{-1}$ ) were purchased from Sigma Aldrich. Toluene and Chloroform were purchased from Fisher Scientific.

Solutions with a total polymer concentration of 15 wt% were prepared by dissolving the weighed polymers together in Chloroform/toluene (80/20 wt%) using a magnetic stirrer. The solutions were extracted from the beakers with syringes connected with 14G needles that were later changed to 21G needles used for the electrospinning process. The flow rate of  $2\text{mL.h}^{-1}$  during electrospinning was controlled with a syringe pump (PHD Ultra, Harvard Apparatus) and the voltage applied to the needle, 15 kV, was controlled by a high voltage power supply (SL40\*150, Spellman). A grounded flat collector was placed 15 cm from the needle. Blends of SEBS with either pure PEO or PEO-PPO-PEO (F127 and P123) were prepared and named as PEO\_x, F127\_x or P123\_x, where x is the wt% (5, 10, 15 and 20 wt%) of each polymer in the blends. Higher contents of these polymers caused process disruption due to their relative low molecular weight. Later, blends with PS matrix were prepared using the same parameters with the exception of the flow rate, which was set at  $1\text{ mL.h}^{-1}$ , and total polymer concentration at 20 wt%. Additionally, glass slides were dip-coated

in the solutions of pure polymers using a dip-coater (Dip-Master 50, Chemat Technology) with a residence time of 3 seconds and speed of 10 mm.min<sup>-1</sup> to prepare flat films for the surface tension/energy analysis.

After electrospinning, several 1×1 cm samples were prepared and kept sealed at room temperature for the surface chemical compositions analysis over time. X-ray photoelectron spectroscopy (XPS) was performed to analyze the first 10 nm of the fibers surface using an ESCALAB 3 MKII with a Mg K $\alpha$  source and 216W (12 kV, 18 mA) of power. The mat area analyzed in each sample was 2×3 mm and so the result is an average of all fibers present in this area.

Contact angle measurements were performed with a goniometer (VCA Optima, AST products Inc.) and ultrapure water (Milli-Q<sup>®</sup>) to verify if the electrospun mats were hydrophobic or hydrophilic (absorbing). The contact angles of both formamide and diiodomethane on flat films of the pure polymers were measured for the surface tension calculation using the Owens-Wendt method (Owens & Wendt, 1969; Żenkiewicz, 2007).

Scanning electron microscopy (SEM) was performed to observe both the mat and fibers surface morphology using a SU-8230 microscope (Hitachi) at 5kV in secondary electrons mode. The samples were coated with platinum (Q150T S sputter coater, Quorum Technologies).

### **5.3 Results and discussion**

Figure 5.1 shows the mat morphology of electrospun pure SEBS (Figure 5.1a) and the blends containing the highest concentration (20 wt%) of F127 (Figure 5.1b), P123 (Figure 5.1c) and pure PEO (Figure 5.1d). Pure SEBS presented uniform fibers with diameter around 11  $\mu$ m. The incorporation of each one of the additives helped to reduce the final diameter possibly due to changes in the electrical properties of the solution. F127\_20, P123\_20 and PEO\_20

mats were composed of fibers with an average diameter of around 5, 7, and 6 micrometers, respectively. The presence of 20 wt% of P123, the smallest molecule used in this study ( $M_w = 5\,800\text{ g}\cdot\text{mol}^{-1}$ ), in the solution caused some disruption during electrospinning, producing more fibers with nonuniform diameter and merged contact points. The mats of Pure SEBS and PEO\_20 were hydrophobic and presented similar high values of static contact angle (Figure 5.1a and d), while the mats of F127\_20 and PEO\_20 (Figure 5.1b and c) were superhydrophilic and absorbed the water droplet.

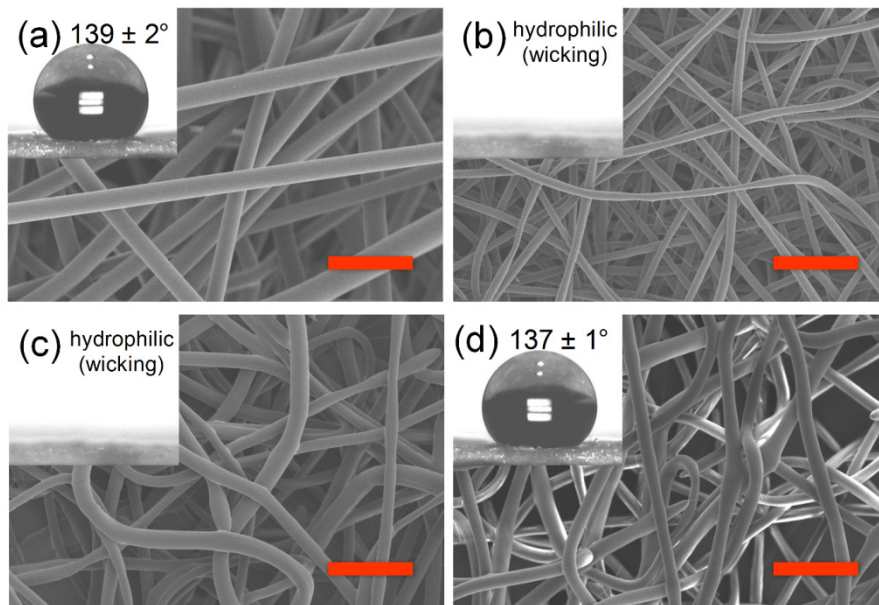


Figure 5.1 – Mat morphology and static contact angle results for (a) pure SEBS, (b) F127\_20, (c) P123\_20 and (d) PEO\_20.

Scale bars = 50 $\mu\text{m}$ .

Figure 5.2 shows the surface chemical composition results obtained by XPS. To allow complete solvent evaporation, the measurements were made 24 hours after electrospinning. The oxygen concentration, calculated from the areas of the photoemission peaks of C 1s and O 1s in the XPS survey spectrum (Figure 5.2a), was used as an indicator of PEO or PEO-PPO-PEO presence at the surface, considering that there is no oxygen in the SEBS matrix (Figure 5.2a). This atomic concentration was then converted to PEO or PEO-PPO-PEO concentration (as shown in Figure 5.2b) using the theoretical carbon to oxygen (C:O) ratio in

each of the pure chemical structures (PEO, F127 or P123). Results of XPS surveys performed on films of the pure polymers revealed good agreement with this theoretical oxygen concentration. The horizontal arrow in Figure 5.2b indicates the point above which all the mats were hydrophilic and started to absorb water (onset of wicking). All mats below the arrow presented high values of water contact angle similar to pure SEBS mats ( $\approx 140^\circ$ ).

SEBS/P123 blends presented the greatest level of PEO-PPO-PEO segregation to the surface, way above the blend bulk composition line, reaching complete hydrophilization at 10 wt% of P123 and almost surface saturation at 20 wt%. Blends with F127 also presented surface enrichment for all compositions due to the segregation of PEO-PPO-PEO, but the onset of wicking was achieved only at 20 wt% of F127. Pure PEO was much less effective to modify the surface of SEBS fibers and the analysis showed PEO depletion up until 15 wt% of PEO, and hydrophobicity for all the SEBS/PEO mats.

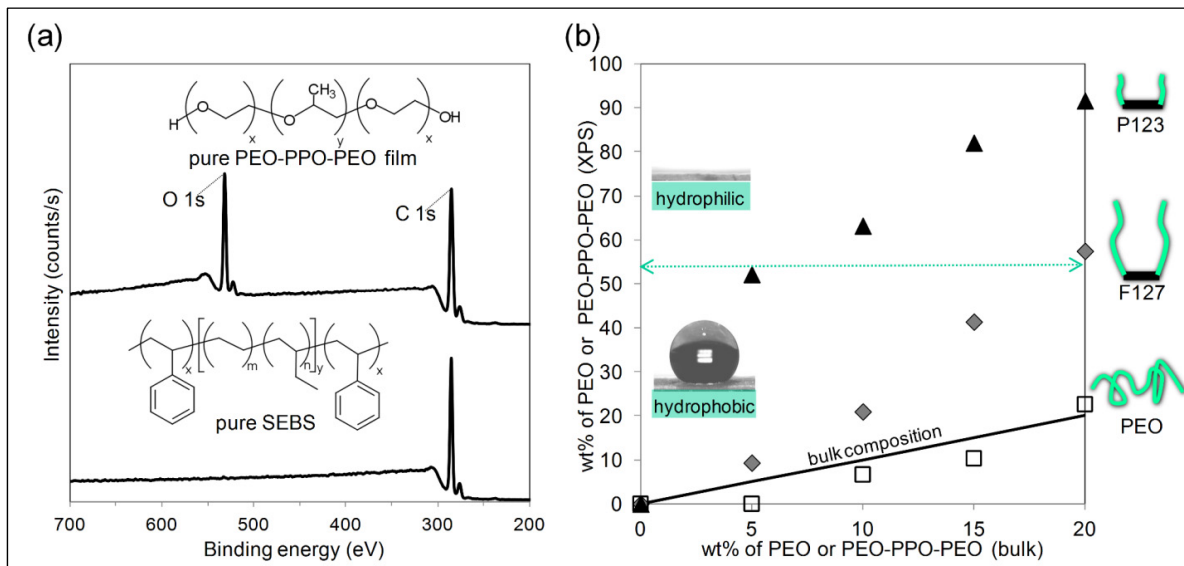


Figure 5.2 – XPS results: (a) Survey spectra for pure PEO-PPO-PEO and pure SEBS showing the photoemission peaks of C 1s and O 1s. (a) Surface chemical composition of SEBS/PEO-PPO-PEO or SEBS/PEO blends after processing (day 1) as a function of PEO-PPO-PEO (F127 or P123) or PEO concentration (0, 5, 10, 15 and 20 wt%).

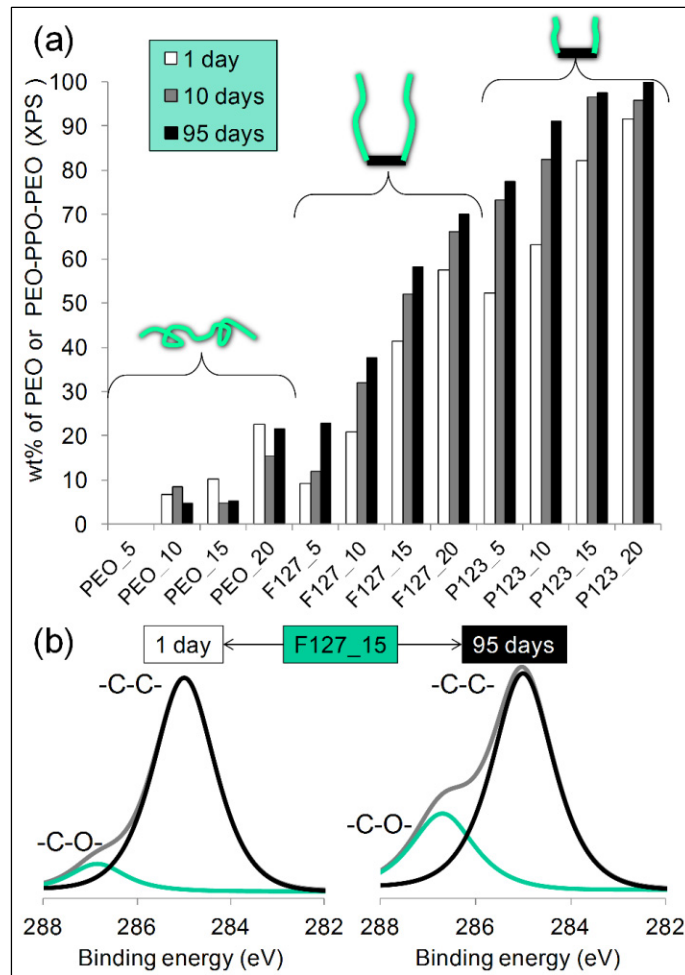


Figure 5.3 – XPS aging results: (a) Survey results showing PEO or PEO-PPO-PEO (F127 or P123) segregation to the surface over time in the SEBS blends; (b) High-resolution spectra showing intensity increase in the  $-C-O-$  peak over time.

One day after the electrospinning process the mat of the blend with 5 wt% of P123 (P123\_5) was hydrophobic. Any blend with higher PEO-PPO-PEO content was completely superhydrophilic while the compositions with lower PEO-PPO-PEO surface concentration were completely hydrophobic (Figure 5.2b). However, days after processing, new water contact angle measurements revealed that the P123\_5 mat was hydrophilic with fast water absorption. Similarly, the F127\_15 mat that was hydrophobic right after processing also became hydrophilic, although the droplet absorption times varied greatly depending on the

mat region (Rafael S. Kurusu & Demarquette, 2016). These results led to the investigation presented in Figure 5.3a that shows the evolution of the surface chemical composition of the mats over time after storage in a sealed package at room temperature (22-23 °C). Surface enrichment by segregation continued even after total solidification. The blends SEBS/P123 showed a sharp segregation in the first 10 days after processing followed by a slight increase/stabilization in the next months. P123\_15 and P123\_20 practically presented a complete surface coverage with PEO-PPO-PEO. SEBS/F127 blends also presented continued, although less sharp, segregation but stabilized at lower values never reaching complete coverage. High resolution XPS (Figure 5.3) in both as processed (1 day after) and aged samples revealed that the increase in oxygen content at the surface was due to the greater presence of -C-O- bonds, which exists in both PEO and PPO blocks, and that no chemical reaction occurred. In the case of SEBS/PEO blends there was no clear continued segregation and some of the blends even presented a lower value of PEO at the surface after 95 days. All the SEBS/PEO mats remained hydrophobic even after aging.

Considering that both PEO and PEO-PPO-PEO are immiscible with SEBS (observed by optical microscopy of films and Differential Scanning Calorimetry, not shown here), an attempt to predict the equilibrium morphology of the blends was made with surface tension measurements and interfacial tension calculations in order to understand the segregation results. The Owens-Wendt method was used to calculate the surface tension of pure SEBS, PS, PEO-PPO-PEO (F127) and PEO films. Formamide was used as the polar test liquid while diiodomethane was the nonpolar test liquid (Owens & Wendt, 1969; Shimizu & Demarquette, 2000; Żenkiewicz, 2007). Contact angle measurements with the liquid pair were performed on the surfaces of flat films of each pure polymer, obtained by dip-coating. The results enabled the surface tension calculation as the sum of dispersion and polar components (Table 5.1).

Table 5.1 – Surface tension values calculated by the Owens-Wendt method, and taken from literature as indicated

polymer	surface tension (mN/m)		
	$\gamma^d$	$\gamma^p$	$\gamma$
SEBS	35.7	2.1	37.8
PS	41.4	0.2	41.6
PEO-PPO-PEO	45.7	0.0	45.7
PEO	44.6	3.8	48.4
PEO <sup>1</sup>	30.7	12.2	42.9
PPO <sup>1</sup>	31.3	0.4	31.7

<sup>1</sup>Values taken from ref (Brandrup, Immergut, Grulke, Abe, & Bloch, 1989)

The harmonic mean equation

$$\gamma_{12} = \gamma_1 + \gamma_2 - \frac{4\gamma_1^d \gamma_2^d}{\gamma_1^d + \gamma_2^d} - \frac{4\gamma_1^p \gamma_2^p}{\gamma_1^p + \gamma_2^p} \quad (5.1)$$

was used to calculate the interfacial tension  $\gamma_{12}$  between the polymers 1 (SEBS or PS) and 2 (PEO, PEO-PPO-PEO or PPO), where  $\gamma_i^d$  and  $\gamma_i^p$  are the dispersion and polar components of the surface tension  $\gamma_i$ , which can also be interpreted as the interfacial tension between polymer  $i$  and air. The interfacial tension values were then used to calculate the three spreading coefficients presented in Figure 5.4 with the possible surface morphologies (Morita et al., 2001; Rezaei Kolahchi et al., 2014). The results are summarized in Table 5.2.

		spreading coefficients		
air		$\gamma_2 - (\gamma_{12} + \gamma_1)$	$\gamma_{12} - (\gamma_1 + \gamma_2)$	$\gamma_1 - (\gamma_{12} + \gamma_2)$
(i)		$> 0$	$< 0$	$< 0$
(ii)		$< 0$	$< 0$	$< 0$
(iii)		$< 0$	$< 0$	$> 0$
(iv)		$< 0$	$> 0$	$< 0$

Figure 5.4 – Possible blend surface morphologies according to surface tension values and spreading coefficients. Polymer 1 (orange) is the SEBS matrix and polymer 2 (green) represents either PEO or PEO-PPO-PEO.

Table 5.2 – Interfacial tension, spreading coefficients and possible morphologies for the polymer blends using either hydrophilic PEO or amphiphilic PEO-PPO-PEO as surface modifying polymers in a SEBS or PS matrix

	$\gamma_{12}$ (mN/m)	$\gamma_2 - (\gamma_{12} + \gamma_1)$	$\gamma_{12} - (\gamma_1 + \gamma_2)$	$\gamma_1 - (\gamma_{12} + \gamma_2)$	Morphology (Fig 3)
SEBS/PEO	1.5	$> 0$	$< 0$	$< 0$	(i)
SEBS/PEO-PPO-PEO	3,3	$> 0$	$< 0$	$< 0$	(i)
SEBS/PEO <sup>1</sup>	7.4	$< 0$	$< 0$	$< 0$	(ii)
SEBS/PPO <sup>1</sup>	1.5	$< 0$	$< 0$	$> 0$	(iii)
PS/PEO	3.4	$> 0$	$< 0$	$< 0$	(i)
PS/PEO-PPO-PEO	0.4	$> 0$	$< 0$	$< 0$	(i)
PS/PEO <sup>1</sup>	13.2	$< 0$	$< 0$	$< 0$	(ii)
PS/PPO <sup>1</sup>	1.5	$< 0$	$< 0$	$> 0$	(iii)

<sup>1</sup>Calculated with the values found in literature (see Table 5.1)

The interfacial energy values calculated from the surface tension measurements for pure SEBS, PEO and PEO-PPO-PEO (F127) reveal that for all blends the equilibrium morphology would be the case (i) presented in Figure 5.4, with the dispersed phase droplet of polymer 2 (PEO or PEO-PPO-PEO) inside the polymer 1 (SEBS) matrix. The morphology would not

change if SEBS was replaced by pure PS. At first, this analysis leads to the conclusion that if the thermodynamic equilibrium was reached the morphology evolution would result in less PEO or PEO-PPO-PEO at the surface, contrary to what was observed in the aging experiments. In fact, Figure 5.3 shows an increase of PEO-PPO-PEO at the surface leading to surface saturation for some compositions. Some factors can contribute to the lack of precision involved in the contact angle measurements. Block copolymers may present a degree of surface roughness that can alter the results. Also, films of PEO or PEO-PPO-PEO (F127) are soluble or leachable when in contact with different liquids like water, formamide and diiodomethane. The contact angle was taken instantly after the droplet deposition, but this probably contributed to increase the measurement error. Moreover, the amphiphilic polymer with smaller molecular weight (P123) did not form a film without cracks and was left out of this analysis. But most importantly, this method does not permit to separate the values for hydrophilic PEO and hydrophobic PPO blocks, giving only an average that does not correspond to the behavior of each block. In order to circumvent these uncertainties, the interfacial tension was also calculated using separate surface tension values for PEO and PPO found in literature (Table 5.1) that were obtained by different methods (Brandrup et al., 1989), such as the pendant drop (Rastogi & St. Pierre, 1969) with molten polymers and extrapolation to room temperature. By recalculating the spreading coefficients for SEBS and pure PEO the new morphology obtained corresponds to the case (ii) in Figure 5.4 with the PEO droplet reaching the air surface while still inside the matrix. The new spreading coefficients for SEBS and pure PPO leads to the morphology (iii) in Figure 5.4, with a wetting layer of PPO separating the SEBS matrix from the air.

These new morphologies help to explain the evolution towards surface enrichment and saturation in the blends tested. As previously proposed, the low surface energy PPO block drives the segregation of the amphiphilic PEO-PPO-PEO to the surface (Rafael S. Kurusu & Demarquette, 2016; Y.-q. Wang et al., 2005). Pure PEO and F127 have a similar molar mass but the segregation is much more effective with the amphiphilic polymer. The size of the molecule and the PPO/PEO ratio will influence the level of PEO-PPO-PEO segregation. F127 and P123 have similar PPO block size but P123 has shorter PEO chain-ends and

therefore lower molar mass, resulting in a more drastic segregation and even surface saturation. Any segregation of higher energy molecules to the surface may be explained by the difference in molecular weight between the modifying polymer and the matrix. As previously reported, two factors may be responsible for this effect: (i) chain ends present lower surface energy than the main chain so that lower  $M_w$  polymers will have greater tendency to segregate to the surface; (ii) a decrease in  $M_w$  leads to a decrease in the conformational entropy penalty for a polymer chain located at the surface so that the enthalpic/energy effects may be overcome (Tanaka et al., 1998). Combining both enthalpic (low surface energy) and entropic (low molar mass) will then lead to a greater segregation, like it was observed for the blends containing P123 ( $M_w = 5\,800\text{ g}\cdot\text{mol}^{-1}$ ) molecules.

Nevertheless, it is still unclear if the fiber surface is covered only by phase-separated PEO-PPO-PEO polymer or if free amphiphilic molecules also contributed to the surface coverage. PEO-PPO-PEO presents surfactant properties, meaning that in aqueous solutions free amphiphilic molecules will tend to segregate to the surface and form a layer until the surface is saturated. By increasing the surfactant concentration micelles will start to form and aggregate inside the solution leading to observable phase separation. The surface saturation is followed by a decrease in surface tension and in the case of PEO-PPO-PEO copolymers, the PPO block will cover the surface with air while the PEO is immersed in the solution. In a solution containing polymers, the surfactant molecules will still form this type of layer even though the interaction with polymer chains makes the segregation more difficult (Kronberg, Holmberg, & Lindman, 2014; Lochhead & Huisinga, 2004). Surface tension values for PEO-PPO-PEO copolymers are usually measured in solution due to this ability to form a layer, and the values reported (Alexandridis & Alan Hatton, 1995) are close to the ones presented in Table 1 for pure PPO, confirming that in aqueous solutions the PPO block covers the surface while the PEO block stays in the aqueous phase. The values in Table 1 also show that the PPO presents the lowest surface tension value in the blends, while the PEO block presents the highest value.

To observe the morphology by SEM, the blends with the highest amount of either PEO-PPO-PEO or PEO were washed and immersed in water for 24h. After that, the procedure was repeated five more times in order to extract PEO-PPO-PEO or PEO. Figure 5.5 shows the edge of a mat and a cross-section of a fiber of PEO\_20 (Figure 5.5a and Figure 5.5b) and P123\_20 (Figure 5.5c and Figure 5.5d). PEO\_20 mats presented more homogeneous fibers (Figure 5.5a) while P123\_20 fibers presented greater variation in diameter and shape (Figure 5.5c). It is possible to observe some holes on the lateral surface that may indicate phase-separated PEO extraction in PEO\_20 (Figure 5.5b). The cross-section revealed elongated droplets (indicated by the arrow) but it is not a clear if this indicates PEO extraction or just surface roughness. Due to the lower presence of PEO on the fibers surface, the extraction did not completely reveal the morphology of PEO\_20 blends (Figure 5.5b). In the case of SEBS/F127\_20 a different type of morphology formed a phase-separated structure that contributed to the homogeneous wetting behavior as previously discussed in more detail in Chapter 3 (Rafael S. Kurusu & Demarquette, 2015). The cross-section of SEBS/P123\_20 fibers (Figure 5.5d) clearly showed the phase separation between the polymers after P123 extraction. The lateral surface of the fiber in Figure 5.5d shows that, different from blends with pure PEO, larger regions were covered by phase-separated P123 leaving a rougher surface after extraction. From the XPS results we know that this composition presented saturated surface even before aging.

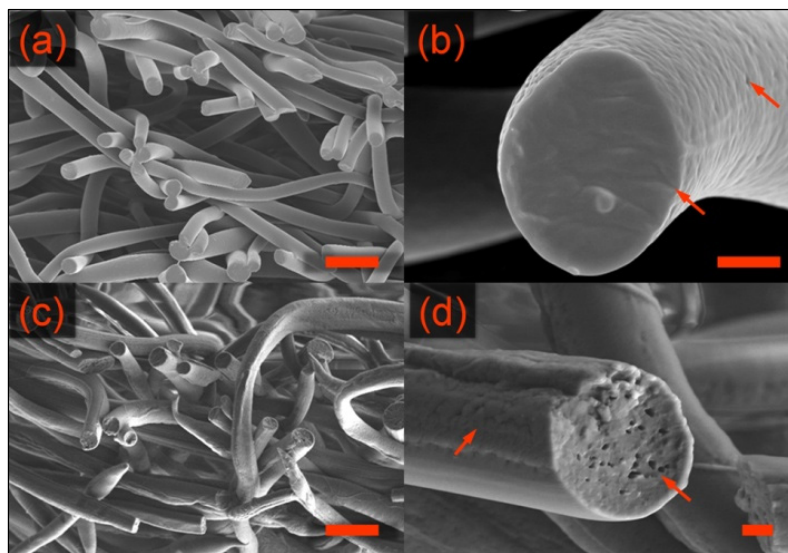


Figure 5.5 – Edge of a cut mat and cross section of a fiber after washing: (a) and (b) PEO\_20; (c) and (d) P123\_20. Scale bars = 20  $\mu\text{m}$  in (a) and (c); 2  $\mu\text{m}$  in (b) and (d).

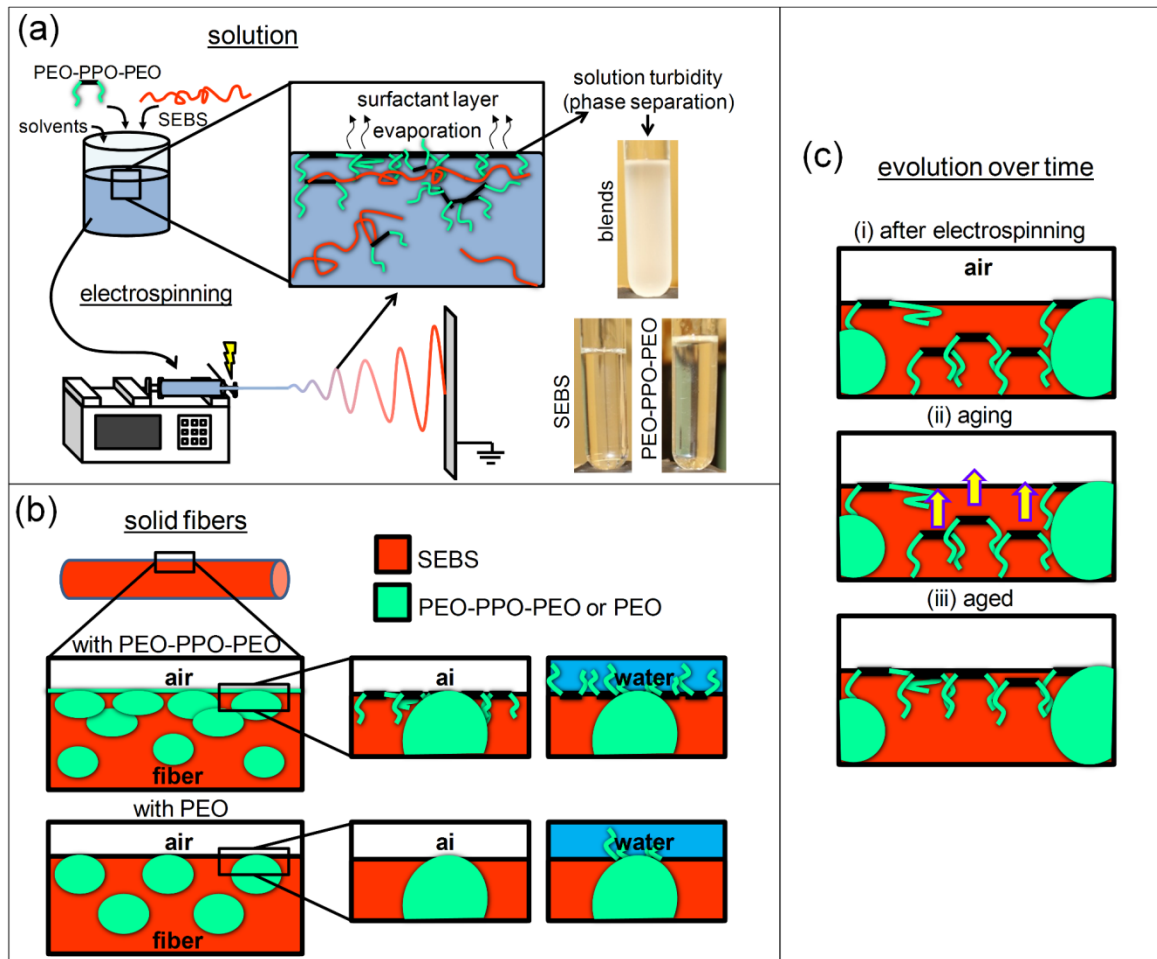


Figure 5.6 – Schematic illustrations: (a) solutions containing SEBS and PEO-PPO-PEO with pictures of representative solutions; (b) surface enrichment and hydrophilization mechanism with amphiphilic PEO-PPO-PEO and pure PEO (out of scale); (c) Aging mechanism showing PEO-PPO-PEO molecules that continue to segregate to the surface over time after solidification.

The clear phase separation (SEM) and surface coverage (XPS) indicate that in the blends with amphiphilic copolymers the morphology evolved as presented in the attempted mechanisms in Figure 5.6. As the organic solvents evaporate, PEO-PPO-PEO molecules will tend to segregate to the polymer-rich solution surface and lower the surface tension (Figure 5.6a). Inside the solution, the amphiphilic molecules will start to interact with SEBS chains and also form micelles, which will lead to phase-separated structures. The turbidity of the solutions containing both polymers is a clear indication of large phase-separated agglomerates, while the solutions of both pure SEBS and pure PEO-PPO-PEO are

transparent (Figure 5.6a). After electrospinning (Figure 5.6b), the chemical composition of the fiber surface will be altered by both this original layer of amphiphilic molecules and also by phase-separated structures that reached the surface, which makes blending with amphiphilic molecules much more effective to hydrophilize the mat. Besides greater surface energy, pure PEO does not have surfactant properties and the main contribution to the surface modification of SEBS/PEO blends comes from phase-separated structures that reached the surface, which was not enough to produce hydrophilic mats.

The surface morphology of the fiber can be divided in three stages (Figure 5.6c). During electrospinning the surfactant layer of the solutions may be disrupted by the rapid jet bending and fiber solidification, “freezing” the microstructure in the after-processing morphology and chemical composition (Figure 5.6c (i)) and, as shown in XPS results, the resulting fiber surface presented great enrichment but it was not completely covered. Molecules close to but not at the surface right after electrospinning continued to move to the surface with time (Figure 5.6c (ii)) and formed the aged morphology (Figure 5.6c (iii)) with increased segregation. In addition, it is much more unlikely that larger, phase-separated structures would be able to move in the solid state.

Another factor that will influence the segregation is the mobility of the surface modifying molecules, which will depend on the matrix free volume. It is known that annealing of polymer blends above the glass transition temperature of the matrix increases the mobility of the polymers and allows surface modification (Campoy-Quiles et al., 2008; Geoghegan & Krausch, 2003). The free volume fraction  $f$  of an amorphous polymer at a given temperature  $T$  can be estimated by the expression (Williams, Landel, & Ferry, 1955)

$$f = f_g + \alpha_2(T - T_g) \quad (5.2)$$

where  $f_g$  is the fraction of free volume at the glass transition temperature  $T_g$ , and  $\alpha_2$  is the difference between the thermal expansion coefficient above and below the glass transition

temperature. As obtained by the Williams–Landel–Ferry equation (Williams et al., 1955),  $f_g = 0.025$  and  $\alpha_2 = 4.8 \times 10^{-4} \text{ K}^{-1}$ , and considering that the overall glass transition temperature of SEBS is  $-42^\circ\text{C}$  due to the presence of 70 wt% elastomeric EB blocks,  $T - T_g \approx 65 \text{ K}$ . In these conditions, the fraction of free volume  $f$  would more than double the  $f_g$  value, increasing the possibility of segregation of other molecules to their equilibrium state without the need for annealing at higher temperatures. To verify this hypothesis blends containing the same amount of P123, which presented marked segregation over time (Figure 5.3), were prepared using either SEBS or pure PS ( $T_g = 100^\circ\text{C}$ ) as matrices. The results presented in Figure 5.7 show practically no sign of aging in the PS/P123 samples. The rigidity and lower free volume of the matrix prevented further movement and the structure obtained after electrospinning is preserved over time.

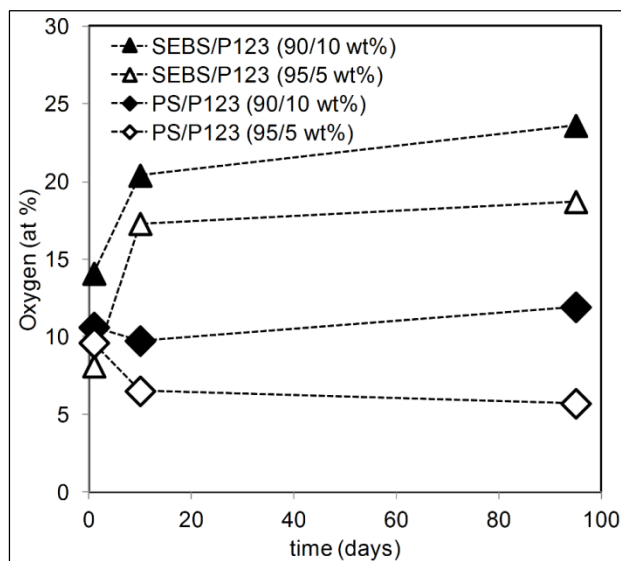


Figure 5.7 – Evolution in oxygen content over time for the blends containing 5 and 10 wt% of P123 in SEBS or PS matrix.

## 5.4 Conclusions

This work investigated polymer blending with hydrophilic or amphiphilic molecules as a technique to hydrophilize the surface of hydrophobic SEBS electrospun mats. After

processing, blends with amphiphilic PEO-PPO-PEO (F127 or P123) copolymers presented a drastic PEO-PPO-PEO segregation to the surface and mat hydrophilization, while the mats of the SEBS/PEO blends were all hydrophobic. P123, the block copolymer with shorter PEO chain-ends and lower molecular weight, segregated more than F127 with longer PEO chain-ends. SEBS/PEO mats revealed depletion of PEO at the surface up until 15 wt% of PEO, and mild enrichment in the blend with 20 wt% of PEO.

Contact angle measurements on some of the mats (P123\_5 and F127\_15) revealed a change in wetting behavior with time at room temperature. A systematic analysis of the surface chemical composition revealed that the segregation of amphiphilic molecules continued over time, stabilizing only after weeks. In the compositions with higher content of P123 the surface practically presented complete coverage. This continued morphology evolution is due to the movement of amphiphilic molecules that have the tendency to move to the surface to decrease the total energy of the system and form a layer of PPO blocks. Mild segregation of PEO probably happened due to entropic factors.

Segregation also seems to be influenced by the mobility (free volume) inside the matrix. Flexible SEBS-based (SEBS glass transition temperature around  $-42^{\circ}\text{C}$ ) blends presented greater segregation than rigid PS-based (PS glass transition temperature around  $100^{\circ}\text{C}$ ) blends.

## 5.5 Acknowledgements

The authors wish to thank *École de Technologie Supérieure (ÉTS)*, the Natural Sciences and Engineering Research Council of Canada (NSERC), and the *Fond de recherche du Québec (FRQ)* for financial support, and Jessica De La Torre and Professor Sophie Lerouge for helping with the contact angle measurements.



## **CHAPTER 6**

### **DISCUSSION**

This thesis investigated the hydrophilization of electrospun mats by blending, which involved many technical challenges. This Chapter has four sections (wetting of electrospun mats, electrospinning of SEBS and SEBS/PEO-PPO-PEO blends, hydrophilization of SEBS with PEO-PPO-PEO and morphology evolution of electrospun blends) to discuss some of the challenges encountered and also to evaluate if the research objectives were achieved. The main contributions to knowledge close each section.

#### **6.1 Wetting of electrospun mats**

In Chapter 1, a thorough literature review about surface modification techniques to control the wettability of electrospun mats was presented. Before the introduction of each technique, some basic principles of wetting theories were discussed, highlighting the typical behavior expected for the interaction of water with porous structures such as electrospun mats. As explained in the Chapter, the mats obtained by electrospinning can be regarded as a surface with high roughness and as a porous structure with usually a high volume of interconnected pores. These characteristics favor extreme wetting behavior, from mats with high values of contact angle or even superhydrophobic to superhydrophilic mats with fast water absorption (wicking). A minor change in the chemical composition of the surface can drastically alter the wettability of the mats. By analysing the recent literature, it is possible to observe the reoccurrence of this switch mechanism. In other cases, there seems to be a confusion about contact angle results that do not corroborate this behavior, particularly in the case of hydrophilic mats. In some cases the contact angle was not measured over time – water absorption occurs sometimes after minutes. In other cases the mat is too thin, with a few fiber

layers, making it hard to affirm that there is no influence from the substrate on which the fibers were deposited during the contact angle measurement. In other exceptions, the mat presents, sometimes after surface modification, a different and more film-like morphology that can explain the contact angle results. The results presented in Chapters 3 to 5 corroborate with the theory of switching wettability of electrospun mats. In the work presented in these Chapters, surface modification did not change the interconnected porous structures formed by fibers. Only the surface chemical composition was altered at different levels, which makes this system ideal to evaluate the changes in wettability after surface modification. Concerning the wetting theories, the results presented in this thesis tried to stress the limitations of a single static contact angle measurement, which should be taken as a starting point in the analysis to evaluate the wettability of electrospun mats.

## **6.2 Electrospinning of SEBS and SEBS/PEO-PPO-PEO blends**

Although relatively simple to perform, the electrospinning process involves the interplay of many solution and processing parameters that have to be optimized in order to produce a mat with homogeneous fibers. The first challenge was the choice of a polymer. SEBS, a flexible thermoplastic elastomer that can be dissolved in many solvents and that is also hydrophobic, was chosen as the matrix. The second challenge was the choice of solvents. In many cases, electrospinning solutions are composed of a mixture of solvents because it is hard to find a single solvent with the appropriate volatility, conductivity and solubility parameters at the same time. Many systems with two solvents were tried for SEBS based on these properties. The system was therefore rather complex, with a polymer composed of two blocks with distinct behavior and two solvents. Fundamental studies on solution are usually performed with a single solvent with higher affinity for one the blocks, but in our case solutions with single solvents did not present appropriate electrospinnability. Some blended solutions presented gel-formation. The solution chosen for this work, a blend of chloroform and toluene (80/20 wt%, respectively), produced uniform fibers with a relatively high diameter (varying from 4 to 10  $\mu\text{m}$ ) possibly due to low conductivity. The next step was to choose a surface modifying polymer that could be incorporated in the same solution and still produce

uniform fibers. PEO-PPO-PEO and PEO with a similar molecular weight ( $M_w \approx 12\,000\text{ g}\cdot\text{mol}^{-1}$ ) could be easily dissolved and electrospun in the same system up to 20 wt%. Solutions with higher content started to present process disruption and nonuniform fiber formation. Although not the main focus of this thesis, the electrospinning process results showed that a blend of a hydrophobic polymer with immiscible PEO or PEO-PPO-PEO could be prepared by electrospinning in the same solution with the same processing parameters used for the pure matrix.

### **6.3 Hydrophilization of SEBS with PEO-PPO-PEO**

The incorporation of amphiphilic PEO-PPO-PEO to hydrophilize SEBS was based on the idea that the low surface energy PPO block could drive segregation to the surface. The first type of PEO-PPO-PEO chosen (Pluronic F127) was effective to hydrophilize the mat when PEO-PPO-PEO content in the SEBS/PEO-PPO-PEO blend reached 15 wt%. However, homogenous surface properties were only achieved for the electrospun mat with 20 wt% of PEO-PPO-PEO. Morphology, chemical composition and water contact angle were investigated in both electrospun mats and dip-coated films. The results revealed a particular morphology shift in the films with 20 wt% of PEO-PPO-PEO, prepared with an identical solution that was used in electrospinning. Since phase-separated structures are readily formed in solution (as seen by the solution turbidity), it is possible that a particular morphology formed prior to processing was preserved in both films and fibers. Another alternative is that the morphology developed from the same solution towards the same equilibrium, but to different extents due to processing differences (dip-coating vs. electrospinning). In dip-coating, the evaporation time is much longer so that there was more time to achieve the equilibrium morphology. In fact, chemical analysis results revealed that the film surface was practically covered by PEO-PPO-PEO at 20 wt% in the blend. In electrospinning, the rapid processing from solution to solid fibers can make it more difficult to achieve the equilibrium morphology. One of the objectives of this study was to stress that films and mats, even with

the same bulk composition, can present completely different surface compositions and therefore any comparison between the contact angle results of films and mats must be analyzed bearing that in mind.

The next step was to incorporate different PEO-PPO-PEO copolymer to SEBS fibers. One of the advantages of working with commercially available PEO-PPO-PEO copolymers is the great variety of molecules in terms of molecular weight and PEO or PPO content. Results revealed that the surface chemical composition and therefore the wettability could be tuned. It is important to stress the need for different wettability characterization methods like wicking rate or high-speed imaging not only to distinguish hydrophilic mats but also to provide important information for possible applications like humidity sensing or liquid transport. In some cases, leaching of PEO-PPO-PEO was observed and, although problematic for applications in which a robust hydrophilicity is required, this characteristic may be interesting in applications in which a controlled leaching is desirable like drug delivery. PEO-PPO-PEO copolymers are approved for biomedical application and could be combined with a therapeutic agent.

These results showed that the main objective of the thesis could be achieved with the materials and processing conditions chosen. Different contributions to knowledge were made: the hydrophilization using PEO-PPO-PEO in an immiscible blend with surface chemical composition and morphology analysis; the differences between films and electrospun mats produced from identical solution; the control of surface segregation in electrospun mats by blending with different PEO-PPO-PEO polymers for the first time, the differences in wettability of hydrophilic mats with similar chemical composition analyzed by alternative characterization methods.

#### **6.4 Morphology evolution of electrospun blends**

The last article of the thesis (Chapter 5) aimed at understanding the fundamental mechanisms involved in surface segregation during and after electrospinning by blending SEBS and PS

with pure PEO, which has a relative high surface energy, and amphiphilic PEO-PPO-PEO, which has a low surface energy PPO block. The results showed that pure PEO could not hydrophilize the mats even when its content reached 20 wt% in the blend, presenting low surface segregation. As previously discussed, PEO-PPO-PEO was quite effective to hydrophilize the mats. Surprising contact angle results, followed by a systematic chemical composition analysis revealed a continued PEO-PPO-PEO segregation to the surface over weeks after electrospinning, in some cases reaching surface saturation. The results indicated the mechanism of morphology evolution in SEBS/PEO-PPO-PEO blends. PEO-PPO-PEO presents surfactant properties so that a wetting layer of PEO-PPO-PEO molecules is formed in the solution prior to electrospinning. With increased PEO-PPO-PEO concentration, phase-separated structures are formed in the solutions. During electrospinning the surfactant layer is disrupted and the final surface morphology is characterized by the presence of both phase-separated structures and some of the molecules from the surfactant layer. As the fibers age some of the molecules that were close but not at the surface continue to move towards the air. This study gave new experimental evidence about the role of energy factor on the segregation of surface modifying polymers in electrospun fibers, although this discussion is far from established. A new mechanism for the evolution of electrospun blends with amphiphilic copolymers with surfactant properties was also proposed. Lastly, the role of the matrix in allowing PEO-PPO-PEO segregation at room temperature was analyzed by comparing the segregation of P123 in SEBS and PS, showing the importance of the glass transition temperature of the matrix to maintain the stability of the blend after processing.



## CONCLUSIONS AND RECOMMENDATIONS

This Chapter summarizes the main findings of each article presented in Chapters 3 to 5, followed by a conclusion for each Chapter. In the end of this Chapter, the main conclusion of this thesis and some recommendations for future work are presented.

### 7.1 Main findings and conclusions

#### 7.1.1 Summary and conclusions of Chapter 3

In Chapter 3, entitled “*Blending and Morphology Control To Turn Hydrophobic SEBS Electrospun Mats Superhydrophilic*”, the first experimental study about the hydrophilization of SEBS mats was presented. As a surface modifying polymer, a commercial amphiphilic PEO-PPO-PEO (Pluronic F127) block copolymer was chosen, based on theories about the preferential segregation of the hydrophobic PPO block that could drag the hydrophilic PEO blocks to the surface to be hydrophilized when in contact with water. The experiments confirmed theoretical predictions, and the SEBS mats became hydrophilic when 15 wt % of PEO-PPO-PEO was added. However, this mat (SEBS with 15 wt% of PEO-PPO-PEO) presented greatly varying droplet absorption times, while the mat with 20 wt% of PEO-PPO-PEO showed a homogeneous absorption time in different mat regions, revealing more uniform surface properties. Chemical composition analysis revealed greater surface coverage for the latter composition. A morphological investigation of dip-coated films of the same system revealed that at 20 wt% of PEO-PPO-PEO the system SEBS/PEO-PPO-PEO assumed a different morphology when compared to the typical droplet dispersion found in the films with smaller PEO-PPO-PEO content. In the film with 20 wt% of PEO-PPO-PEO, the surface was to be covered by an interconnected grain-like morphology similar, but coarser, to what was found in the pure PEO-PPO-PEO films. This particular morphology also increased the

surface roughness of the SEBS/PEO-PPO-PEO (80/20 wt%) film, which presented a smaller contact angle value than the pure PEO-PPO-PEO film. An increase in surface roughness was also observed on the surface of the electrospun fibers of the same composition indicating that similar morphology change has affected the mats and contributed to the more uniform wettability of this mat. Surface analysis of the same composition (20 wt% of PEO-PPO-PEO) revealed a surface coverage of around 70% on the electrospun mats, which was enough to produce homogeneous hydrophilic mat. The conclusions of this study are: SEBS electrospun mats can be hydrophilized by blending with PEO-PPO-PEO in a one-step process; the blends presented great PEO-PPO-PEO segregation to the surface; morphology is an important parameter to be controlled in order to obtain homogeneous surface properties.

#### 7.1.2 Summary and conclusions of Chapter 4

Following the successful hydrophilization presented in Chapter 3, SEBS blends with three different types of PEO-PPO-PEO copolymers were produced. The study was presented in Chapter 4, entitled “*Wetting of Hydrophilic Electrospun Mats Produced by Blending SEBS with PEO–PPO–PEO Copolymers of Different Molecular Weight*”. F127, the molecule previously presented in Chapter 3, has a molecular weight ( $M_w$ ) of 12 600 g.mol<sup>-1</sup> and 73.2 wt % of PEO. The other two PEO-PPO-PEO molecules chosen were P123 ( $M_w = 5\ 800$  g.mol<sup>-1</sup> and 30 wt % of PEO) and L61 ( $M_w = 2\ 000$  g.mol<sup>-1</sup> and 10 wt % of PEO). The hydrophilization of SEBS/P123 and SEBS/L61 blends was achieved with as little as 5 wt% of each PEO-PPO-PEO. Surface chemical analysis results revealed a massive P123 and L61 segregation to the surface with complete surface coverage achieved at 10 wt% of L61 and 15 wt% of P123. The size of the molecules, which decreased in the order F127>P123>L61, and the proportion of hydrophobic PPO blocks, which increased in the order F127<P123<L61, both contributed to the results. Having different hydrophilic mats, the second objective of this study was to explore different techniques to evaluate the wettability differences between them, highlighting again the limitations of a single static water contact angle measurement. The first and most intuitive method is the comparison of the droplet absorption time in each hydrophilic mat. Since the absorption in some cases was extremely fast (less than 1 second),

high-speed imaging was used to observe the dynamics of droplet spreading and impact. For this analysis only the mats with the highest content of PEO-PPO-PEO, 20 wt%, were used. The results revealed that in the first instant, the contact angle value on all mats is similar to that of pure SEBS, around  $140^\circ$ . After that the droplet is completely absorbed in two seconds (2000 milliseconds) by the SEBS/F127 (80/20 wt%) mats, in about two hundred milliseconds by the SEBS/P123 (80/20 wt%) mats and in less than a hundred milliseconds by the SEBS/L61 (80/20 wt%) mats. The analysis also revealed that the spreading had two regimes, a faster decrease until around  $30\text{-}40^\circ$  followed by a slower decrease until practically zero. The second method to distinguish between hydrophilic mats was the analysis of wicking based on the measured rise of water in a mat strip of defined dimensions. The mats with PEO-PPO-PEO-saturated surfaces presented similar wicking behavior but the highest wicking rate was achieved with blends containing L61. Interestingly, blends with the same surface chemical composition but different PEO-PPO-PEO molecules presented remarkably different wicking behavior. SEBS/P123 (95/5 wt%) and SEBS/F127 (80/20 wt%) presented similar chemical composition but the first blend showed much higher wicking rate. The shorter PEO arms of P123 were more effective to hydrophilize the surface. As the last important result, leaching of PEO-PPO-PEO in the SEBS/L61 blends was clearly observed by the presence of liquid L61 on the substrate and by optical microscopy. The conclusions of this study are: the segregation of PEO-PPO-PEO polymers in SEBS fibers can be tuned by using different molecular weights and PPO content; surface saturation can be achieved with the smaller molecules; wicking rate and droplet spreading can be controlled according to the chemical composition and type of molecule at the surface; the molecule with the smallest molecular weight (L61) could be easily leached when washed.

### 7.1.3 Summary and conclusions of Chapter 5

In Chapter 5, entitled “*Surface morphology evolution in polymer blends by segregation of hydrophilic or amphiphilic molecules during and after electrospinning*”, a hydrophilic

polymer, pure PEO, was used as a surface modifying polymer compared with amphiphilic PEO-PPO-PEO copolymers. The idea was to evaluate the role of surface energy on the segregation to the surface compared to entropic factor such as the differences in molecular weight between the matrix and the modifying molecules. Surface analysis results revealed a depletion of PEO on the surface of the fibers compared to the bulk composition while the blends with PEO-PPO-PEO presented massive segregation. To eliminate the influence of molecular weight, blends of SEBS with F127 (PEO-PPO-PEO with  $M_w$  of 12 600 g.mol<sup>-1</sup>) were compared with blends of SEBS with PEO ( $M_w$  of 12 000 g.mol<sup>-1</sup>). The results showed that, even with the rapid processing time during electrospinning, the energy factors still play a major role on the surface segregation. It was later observed that some of the mats became hydrophilic after time (even weeks), which led to the second part of this manuscript in which the surface chemical composition was measured over time. The results showed that in blends SEBS/PEO-PPO-PEO there was a continued PEO-PPOPEO enrichment after weeks of storage at room temperature. This continued segregation was particularly remarkable for the blends with P123. A surface/interfacial tension analysis was performed to find the equilibrium morphology for the blends with either pure PEO or PEO-PPO-PEO. According to theoretical values, blends of SEBS/PEO would have PEO droplets reaching the surface but mostly buried in the SEBS matrix if the equilibrium was reached. Blends of SEBS/PPO would have a complete PPO wetting layer over SEBS, which corroborates with the aging results of continued enrichment towards saturation in the SEBS/PEO-PPO-PEO blends. The last part of this Chapter included a comparison of PEO-PPO-PEO (P123) segregation in different matrices: elastomer SEBS with a glass transition temperature around -42°C; and pure PS with a glass transition temperature around +100°C. At room temperature, SEBS will have a much higher free volume fraction compared to PS. To have the same free volume fraction, PS would have to be annealed above 100°C. The results confirmed the theoretical predictions that an elastomeric matrix allows more segregation over time. The conclusions of this study are: energy factors are important to control the segregation of surface modifying polymers; high energy PEO was not effective to hydrophilize SEBS mats; the segregation of PEO-PPO-PEO continues over time at room temperature; the low glass transition temperature of SEBS allows more segregation at room temperature.

#### **7.1.4 Main Conclusion**

Based on these results, it can be concluded that blending is an effective technique to alter the surface properties of electrospun mats. The example used in this work was the hydrophilization of hydrophobic SEBS mats with amphiphilic PEO-PPO-PEO copolymers. Many fundamental aspects of materials processing must be taken into account in order to produce homogeneous surface properties, such as blend morphology or preferential surface segregation. Hydrophilic electrospun mats have a great potential in many different areas and this work tried to clarify some questions whose answers can help in the future development of applications.

#### **7.2 Recommendations**

Many aspects of this work could be further developed. The following recommendations should be considered in case of future work:

1. Electrospinning blends with PEO-PPO-PEO copolymers in different matrices and solutions could lead to the formation of fibers of smaller diameter. A mat composed of thinner fibers would have higher surface area and thus it should be easier to place surface modifying polymers on the surface. At the same time, PEO-PPO-PEO copolymers, which are not electrospinnable, would affect more fiber formation and the mechanical properties of the fibers.
2. Considering the aging results, the surface composition of the PEO-PPO-PEO-containing blends could be even more fine-tuned by controlling the segregation of surface modifying molecules during and after electrospinning. This control could be done by choosing a specific amphiphilic molecule or a specific matrix that could allow more or less segregation.

3. To further investigate the morphology evolution of the blends with PEO-PPO-PEO amphiphilic polymers, micelle formation in solution could be further investigated. This represents a connection with a completely different research area in which fundamental studies are generally performed in dilute aqueous solutions and thus it is possible to foresee many challenges since electrospinning solutions usually have high concentration and viscosity, and are composed of volatile solvents. Melt-electrospinning could be an alternative to work with a simpler system using the more well-known blend morphology evolution theories for polymer processing.
  
4. The robustness of the hydrophilization by blending is also an important theme. It was observed that in some cases the PEO-PPO-PEO molecules were easily leached while in other cases the mats remained hydrophilic after washing. The size of PPO block seems to be the key parameter to achieve a good “anchorage” in the matrix but new experiments are needed. The performance in specific and more applied experiments could guide the morphology requirements to obtain the appropriate hydrophilic mats. Tissue engineering and drug delivery are the examples that come to mind in light of the need for hydrophilic scaffold and the current use of PEO-PPO-PEO copolymers in these domains. Controlled leaching or stable hydrophilicity can be achieved by blending. Drugs could be combined with PEO-PPO-PEO copolymers that segregate to the surface and are leached when in contact with the body, for instance. The more robust compositions could be used to provide a scaffold for tissue growth with stable wettability.

## ANNEX I

### ABOUT THE AUTHOR - ACADEMIC ACHIEVEMENTS

#### EDUCATION

- *Doctor of Philosophy* – *École de Technologie Supérieure* (ÉTS). Advisor: Prof Nicole R. Demarquette. From September 2012 to December 2016 (expected). Montréal, QC – Canada.
- *Master of Science* – Polytechnic School of the University of São Paulo. Advisor: Prof. Nicole R. Demarquette. From April 2009 to August 2011. São Paulo, SP – Brazil.
- *Bachelor of Materials Engineering* - Polytechnic School of the University of São Paulo. From February 2004 to December 2008. São Paulo, SP – Brazil.

#### AWARDS AND SCHOLARSHIPS

- Polymer Processing Society Graduate Travel Award 2016. July 2016. Lyon – France.
- Travel award to attend conference – Society of Plastics Engineers Québec Section. September 2015 Montreal, Quebec – Canada.
- Full ride scholarship and excellence Ph.D award for international students. *École de Technologie Supérieure* (ÉTS). From September 2012 to September 2016 Montreal, Quebec – Canada.
- Third prize in the best poster competition at the 12<sup>th</sup> International Conference on Biocomposites: Transition to Green Materials. May 2012 Niagara Falls, Ontario – Canada.
- First prize in the VIII MetMat Micrography contest - Gerdau and University of São Paulo. São Paulo, SP – Brazil.

**JOURNAL PUBLICATIONS**

- Kurusu, R. S., & Demarquette, N. R. *Surface morphology evolution in polymer blends by segregation of hydrophilic or amphiphilic molecules during and after electrospinning*. Submitted on 11/2016.
- Crétois, R., Chenal, J. M., Sheibat-Othman, N., Monnier, A., Martin, C., Astruz, O., Kurusu, R., Demarquette, N. R. M. *Physical explanations about the improvement of PolyHydroxyButyrate ductility: Hidden effect of plasticizer on physical aging*. *Polymer*, 102, 176-182, 2016.
- Kurusu, R. S., & Demarquette, N. R. *Wetting of Hydrophilic Electrospun Mats Produced by Blending SEBS with PEO-PPO-PEO Copolymers of Different Molecular Weight*. *Langmuir*, 32(7), 1846-1853, 2016.
- Kurusu, R. S., & Demarquette, N. R. *Blending and morphology control to turn hydrophobic SEBS electrospun mats superhydrophilic*. *Langmuir*, 31 (19), pp 5495–5503, 2015.
- Kurusu, R. S., Siliki, C. A., David, É., Demarquette, N. R., Gauthier, C., & Chenal, J. M. *Incorporation of plasticizers in sugarcane-based poly (3-hydroxybutyrate)(PHB): Changes in microstructure and properties through aging and annealing*. *Industrial Crops and Products*, 72, 15, 166–174, 2015.
- Kurusu, R. S., Demarquette, N. R., Gauthier, C., & Chenal, J. M. *Effect of aging and annealing on the mechanical behaviour and biodegradability of a poly (3-hydroxybutyrate) and poly (ethylene-co-methyl-acrylate-co-glycidyl-methacrylate) blend*. *Polymer International*, 63(6), 1085-1093, 2014.
- Sadi, R. K.; Kurusu, R. S.; Fechine, G. J. M.; Demarquette, N. R., *Compatibilization of polypropylene/ poly(3-hydroxybutyrate) blends*. *J Appl Polym Sci*, 123 (6), 3511-3519, 2012.

**CONFERENCE PRESENTATIONS**

- Kurusu, R. S., Demarquette, N. R. International Conference of the Polymer Processing Society (PPS-32), Lyon, France, July 25-29, 2016.

- Kurusu, R. S., Demarquette, N. R. International Smart Materials & Surfaces Conference, Incheon, South Korea, March 23-25, 2016.
- Kurusu, R. S., Demarquette, N. R. Regional Polymer Processing Society Conference 2015, Graz, Austria, September 21-25, 2015.
- Kurusu, R. S., Demarquette, N. R., Gauthier, C., & Chenal, J. M. 9th CREPEC Colloquium, Concordia University, December 10, 2014.
- Kurusu, R. S., Demarquette, N. R. International Conference of the Polymer Processing Society (PPS-30), Cleveland, Ohio, USA, June 8-12, 2014.
- Kurusu, R. S., Demarquette, N. R., Gauthier, C., & Chenal, J. M. International Conference on Biobased Materials and Composites, Montreal, Canada, May 13-16, 2014.
- Sadi, R. K., Kurusu, R. S., Fehine, G. J. M., Demarquette, N.R. Polymer Processing Society Americas Conference. 2 pages. Niagara Falls, Ontario – Canada. May 2012.
- Kurusu, R. S., Demarquette, N.R., Gauthier, G., Chenal, J-M. 12<sup>th</sup> International Conference on Biocomposites: Transition to Green Materials. 5 pages. Niagara Falls, Ontario – Canada. May 2012.
- Sadi, R. K., Kurusu, R. S., Fehine, G. J. M., Demarquette, N.R. 7<sup>th</sup> International Symposium on Natural Polymers and Composites. 5 pages. Gramado, RS - Brazil. September, 2010.



## LIST OF BIBLIOGRAPHICAL REFERENCES

- Abdal-hay, A., Pant, H. R., & Lim, J. K. (2013). Super-hydrophilic electrospun nylon-6/hydroxyapatite membrane for bone tissue engineering. *European Polymer Journal*, 49(6), 1314-1321. doi: <http://dx.doi.org/10.1016/j.eurpolymj.2013.02.004>. Repéré à <http://www.sciencedirect.com/science/article/pii/S0014305713000645>
- Abdal-hay, A., Tijing, L. D., & Lim, J. K. (2013). Characterization of the surface biocompatibility of an electrospun nylon 6/CaP nanofiber scaffold using osteoblasts. *Chemical Engineering Journal*, 215–216, 57-64. doi: <http://dx.doi.org/10.1016/j.cej.2012.10.046>. Repéré à <http://www.sciencedirect.com/science/article/pii/S1385894712013836>
- Agarwal, S., Wendorff, J. H., & Greiner, A. (2008). Use of electrospinning technique for biomedical applications. *Polymer*, 49(26), 5603-5621. doi: <http://dx.doi.org/10.1016/j.polymer.2008.09.014>. Repéré à <http://www.sciencedirect.com/science/article/pii/S0032386108007994>
- Aghdam, R. M., Najarian, S., Shakhesi, S., Khanlari, S., Shaabani, K., & Sharifi, S. (2012). Investigating the effect of PGA on physical and mechanical properties of electrospun PCL/PGA blend nanofibers. *Journal of Applied Polymer Science*, 124(1), 123-131. doi: 10.1002/app.35071. Repéré à <http://dx.doi.org/10.1002/app.35071>
- Alexandridis, P., & Alan Hatton, T. (1995). Poly(ethylene oxide) • poly(propylene oxide) • poly(ethylene oxide) block copolymer surfactants in aqueous solutions and at interfaces: thermodynamics, structure, dynamics, and modeling. *Colloids and Surfaces A: Physicochemical and Engineering Aspects*, 96(1–2), 1-46. doi: [http://dx.doi.org/10.1016/0927-7757\(94\)03028-X](http://dx.doi.org/10.1016/0927-7757(94)03028-X). Repéré à <http://www.sciencedirect.com/science/article/pii/092777579403028X>
- Araki, J. (2013). Electrostatic or steric? - preparations and characterizations of well-dispersed systems containing rod-like nanowhiskers of crystalline polysaccharides. *Soft Matter*, 9(16), 4125-4141. doi: 10.1039/C3SM27514K. Repéré à <http://dx.doi.org/10.1039/C3SM27514K>

- Araujo, J. V., Martins, A., Leonor, I. B., Pinho, E. D., Reis, R. L., & Neves, N. M. (2008). Surface controlled biomimetic coating of polycaprolactone nanofiber meshes to be used as bone extracellular matrix analogues. *Journal of Biomaterials Science, Polymer Edition*, 19(10), 1261-1278. doi: 10.1163/156856208786052335. Repéré à <http://dx.doi.org/10.1163/156856208786052335>
- Aussawasathien, D., Dong, J. H., & Dai, L. (2005). Electrospun polymer nanofiber sensors. *Synthetic Metals*, 154(1-3), 37-40. doi: <http://dx.doi.org/10.1016/j.synthmet.2005.07.018>. Repéré à <http://www.sciencedirect.com/science/article/pii/S0379677905004649>
- Banerjee, I., Pangule, R. C., & Kane, R. S. (2011). Antifouling Coatings: Recent Developments in the Design of Surfaces That Prevent Fouling by Proteins, Bacteria, and Marine Organisms. *Advanced Materials*, 23(6), 690-718. doi: 10.1002/adma.201001215. Repéré à <http://dx.doi.org/10.1002/adma.201001215>
- Bhardwaj, N., & Kundu, S. C. (2010). Electrospinning: a fascinating fiber fabrication technique. *Biotechnology advances*, 28(3), 325-347. doi: 10.1016/j.biotechadv.2010.01.004. Repéré à <http://www.ncbi.nlm.nih.gov/pubmed/20100560>
- Bico, J., Marzolin, C., & Quéré, D. (1999). Pearl drops. *EPL (Europhysics Letters)*, 47(2), 220.
- Bico, J., Thiele, U., & Quéré, D. (2002). Wetting of textured surfaces. *Colloids and Surfaces A: Physicochemical and Engineering Aspects*, 206(1), 41-46.
- Bico, J., Tordeux, C., & Quéré, D. (2001). Rough wetting. *EPL (Europhysics Letters)*, 55(2), 214. Repéré à <http://stacks.iop.org/0295-5075/55/i=2/a=214>
- Bishi, D. K., Mathapati, S., Venugopal, J. R., Guhathakurta, S., Cherian, K. M., Ramakrishna, S., & Verma, R. S. (2013). Trans-differentiation of human mesenchymal stem cells generates functional hepatospheres on poly(l-lactic acid)-co-poly(?-caprolactone)/collagen nanofibrous scaffolds. *Journal of Materials Chemistry B*, 1(32), 3972-3984. doi: 10.1039/C3TB20241K. Repéré à <http://dx.doi.org/10.1039/C3TB20241K>
- Brandrup, J., Immergut, E. H., Grulke, E. A., Abe, A., & Bloch, D. R. (1989). *Polymer handbook* (Vol. 7). Wiley New York etc.

- Callies, M., & Quere, D. (2005). On water repellency. *Soft Matter*, 1(1), 55-61. doi: 10.1039/B501657F. Repéré à <http://dx.doi.org/10.1039/B501657F>
- Campoy-Quiles, M., Ferenczi, T., Agostinelli, T., Etchegoin, P. G., Kim, Y., Anthopoulos, T. D., . . . Nelson, J. (2008). Morphology evolution via self-organization and lateral and vertical diffusion in polymer:fullerene solar cell blends. *Nat Mater*, 7(2), 158-164. doi: [http://www.nature.com/nmat/journal/v7/n2/supinfo/nmat2102\\_S1.html](http://www.nature.com/nmat/journal/v7/n2/supinfo/nmat2102_S1.html). Repéré à <http://dx.doi.org/10.1038/nmat2102>
- Cécile, C., & Hsieh, Y.-L. (2010). Hydrophilic polystyrene/maleic anhydride ultrafine fibrous membranes. *Journal of Applied Polymer Science*, 115(2), 723-730. doi: 10.1002/app.31003. Repéré à <http://dx.doi.org/10.1002/app.31003>
- Chandrasekaran, A. R., Venugopal, J., Sundarrajan, S., & Ramakrishna, S. (2011). Fabrication of a nanofibrous scaffold with improved bioactivity for culture of human dermal fibroblasts for skin regeneration. *Biomedical Materials*, 6(1), 015001. Repéré à <http://stacks.iop.org/1748-605X/6/i=1/a=015001>
- Cho, S. J., Nam, H., Ryu, H., & Lim, G. (2013). A Rubberlike Stretchable Fibrous Membrane with Anti-Wettability and Gas Breathability. *Advanced Functional Materials*, 23(45), 5577-5584. doi: 10.1002/adfm.201300442. Repéré à <http://dx.doi.org/10.1002/adfm.201300442>
- Cho, W. J., Kim, J. H., Oh, S. H., Nam, H. H., Kim, J. M., & Lee, J. H. (2009). Hydrophilized polycaprolactone nanofiber mesh-embedded poly(glycolic-co-lactic acid) membrane for effective guided bone regeneration. *Journal of Biomedical Materials Research Part A*, 91A(2), 400-407. doi: 10.1002/jbm.a.32264. Repéré à <http://dx.doi.org/10.1002/jbm.a.32264>
- Clarke, A., Blake, T. D., Carruthers, K., & Woodward, A. (2002). Spreading and Imbibition of Liquid Droplets on Porous Surfaces. *Langmuir*, 18(8), 2980-2984. doi: 10.1021/la0117810. Repéré à <http://dx.doi.org/10.1021/la0117810>
- Corey, J. M., Gertz, C. C., Wang, B.-S., Birrell, L. K., Johnson, S. L., Martin, D. C., & Feldman, E. L. (2008). The design of electrospun PLLA nanofiber scaffolds compatible with serum-free growth of primary motor and sensory neurons. *Acta*

*biomaterialia*, 4(4), 863-875. doi: <http://dx.doi.org/10.1016/j.actbio.2008.02.020>.

Repéré à <http://www.sciencedirect.com/science/article/pii/S1742706108000470>

Correia, D. M., Ribeiro, C., Sencadas, V., Botelho, G., Carabineiro, S. A. C., Ribelles, J. L. G., & Lanceros-Méndez, S. (2015). Influence of oxygen plasma treatment parameters on poly(vinylidene fluoride) electrospun fiber mats wettability. *Progress in Organic Coatings*, 85, 151-158. doi: <http://dx.doi.org/10.1016/j.porgcoat.2015.03.019>. Repéré à <http://www.sciencedirect.com/science/article/pii/S0300944015001009>

Courbin, L., Bird, J. C., Reyssat, M., & Stone, H. A. (2009). Dynamics of wetting: from inertial spreading to viscous imbibition. *Journal of Physics: Condensed Matter*, 21(46), 464127. Repéré à <http://stacks.iop.org/0953-8984/21/i=46/a=464127>

Croll, T. I., O'Connor, A. J., Stevens, G. W., & Cooper-White, J. J. (2004). Controllable Surface Modification of Poly(lactic-co-glycolic acid) (PLGA) by Hydrolysis or Aminolysis I: Physical, Chemical, and Theoretical Aspects. *Biomacromolecules*, 5(2), 463-473. doi: 10.1021/bm0343040. Repéré à <http://dx.doi.org/10.1021/bm0343040>

Cui, W., Li, X., Xie, C., Chen, J., Zou, J., Zhou, S., & Weng, J. (2010). Controllable growth of hydroxyapatite on electrospun poly(dl-lactide) fibers grafted with chitosan as potential tissue engineering scaffolds. *Polymer*, 51(11), 2320-2328. doi: <http://dx.doi.org/10.1016/j.polymer.2010.03.037>. Repéré à <http://www.sciencedirect.com/science/article/pii/S0032386110002636>

Darmanin, T., & Guittard, F. (2014). Recent advances in the potential applications of bioinspired superhydrophobic materials. *Journal of Materials Chemistry A*, 2(39), 16319-16359. doi: 10.1039/C4TA02071E. Repéré à <http://dx.doi.org/10.1039/C4TA02071E>

De Schoenmaker, B., Van der Schueren, L., De Vrieze, S., Westbroek, P., & De Clerck, K. (2011). Wicking properties of various polyamide nanofibrous structures with an optimized method. *Journal of Applied Polymer Science*, 120(1), 305-310. doi: 10.1002/app.33117. Repéré à <http://dx.doi.org/10.1002/app.33117>

Deitzel, J. M., Kleinmeyer, J., Harris, D., & Beck Tan, N. C. (2001). The effect of processing variables on the morphology of electrospun nanofibers and textiles. *Polymer*, 42(1), 261-272. doi: [http://dx.doi.org/10.1016/S0032-3861\(00\)00250-0](http://dx.doi.org/10.1016/S0032-3861(00)00250-0). Repéré à <http://www.sciencedirect.com/science/article/pii/S0032386100002500>

- Desmet, T., Morent, R., Geyter, N. D., Leys, C., Schacht, E., & Dubruel, P. (2009). Nonthermal Plasma Technology as a Versatile Strategy for Polymeric Biomaterials Surface Modification: A Review. *Biomacromolecules*, *10*(9), 2351-2378. doi: 10.1021/bm900186s. Repéré à <http://dx.doi.org/10.1021/bm900186s>
- Ding, B., Li, C., Hotta, Y., Kim, J., Kuwaki, O., & Shiratori, S. (2006). Conversion of an electrospun nanofibrous cellulose acetate mat from a super-hydrophilic to super-hydrophobic surface. *Nanotechnology*, *17*(17), 4332. Repéré à <http://stacks.iop.org/0957-4484/17/i=17/a=009>
- Ding, B., Ogawa, T., Kim, J., Fujimoto, K., & Shiratori, S. (2008). Fabrication of a super-hydrophobic nanofibrous zinc oxide film surface by electrospinning. *Thin Solid Films*, *516*(9), 2495-2501. doi: <http://dx.doi.org/10.1016/j.tsf.2007.04.086>. Repéré à <http://www.sciencedirect.com/science/article/pii/S0040609007006906>
- Dolci, L. S., Quiroga, S. D., Gherardi, M., Laurita, R., Liguori, A., Sanibondi, P., . . . Focarete, M. L. (2014). Carboxyl Surface Functionalization of Poly(L-lactic acid) Electrospun Nanofibers through Atmospheric Non-Thermal Plasma Affects Fibroblast Morphology. *Plasma Processes and Polymers*, *11*(3), 203-213. doi: 10.1002/ppap.201300104. Repéré à <http://dx.doi.org/10.1002/ppap.201300104>
- Dong, Y., Kong, J., Phua, S. L., Zhao, C., Thomas, N. L., & Lu, X. (2014). Tailoring Surface Hydrophilicity of Porous Electrospun Nanofibers to Enhance Capillary and Push–Pull Effects for Moisture Wicking. *ACS Applied Materials & Interfaces*, *6*(16), 14087-14095. doi: 10.1021/am503417w. Repéré à <http://dx.doi.org/10.1021/am503417w>
- Doshi, J. R., Darrell H. (1995). Electrospinning Process and Applications of Electrospun Fibers. *Journal of Electrostatics*, *35*(2), 151-160. doi: 10.1016/0304-3886(95)00041-8
- Duan, B., Yuan, X., Zhu, Y., Zhang, Y., Li, X., Zhang, Y., & Yao, K. (2006). A nanofibrous composite membrane of PLGA–chitosan/PVA prepared by electrospinning. *European Polymer Journal*, *42*(9), 2013-2022. doi: <http://dx.doi.org/10.1016/j.eurpolymj.2006.04.021>. Repéré à <http://www.sciencedirect.com/science/article/pii/S0014305706001479>

- Duan, Y., Wang, Z., Yan, W., Wang, S., Zhang, S., & Jia, J. (2007). Preparation of collagen-coated electrospun nanofibers by remote plasma treatment and their biological properties. *Journal of Biomaterials Science, Polymer Edition*, 18(9), 1153-1164. doi: 10.1163/156856207781554019. Repéré à <http://dx.doi.org/10.1163/156856207781554019>
- Dufficy, M. K., Geiger, M. T., Bonino, C. A., & Khan, S. A. (2015). Electrospun Ultrafine Fiber Composites Containing Fumed Silica: From Solution Rheology to Materials with Tunable Wetting. *Langmuir*, 31(45), 12455-12463. doi: 10.1021/acs.langmuir.5b03545. Repéré à <http://dx.doi.org/10.1021/acs.langmuir.5b03545>
- Feng, L., Zhang, Y., Xi, J., Zhu, Y., Wang, N., Xia, F., & Jiang, L. (2008). Petal Effect: A Superhydrophobic State with High Adhesive Force. *Langmuir*, 24(8), 4114-4119. doi: 10.1021/la703821h. Repéré à <http://dx.doi.org/10.1021/la703821h>
- Ferrero, F. (2003). Wettability measurements on plasma treated synthetic fabrics by capillary rise method. *Polymer Testing*, 22(5), 571-578. doi: [http://dx.doi.org/10.1016/S0142-9418\(02\)00153-8](http://dx.doi.org/10.1016/S0142-9418(02)00153-8). Repéré à <http://www.sciencedirect.com/science/article/pii/S0142941802001538>
- Filip, D., Macocinschi, D., Paslaru, E., Munteanu, B. S., Dumitriu, R. P., Lungu, M., & Vasile, C. (2014). Polyurethane biocompatible silver bionanocomposites for biomedical applications. *Journal of Nanoparticle Research*, 16(11), 2710. doi: 10.1007/s11051-014-2710-x. Repéré à <http://dx.doi.org/10.1007/s11051-014-2710-x>
- Fortunato, G., Guex, A. G., Popa, A. M., Rossi, R. M., & Hufenus, R. (2014). Molecular weight driven structure formation of PEG based e-spun polymer blend fibres. *Polymer*, 55(14), 3139-3148. doi: <http://dx.doi.org/10.1016/j.polymer.2014.04.053>. Repéré à <http://www.sciencedirect.com/science/article/pii/S0032386114003656>
- Ganesh, V. A., Nair, A. S., Raut, H. K., Walsh, T. M., & Ramakrishna, S. (2012). Photocatalytic superhydrophilic TiO<sub>2</sub> coating on glass by electrospinning. *RSC Advances*, 2(5), 2067-2072.
- Geoghegan, M., & Krausch, G. (2003). Wetting at polymer surfaces and interfaces. *Progress in Polymer Science*, 28(2), 261-302. doi: [http://dx.doi.org/10.1016/S0079-6700\(02\)00080-1](http://dx.doi.org/10.1016/S0079-6700(02)00080-1). Repéré à <http://www.sciencedirect.com/science/article/pii/S0079670002000801>

- Ghofraniha, N., Tamborini, E., Oberdisse, J., Cipelletti, L., & Ramos, L. (2012). Grain refinement and partitioning of impurities in the grain boundaries of a colloidal polycrystal. *Soft Matter*, 8(23), 6214-6219. doi: 10.1039/C2SM25488C. Repéré à <http://dx.doi.org/10.1039/C2SM25488C>
- Gleason, K. K. (2015). Overview of Chemically Vapor Deposited (CVD) Polymers. Dans *CVD Polymers* (pp. 1-11). Wiley-VCH Verlag GmbH & Co. KGaA. doi: 10.1002/9783527690275.ch1. Repéré à <http://dx.doi.org/10.1002/9783527690275.ch1>
- Gopal, R., Kaur, S., Ma, Z., Chan, C., Ramakrishna, S., & Matsuura, T. (2006). Electrospun nanofibrous filtration membrane. *Journal of Membrane Science*, 281(1-2), 581-586. doi: <http://dx.doi.org/10.1016/j.memsci.2006.04.026>. Repéré à <http://www.sciencedirect.com/science/article/pii/S0376738806002651>
- Grynyov, R., Bormashenko, E., Whyman, G., Bormashenko, Y., Musin, A., Pogreb, R., . . . Kolagatla, S. (2016). Superoleophobic Surfaces Obtained via Hierarchical Metallic Meshes. *Langmuir*, 32(17), 4134-4140. doi: 10.1021/acs.langmuir.6b00248. Repéré à <http://dx.doi.org/10.1021/acs.langmuir.6b00248>
- Guo, M., Ding, B., Li, X., Wang, X., Yu, J., & Wang, M. (2010). Amphiphobic Nanofibrous Silica Mats with Flexible and High-Heat-Resistant Properties. *The Journal of Physical Chemistry C*, 114(2), 916-921. doi: 10.1021/jp909672r. Repéré à <http://dx.doi.org/10.1021/jp909672r>
- Hacker, C., Karahaliloglu, Z., Seide, G., Denkbaz, E. B., & Gries, T. (2014). Functionally modified, melt-electrospun thermoplastic polyurethane mats for wound-dressing applications. *Journal of Applied Polymer Science*, 131(8), n/a-n/a. doi: 10.1002/app.40132. Repéré à <http://dx.doi.org/10.1002/app.40132>
- Hakamada, Y., Ohgushi, N., Fujimura-Kondo, N., & Matsuda, T. (2012). Electrospun Poly( $\gamma$ -Benzyl-L-Glutamate) and Its Alkali-Treated Meshes: Their Water Wettability and Cell-Adhesion Potential. *Journal of Biomaterials Science, Polymer Edition*, 23(8), 1055-1067. doi: 10.1163/092050611X572057. Repéré à <http://dx.doi.org/10.1163/092050611X572057>

- Herminghaus, S. (2000). Roughness-induced non-wetting. *EPL (Europhysics Letters)*, 52(2), 165. Repéré à <http://stacks.iop.org/0295-5075/52/i=2/a=165>
- Hotaling, N. A., Bharti, K., Kriel, H., & Simon Jr, C. G. (2015). DiameterJ: A validated open source nanofiber diameter measurement tool. *Biomaterials*, 61, 327-338. doi: <http://dx.doi.org/10.1016/j.biomaterials.2015.05.015>. Repéré à <http://www.sciencedirect.com/science/article/pii/S0142961215004652>
- Hu, H.-T., Lee, S.-Y., Chen, C.-C., Yang, Y.-C., & Yang, J.-C. (2013). Processing and properties of hydrophilic electrospun polylactic acid/beta-tricalcium phosphate membrane for dental applications. *Polymer Engineering & Science*, 53(4), 833-842. doi: 10.1002/pen.23329. Repéré à <http://dx.doi.org/10.1002/pen.23329>
- Huang, L., Arena, J. T., Manickam, S. S., Jiang, X., Willis, B. G., & McCutcheon, J. R. (2014). Improved mechanical properties and hydrophilicity of electrospun nanofiber membranes for filtration applications by dopamine modification. *Journal of Membrane Science*, 460, 241-249. doi: <http://dx.doi.org/10.1016/j.memsci.2014.01.045>. Repéré à <http://www.sciencedirect.com/science/article/pii/S0376738814000581>
- Hutmacher, D. W. (2000). Scaffolds in tissue engineering bone and cartilage. *Biomaterials*, 21(24), 2529-2543. doi: [http://dx.doi.org/10.1016/S0142-9612\(00\)00121-6](http://dx.doi.org/10.1016/S0142-9612(00)00121-6). Repéré à <http://www.sciencedirect.com/science/article/pii/S0142961200001216>
- Hwa Hong, K., & Jin Kang, T. (2006). Hydraulic permeabilities of PET and nylon 6 electrospun fiber webs. *Journal of Applied Polymer Science*, 100(1), 167-177. doi: 10.1002/app.22651. Repéré à <http://dx.doi.org/10.1002/app.22651>
- Ishino, C., Reyssat, M., Reyssat, E., Okumura, K., & Quéré, D. (2007). Wicking within forests of micropillars. *EPL (Europhysics Letters)*, 79(5), 56005. Repéré à <http://stacks.iop.org/0295-5075/79/i=5/a=56005>
- Ito, Y., Hasuda, H., Kamitakahara, M., Ohtsuki, C., Tanihara, M., Kang, I. K., & Kwon, O. H. (2005). A composite of hydroxyapatite with electrospun biodegradable nanofibers as a tissue engineering material. *Journal of bioscience and bioengineering*, 100(1), 43-49. doi: 10.1263/jbb.100.43. Repéré à <http://www.ncbi.nlm.nih.gov/pubmed/16233849>

- Jang, W., Yun, J., Jeon, K., & Byun, H. (2015). PVdF/graphene oxide hybrid membranes via electrospinning for water treatment applications. *RSC Advances*, 5(58), 46711-46717. doi: 10.1039/C5RA04439A. Repéré à <http://dx.doi.org/10.1039/C5RA04439A>
- Jeon, H., & Kim, G. (2014). Preparation and characterization of an electrospun polycaprolactone (PCL) fibrous mat and multi-layered PCL scaffolds having a nanosized pattern-surface for tissue regeneration. *Journal of Materials Chemistry B*, 2(2), 171-180. doi: 10.1039/C3TB21230K. Repéré à <http://dx.doi.org/10.1039/C3TB21230K>
- Ji, Y., Liang, K., Shen, X., & Bowlin, G. L. (2014). Electrospinning and characterization of chitin nanofibril/polycaprolactone nanocomposite fiber mats. *Carbohydrate Polymers*, 101, 68-74. doi: <http://dx.doi.org/10.1016/j.carbpol.2013.09.012>. Repéré à <http://www.sciencedirect.com/science/article/pii/S0144861713009028>
- Jiang, L., Zhao, Y., & Zhai, J. (2004). A Lotus-Leaf-like Superhydrophobic Surface: A Porous Microsphere/Nanofiber Composite Film Prepared by Electrohydrodynamics. *Angewandte Chemie*, 116(33), 4438-4441. doi: 10.1002/ange.200460333. Repéré à <http://dx.doi.org/10.1002/ange.200460333>
- Joshi, M. K., Tiwari, A. P., Pant, H. R., Shrestha, B. K., Kim, H. J., Park, C. H., & Kim, C. S. (2015). In Situ Generation of Cellulose Nanocrystals in Polycaprolactone Nanofibers: Effects on Crystallinity, Mechanical Strength, Biocompatibility, and Biomimetic Mineralization. *ACS Applied Materials & Interfaces*, 7(35), 19672-19683. doi: 10.1021/acsami.5b04682. Repéré à <http://dx.doi.org/10.1021/acsami.5b04682>
- Kabanov, A. V., Batrakova, E. V., & Alakhov, V. Y. (2002). Pluronic® block copolymers as novel polymer therapeutics for drug and gene delivery. *Journal of Controlled Release*, 82(2-3), 189-212. doi: [http://dx.doi.org/10.1016/S0168-3659\(02\)00009-3](http://dx.doi.org/10.1016/S0168-3659(02)00009-3). Repéré à <http://www.sciencedirect.com/science/article/pii/S0168365902000093>
- Kaur, S., Ma, Z., Gopal, R., Singh, G., Ramakrishna, S., & Matsuura, T. (2007). Plasma-Induced Graft Copolymerization of Poly(methacrylic acid) on Electrospun Poly(vinylidene fluoride) Nanofiber Membrane. *Langmuir*, 23(26), 13085-13092. doi: 10.1021/la701329r. Repéré à <http://dx.doi.org/10.1021/la701329r>

- Kaur, S., Rana, D., Matsuura, T., Sundarrajan, S., & Ramakrishna, S. (2012). Preparation and characterization of surface modified electrospun membranes for higher filtration flux. *Journal of Membrane Science*, 390–391(0), 235-242. doi: <http://dx.doi.org/10.1016/j.memsci.2011.11.045>. Repéré à <http://www.sciencedirect.com/science/article/pii/S0376738811008726>
- Kedroňová, E., Zajíčková, L., Hegemann, D., Klíma, M., Michlíček, M., & Manakhov, A. (2015). Plasma Enhanced CVD of Organosilicon Thin Films on Electrospun Polymer Nanofibers. *Plasma Processes and Polymers*, 12(11), 1231-1243. doi: 10.1002/ppap.201400235. Repéré à <http://dx.doi.org/10.1002/ppap.201400235>
- Kell, M. (1996). Structural studies of aqueous solutions of PEO - PPO - PEO triblock copolymers, their micellar aggregates and mesophases; a small-angle neutron scattering study. *Journal of Physics: Condensed Matter*, 8(25A), A103. Repéré à <http://stacks.iop.org/0953-8984/8/i=25A/a=008>
- Khatri, Z., Wei, K., Kim, B.-S., & Kim, I.-S. (2012). Effect of deacetylation on wicking behavior of co-electrospun cellulose acetate/polyvinyl alcohol nanofibers blend. *Carbohydrate Polymers*, 87(3), 2183-2188. doi: <http://dx.doi.org/10.1016/j.carbpol.2011.10.046>. Repéré à <http://www.sciencedirect.com/science/article/pii/S0144861711009520>
- Kim, C. H., Khil, M. S., Kim, H. Y., Lee, H. U., & Jahng, K. Y. (2006). An improved hydrophilicity via electrospinning for enhanced cell attachment and proliferation. *Journal of Biomedical Materials Research Part B: Applied Biomaterials*, 78B(2), 283-290. doi: 10.1002/jbm.b.30484. Repéré à <http://dx.doi.org/10.1002/jbm.b.30484>
- Kim, H. S., Ham, H. O., Son, Y. J., Messersmith, P. B., & Yoo, H. S. (2013). Electrospun catechol-modified poly(ethyleneglycol) nanofibrous mesh for anti-fouling properties. *Journal of Materials Chemistry B*, 1(32), 3940-3949. doi: 10.1039/C3TB20444H. Repéré à <http://dx.doi.org/10.1039/C3TB20444H>
- Kim, K., Luu, Y. K., Chang, C., Fang, D., Hsiao, B. S., Chu, B., & Hadjiargyrou, M. (2004). Incorporation and controlled release of a hydrophilic antibiotic using poly(lactide-co-glycolide)-based electrospun nanofibrous scaffolds. *Journal of Controlled Release*, 98(1), 47-56. doi: <http://dx.doi.org/10.1016/j.jconrel.2004.04.009>. Repéré à <http://www.sciencedirect.com/science/article/pii/S0168365904001932>
- Kim, K., Yu, M., Zong, X., Chiu, J., Fang, D., Seo, Y.-S., . . . Hadjiargyrou, M. (2003a). Control of degradation rate and hydrophilicity in electrospun non-woven poly (D, L-

lactide) nanofiber scaffolds for biomedical applications. *Biomaterials*, 24(27), 4977-4985.

- Kim, K., Yu, M., Zong, X., Chiu, J., Fang, D., Seo, Y.-S., . . . Hadjiargyrou, M. (2003b). Control of degradation rate and hydrophilicity in electrospun non-woven poly(D,L-lactide) nanofiber scaffolds for biomedical applications. *Biomaterials*, 24(27), 4977-4985. doi: [http://dx.doi.org/10.1016/S0142-9612\(03\)00407-1](http://dx.doi.org/10.1016/S0142-9612(03)00407-1). Repéré à <http://www.sciencedirect.com/science/article/pii/S0142961203004071>
- Kolahchi, A. R. (2014). *Polyethylene Terephthalate (PET) Films Surface Modification Through Blending* (École Polytechnique de Montréal).
- Kota, A. K., Li, Y., Mabry, J. M., & Tuteja, A. (2012). Hierarchically Structured Superoleophobic Surfaces with Ultralow Contact Angle Hysteresis. *Advanced Materials*, 24(43), 5838-5843. doi: 10.1002/adma.201202554. Repéré à <http://dx.doi.org/10.1002/adma.201202554>
- Kronberg, B., Holmberg, K., & Lindman, B. (2014). *Surface chemistry of surfactants and polymers*. John Wiley & Sons. Repéré à <https://books.google.ca/books?id=11CnBAAQBAJ&lpg=PA137&ots=RSWwiSabKK&dq=Surface%20Chemistry%20of%20Surfactants%20and%20Polymers&lr&pg=PA137#v=onepage&q=Surface%20Chemistry%20of%20Surfactants%20and%20Polymers&f=false>
- Kurusu, R. S., & Demarquette, N. R. (2015). Blending and Morphology Control To Turn Hydrophobic SEBS Electrospun Mats Superhydrophilic. *Langmuir*, 31(19), 5495-5503. doi: 10.1021/acs.langmuir.5b00814. Repéré à <http://dx.doi.org/10.1021/acs.langmuir.5b00814>
- Kurusu, R. S., & Demarquette, N. R. (2016). Wetting of Hydrophilic Electrospun Mats Produced by Blending SEBS with PEO–PPO–PEO Copolymers of Different Molecular Weight. *Langmuir*, 32(7), 1846-1853. doi: 10.1021/acs.langmuir.5b04287. Repéré à <http://dx.doi.org/10.1021/acs.langmuir.5b04287>
- Kurusu, R. S., Demarquette, N. R., Gauthier, C., & Chenal, J.-M. (2014). Effect of ageing and annealing on the mechanical behaviour and biodegradability of a poly(3-hydroxybutyrate) and poly(ethylene-co-methyl-acrylate-co-glycidyl-

- methacrylate)blend. *Polymer International*, 63(6), 1085-1093. doi: 10.1002/pi.4616. Repéré à <http://dx.doi.org/10.1002/pi.4616>
- Lee, J. H., Ju, Y. M., & Kim, D. M. (2000). Platelet adhesion onto segmented polyurethane film surfaces modified by addition and crosslinking of PEO-containing block copolymers. *Biomaterials*, 21(7), 683-691. doi: [http://dx.doi.org/10.1016/S0142-9612\(99\)00197-0](http://dx.doi.org/10.1016/S0142-9612(99)00197-0). Repéré à <http://www.sciencedirect.com/science/article/pii/S0142961299001970>
- Lee, M., Lee, T., & Park, W. (2013). Highly hydrophobic nanofibrous surfaces generated by poly(vinylidene fluoride). *Fibers and Polymers*, 14(8), 1271-1275. doi: 10.1007/s12221-013-1271-4. Repéré à <http://dx.doi.org/10.1007/s12221-013-1271-4>
- Lee, M. W., An, S., Latthe, S. S., Lee, C., Hong, S., & Yoon, S. S. (2013). Electrospun Polystyrene Nanofiber Membrane with Superhydrophobicity and Superoleophilicity for Selective Separation of Water and Low Viscous Oil. *ACS Applied Materials & Interfaces*, 5(21), 10597-10604. doi: 10.1021/am404156k. Repéré à <http://dx.doi.org/10.1021/am404156k>
- Lembach, A. N., Tan, H.-B., Roisman, I. V., Gambaryan-Roisman, T., Zhang, Y., Tropea, C., & Yarin, A. L. (2010). Drop Impact, Spreading, Splashing, and Penetration into Electrospun Nanofiber Mats. *Langmuir*, 26(12), 9516-9523. doi: 10.1021/la100031d. Repéré à <http://dx.doi.org/10.1021/la100031d>
- Li, D., Wang, Y., & Xia, Y. (2003). Electrospinning of Polymeric and Ceramic Nanofibers as Uniaxially Aligned Arrays. *Nano Letters*, 3(8), 1167-1171. doi: 10.1021/nl0344256. Repéré à <http://dx.doi.org/10.1021/nl0344256>
- Li, G., Zhao, Y., Lv, M., Shi, Y., & Cao, D. (2013). Super hydrophilic poly(ethylene terephthalate) (PET)/poly(vinyl alcohol) (PVA) composite fibrous mats with improved mechanical properties prepared via electrospinning process. *Colloids and Surfaces A: Physicochemical and Engineering Aspects*, 436(0), 417-424. doi: <http://dx.doi.org/10.1016/j.colsurfa.2013.07.014>. Repéré à <http://www.sciencedirect.com/science/article/pii/S0927775713005700>
- Li, J., Cao, J., Wei, Z., Yang, M., Yin, W., Yu, K., . . . Leng, J. (2014). Electrospun silica/naion hybrid products: mechanical property improvement, wettability tuning and periodic structure adjustment. *Journal of Materials Chemistry A*, 2(39), 16569-16576. doi: 10.1039/C4TA03183K. Repéré à <http://dx.doi.org/10.1039/C4TA03183K>

- Li, L., Qian, Y., Lin, C., Li, H., Jiang, C., Lv, Y., . . . Yang, L. (2015). The effect of silk gland sericin protein incorporation into electrospun polycaprolactone nanofibers on in vitro and in vivo characteristics. *Journal of Materials Chemistry B*, 3(5), 859-870. doi: 10.1039/C4TB00653D. Repéré à <http://dx.doi.org/10.1039/C4TB00653D>
- Li, M., Mondrinos, M. J., Chen, X., Gandhi, M. R., Ko, F. K., & Lelkes, P. I. (2006). Co-electrospun poly(lactide-co-glycolide), gelatin, and elastin blends for tissue engineering scaffolds. *Journal of Biomedical Materials Research Part A*, 79A(4), 963-973. doi: 10.1002/jbm.a.30833. Repéré à <http://dx.doi.org/10.1002/jbm.a.30833>
- Li, X., Wang, M., Wang, C., Cheng, C., & Wang, X. (2014). Facile Immobilization of Ag Nanocluster on Nanofibrous Membrane for Oil/Water Separation. *ACS Applied Materials & Interfaces*, 6(17), 15272-15282. doi: 10.1021/am503721k. Repéré à <http://dx.doi.org/10.1021/am503721k>
- Li, Y.-F., Rubert, M., Aslan, H., Yu, Y., Howard, K. A., Dong, M., . . . Chen, M. (2014). Ultraporous interweaving electrospun microfibers from PCL-PEO binary blends and their inflammatory responses. *Nanoscale*, 6(6), 3392-3402. doi: 10.1039/C3NR06197C. Repéré à <http://dx.doi.org/10.1039/C3NR06197C>
- Li, Y., Zhu, Z., Yu, J., & Ding, B. (2015). Carbon Nanotubes Enhanced Fluorinated Polyurethane Macroporous Membranes for Waterproof and Breathable Application. *ACS Applied Materials & Interfaces*, 7(24), 13538-13546. doi: 10.1021/acsami.5b02848. Repéré à <http://dx.doi.org/10.1021/acsami.5b02848>
- Liang, D., Hsiao, B. S., & Chu, B. (2007). Functional electrospun nanofibrous scaffolds for biomedical applications. *Advanced drug delivery reviews*, 59(14), 1392-1412. doi: <http://dx.doi.org/10.1016/j.addr.2007.04.021>. Repéré à <http://www.sciencedirect.com/science/article/pii/S0169409X07001858>
- Lim, G. T., Puskas, J. E., Reneker, D. H., Jákli, A., & Horton, W. E. (2011). Highly Hydrophobic Electrospun Fiber Mats from Polyisobutylene-Based Thermoplastic Elastomers. *Biomacromolecules*, 12(5), 1795-1799. doi: 10.1021/bm200157b. Repéré à <http://dx.doi.org/10.1021/bm200157b>

- Lim, H. S., Park, S. H., Koo, S. H., Kwark, Y.-J., Thomas, E. L., Jeong, Y., & Cho, J. H. (2010). Superamphiphilic Janus Fabric. *Langmuir*, 26(24), 19159-19162. doi: 10.1021/la103829c. Repéré à <http://dx.doi.org/10.1021/la103829c>
- Lin, J., Ding, B., Yang, J., Yu, J., & Sun, G. (2012). Subtle regulation of the micro- and nanostructures of electrospun polystyrene fibers and their application in oil absorption. *Nanoscale*, 4(1), 176-182. doi: 10.1039/C1NR10895F. Repéré à <http://dx.doi.org/10.1039/C1NR10895F>
- Lin, J., Shang, Y., Ding, B., Yang, J., Yu, J., & Al-Deyab, S. S. (2012). Nanoporous polystyrene fibers for oil spill cleanup. *Marine Pollution Bulletin*, 64(2), 347-352. doi: <http://dx.doi.org/10.1016/j.marpolbul.2011.11.002>. Repéré à <http://www.sciencedirect.com/science/article/pii/S0025326X11005790>
- Lin, Q., Li, Y., & Yang, M. (2012). Highly sensitive and ultrafast response surface acoustic wave humidity sensor based on electrospun polyaniline/poly(vinyl butyral) nanofibers. *Analytica Chimica Acta*, 748, 73-80. doi: <http://dx.doi.org/10.1016/j.aca.2012.08.041>. Repéré à <http://www.sciencedirect.com/science/article/pii/S0003267012012718>
- Liu, H., & Hsieh, Y.-L. (2002). Ultrafine fibrous cellulose membranes from electrospinning of cellulose acetate. *Journal of Polymer Science Part B: Polymer Physics*, 40(18), 2119-2129. doi: 10.1002/polb.10261. Repéré à <http://dx.doi.org/10.1002/polb.10261>
- Liu, N.-h., Pan, J.-f., Miao, Y.-E., Liu, T.-x., Xu, F., & Sun, H. (2014). Electrospinning of poly ( $\epsilon$ -caprolactone-co-lactide)/Pluronic blended scaffolds for skin tissue engineering. *Journal of Materials Science*, 49(20), 7253-7262.
- Liu, X., Lin, T., Fang, J., Yao, G., Zhao, H., Dodson, M., & Wang, X. (2010). In vivo wound healing and antibacterial performances of electrospun nanofibre membranes. *Journal of Biomedical Materials Research Part A*, 94A(2), 499-508. doi: 10.1002/jbm.a.32718. Repéré à <http://dx.doi.org/10.1002/jbm.a.32718>
- Lochhead, R. Y., & Huisinga, L. R. (2004). A brief review of polymer/surfactant interaction. *Cosmetics and toiletries*, 119(2), 37-45.
- Lowery, J. L., Datta, N., & Rutledge, G. C. (2010). Effect of fiber diameter, pore size and seeding method on growth of human dermal fibroblasts in electrospun poly( $\epsilon$ -caprolactone) fibrous mats. *Biomaterials*, 31(3), 491-504. doi:

<http://dx.doi.org/10.1016/j.biomaterials.2009.09.072>. Repéré à  
<http://www.sciencedirect.com/science/article/pii/S0142961209010242>

- Lu, P., & Hsieh, Y.-L. (2010). Multiwalled Carbon Nanotube (MWCNT) Reinforced Cellulose Fibers by Electrospinning. *ACS Applied Materials & Interfaces*, 2(8), 2413-2420. doi: 10.1021/am1004128. Repéré à <http://dx.doi.org/10.1021/am1004128>
- Ma, M., Gupta, M., Li, Z., Zhai, L., Gleason, K. K., Cohen, R. E., . . . Rutledge, G. C. (2007). Decorated Electrospun Fibers Exhibiting Superhydrophobicity. *Advanced Materials*, 19(2), 255-259. doi: 10.1002/adma.200601449. Repéré à <http://dx.doi.org/10.1002/adma.200601449>
- Ma, M., Hill, R. M., Lowery, J. L., Fridrikh, S. V., & Rutledge, G. C. (2005). Electrospun Poly(Styrene-block-dimethylsiloxane) Block Copolymer Fibers Exhibiting Superhydrophobicity. *Langmuir*, 21(12), 5549-5554. doi: 10.1021/la047064y. Repéré à <http://dx.doi.org/10.1021/la047064y>
- Ma, M., Mao, Y., Gupta, M., Gleason, K. K., & Rutledge, G. C. (2005). Superhydrophobic Fabrics Produced by Electrospinning and Chemical Vapor Deposition. *Macromolecules*, 38(23), 9742-9748. doi: 10.1021/ma0511189. Repéré à <http://dx.doi.org/10.1021/ma0511189>
- Ma, Z., Kotaki, M., & Ramakrishna, S. (2005). Electrospun cellulose nanofiber as affinity membrane. *Journal of Membrane Science*, 265(1-2), 115-123. doi: <http://dx.doi.org/10.1016/j.memsci.2005.04.044>. Repéré à <http://www.sciencedirect.com/science/article/pii/S0376738805003790>
- Ma, Z., Kotaki, M., Yong, T., He, W., & Ramakrishna, S. (2005). Surface engineering of electrospun polyethylene terephthalate (PET) nanofibers towards development of a new material for blood vessel engineering. *Biomaterials*, 26(15), 2527-2536. doi: <http://dx.doi.org/10.1016/j.biomaterials.2004.07.026>. Repéré à <http://www.sciencedirect.com/science/article/pii/S0142961204006775>
- Marx, K. A. (2003). Quartz Crystal Microbalance: A Useful Tool for Studying Thin Polymer Films and Complex Biomolecular Systems at the Solution-Surface Interface. *Biomacromolecules*, 4(5), 1099-1120. doi: 10.1021/bm020116i. Repéré à <http://dx.doi.org/10.1021/bm020116i>

- Miyauchi, Y., Ding, B., & Shiratori, S. (2006). Fabrication of a silver-ragwort-leaf-like super-hydrophobic micro/nanoporous fibrous mat surface by electrospinning. *Nanotechnology*, 17(20), 5151. Repéré à <http://stacks.iop.org/0957-4484/17/i=20/a=019>
- Morent, R., De Geyter, N., Desmet, T., Dubruel, P., & Leys, C. (2011). Plasma Surface Modification of Biodegradable Polymers: A Review. *Plasma Processes and Polymers*, 8(3), 171-190. doi: 10.1002/ppap.201000153. Repéré à <http://dx.doi.org/10.1002/ppap.201000153>
- Morita, H., Kawakatsu, T., & Doi, M. (2001). Dynamic Density Functional Study on the Structure of Thin Polymer Blend Films with a Free Surface. *Macromolecules*, 34(25), 8777-8783. doi: 10.1021/ma010346+. Repéré à <http://dx.doi.org/10.1021/ma010346+>
- Muthiah, P., Hoppe, S. M., Boyle, T. J., & Sigmund, W. (2011). Thermally Tunable Surface Wettability of Electrospun Fiber Mats: Polystyrene/Poly(N-isopropylacrylamide) Blended versus Crosslinked Poly[(N-isopropylacrylamide)-co-(methacrylic acid)]. *Macromolecular Rapid Communications*, 32(21), 1716-1721. doi: 10.1002/marc.201100373. Repéré à <http://dx.doi.org/10.1002/marc.201100373>
- Nishimoto, S., & Bhushan, B. (2013). Bioinspired self-cleaning surfaces with superhydrophobicity, superoleophobicity, and superhydrophilicity. *RSC Advances*, 3(3), 671-690. doi: 10.1039/C2RA21260A. Repéré à <http://dx.doi.org/10.1039/C2RA21260A>
- Nosonovsky, M. (2007). On the Range of Applicability of the Wenzel and Cassie Equations. *Langmuir*, 23(19), 9919-9920. doi: 10.1021/la701324m. Repéré à <http://dx.doi.org/10.1021/la701324m>
- Nuraje, N., Khan, W. S., Lei, Y., Ceylan, M., & Asmatulu, R. (2013). Superhydrophobic electrospun nanofibers. *Journal of Materials Chemistry A*, 1(6), 1929-1946. doi: 10.1039/C2TA00189F. Repéré à <http://dx.doi.org/10.1039/C2TA00189F>
- Oh, S. H., & Lee, J. H. (2013). Hydrophilization of synthetic biodegradable polymer scaffolds for improved cell/tissue compatibility. *Biomedical Materials*, 8(1), 014101. Repéré à <http://stacks.iop.org/1748-605X/8/i=1/a=014101>

- Öner, D., & McCarthy, T. J. (2000). Ultrahydrophobic Surfaces. Effects of Topography Length Scales on Wettability. *Langmuir*, 16(20), 7777-7782. doi: 10.1021/la000598o. Repéré à <http://dx.doi.org/10.1021/la000598o>
- Owens, D. K., & Wendt, R. C. (1969). Estimation of the surface free energy of polymers. *Journal of Applied Polymer Science*, 13(8), 1741-1747. doi: 10.1002/app.1969.070130815. Repéré à <http://dx.doi.org/10.1002/app.1969.070130815>
- Özçam, A. E., Roskov, K. E., Genzer, J., & Spontak, R. J. (2012). Responsive PET Nano/Microfibers via Surface-Initiated Polymerization. *ACS Applied Materials & Interfaces*, 4(1), 59-64. doi: 10.1021/am201559f. Repéré à <http://dx.doi.org/10.1021/am201559f>
- Pai, C.-L., Boyce, M. C., & Rutledge, G. C. (2009). Morphology of Porous and Wrinkled Fibers of Polystyrene Electrospun from Dimethylformamide. *Macromolecules*, 42(6), 2102-2114. doi: 10.1021/ma802529h. Repéré à <http://dx.doi.org/10.1021/ma802529h>
- Park, K., Ju, Y. M., Son, J. S., Ahn, K.-D., & Han, D. K. (2007). Surface modification of biodegradable electrospun nanofiber scaffolds and their interaction with fibroblasts. *Journal of Biomaterials Science, Polymer Edition*, 18(4), 369-382. doi: 10.1163/156856207780424997. Repéré à <http://dx.doi.org/10.1163/156856207780424997>
- Park, S. H., Ryu, Y. S., & Kim, S. H. (2015). Effect of modified silica nanoparticle on the properties of bio-based polyurethane ultrafine fibers. *Journal of Materials Science*, 50(4), 1760-1769. doi: 10.1007/s10853-014-8739-5. Repéré à <http://dx.doi.org/10.1007/s10853-014-8739-5>
- Patankar, N. A. (2004). Mimicking the Lotus Effect: Influence of Double Roughness Structures and Slender Pillars. *Langmuir*, 20(19), 8209-8213. doi: 10.1021/la048629t. Repéré à <http://dx.doi.org/10.1021/la048629t>
- Persano, L., Dagdeviren, C., Su, Y., Zhang, Y., Girardo, S., Pisignano, D., . . . Rogers, J. A. (2013). High performance piezoelectric devices based on aligned arrays of nanofibers of poly (vinylidene fluoride-co-trifluoroethylene). *Nature communications*, 4, 1633.

- Pisuchpen, T., Chaim-ngoen, N., Intasanta, N., Supaphol, P., & Hoven, V. P. (2011). Tuning Hydrophobicity and Water Adhesion by Electrospinning and Silanization. *Langmuir*, 27(7), 3654-3661. doi: 10.1021/la104978e. Repéré à <http://dx.doi.org/10.1021/la104978e>
- Range, K., & Feuillebois, F. (1998). Influence of Surface Roughness on Liquid Drop Impact. *Journal of Colloid and Interface Science*, 203(1), 16-30. doi: <http://dx.doi.org/10.1006/jcis.1998.5518>. Repéré à <http://www.sciencedirect.com/science/article/pii/S0021979798955187>
- Rastogi, A. K., & St. Pierre, L. E. (1969). Papers Presented at the 43rd National Colloid Symposium Interfacial phenomena in macromolecular systems. *Journal of Colloid and Interface Science*, 31(2), 168-175. doi: [http://dx.doi.org/10.1016/0021-9797\(69\)90323-3](http://dx.doi.org/10.1016/0021-9797(69)90323-3). Repéré à <http://www.sciencedirect.com/science/article/pii/0021979769903233>
- Reneker, D. H., & Yarin, A. L. (2008). Electrospinning jets and polymer nanofibers. *Polymer*, 49(10), 2387-2425. doi: 10.1016/j.polymer.2008.02.002
- Reyssat, M., Pépin, A., Marty, F., Chen, Y., & Quéré, D. (2006). Bouncing transitions on microtextured materials. *EPL (Europhysics Letters)*, 74(2), 306. Repéré à <http://stacks.iop.org/0295-5075/74/i=2/a=306>
- Rezaei Kolahchi, A., Ajjji, A., & Carreau, P. J. (2014). Surface Morphology and Properties of Ternary Polymer Blends: Effect of the Migration of Minor Components. *The Journal of Physical Chemistry B*, 118(23), 6316-6323. doi: 10.1021/jp502081g. Repéré à <http://dx.doi.org/10.1021/jp502081g>
- Rezaei Kolahchi, A., Ajjji, A., & Carreau, P. J. (2015). Enhancing hydrophilicity of polyethylene terephthalate surface through melt blending. *Polymer Engineering & Science*, 55(2), 349-358. doi: 10.1002/pen.23910. Repéré à <http://dx.doi.org/10.1002/pen.23910>
- Rodriguez-Hernandez, J., Ibarboure, E., & Papon, E. (2011). Surface segregation of polypeptide-based block copolymer micelles: An approach to engineer nanostructured and stimuli responsive surfaces. *European Polymer Journal*, 47(11), 2063-2068. doi: <http://dx.doi.org/10.1016/j.eurpolymj.2011.07.011>. Repéré à <http://www.sciencedirect.com/science/article/pii/S001430571100259X>

- Rösler, A., Vandermeulen, G. W. M., & Klok, H.-A. (2012). Advanced drug delivery devices via self-assembly of amphiphilic block copolymers. *Advanced drug delivery reviews*, 64, Supplement, 270-279. doi: <http://dx.doi.org/10.1016/j.addr.2012.09.026>. Repéré à <http://www.sciencedirect.com/science/article/pii/S0169409X12002864>
- Rungswang, W., Kotaki, M., Shimojima, T., Kimura, G., Sakurai, S., & Chirachanchai, S. (2011a). Directing Thermoplastic Elastomer Microdomain Parallel to Fiber Axis: A Model Case of SEBS with Benzoxazine through  $\pi$ - $\pi$  Stacking. *Macromolecules*, 44(23), 9276-9285. doi: 10.1021/ma2017315. Repéré à <http://dx.doi.org/10.1021/ma2017315>
- Rungswang, W., Kotaki, M., Shimojima, T., Kimura, G., Sakurai, S., & Chirachanchai, S. (2011b). Existence of microdomain orientation in thermoplastic elastomer through a case study of SEBS electrospun fibers. *Polymer*, 52(3), 844-853. doi: <http://dx.doi.org/10.1016/j.polymer.2010.12.019>. Repéré à <http://www.sciencedirect.com/science/article/pii/S0032386110010876>
- Rungswang, W., Kotaki, M., Shimojima, T., Kimura, G., Sakurai, S., & Chirachanchai, S. (2014). Role of surfactant on inducing specific microdomains of block copolymer: An example case from polystyrene-b-poly(ethylene-co-1-butene)-b-polystyrene (SEBS) electrospun thermoplastic-elastomer fiber containing polyethylene glycol lauryl ether (PGLE). *Polymer*, 55(8), 2068-2076. doi: <http://dx.doi.org/10.1016/j.polymer.2014.02.057>. Repéré à <http://www.sciencedirect.com/science/article/pii/S0032386114001724>
- Rutledge, G. C., & Fridrikh, S. V. (2007). Formation of fibers by electrospinning. *Advanced drug delivery reviews*, 59(14), 1384-1391. doi: 10.1016/j.addr.2007.04.020. Repéré à <http://www.ncbi.nlm.nih.gov/pubmed/17889398>
- Sahu, R. P., Sinha-Ray, S., Yarin, A. L., & Pourdeyhimi, B. (2012). Drop impacts on electrospun nanofiber membranes. *Soft Matter*, 8(14), 3957-3970. doi: 10.1039/c2sm06744g. Repéré à <http://dx.doi.org/10.1039/C2SM06744G>
- Sas, I., Gorga, R. E., Joines, J. A., & Thoney, K. A. (2012). Literature review on superhydrophobic self-cleaning surfaces produced by electrospinning. *Journal of Polymer Science Part B: Polymer Physics*, 50(12), 824-845. doi: 10.1002/polb.23070. Repéré à <http://dx.doi.org/10.1002/polb.23070>

- Savoji, H., Lerouge, S., Aiji, A., & Wertheimer, M. R. (2015). Plasma-Etching for Controlled Modification of Structural and Mechanical Properties of Electrospun PET Scaffolds. *Plasma Processes and Polymers*, 12(4), 314-327. doi: 10.1002/ppap.201400147. Repéré à <http://dx.doi.org/10.1002/ppap.201400147>
- Savoji, H., Rana, D., Matsuura, T., Tabe, S., & Feng, C. (2013). Development of plasma and/or chemically induced graft co-polymerized electrospun poly(vinylidene fluoride) membranes for solute separation. *Separation and Purification Technology*, 108, 196-204. doi: <http://dx.doi.org/10.1016/j.seppur.2013.02.013>. Repéré à <http://www.sciencedirect.com/science/article/pii/S1383586613001007>
- Seveno, D., Ledauphin, V., Martic, G., Voué, M., & De Coninck, J. (2002). Spreading Drop Dynamics on Porous Surfaces. *Langmuir*, 18(20), 7496-7502. doi: 10.1021/la025520h. Repéré à <http://dx.doi.org/10.1021/la025520h>
- Shi, Q., Ye, S., Kristalyn, C., Su, Y., Jiang, Z., & Chen, Z. (2008). Probing Molecular-Level Surface Structures of Polyethersulfone/Pluronic F127 Blends Using Sum-Frequency Generation Vibrational Spectroscopy. *Langmuir*, 24(15), 7939-7946. doi: 10.1021/la800570a. Repéré à <http://dx.doi.org/10.1021/la800570a>
- Shimizu, R. N., & Demarquette, N. R. (2000). Evaluation of surface energy of solid polymers using different models. *Journal of Applied Polymer Science*, 76(12), 1831-1845. doi: 10.1002/(SICI)1097-4628(20000620)76:12<1831::AID-APP14>3.0.CO;2-Q. Repéré à [http://dx.doi.org/10.1002/\(SICI\)1097-4628\(20000620\)76:12<1831::AID-APP14>3.0.CO;2-Q](http://dx.doi.org/10.1002/(SICI)1097-4628(20000620)76:12<1831::AID-APP14>3.0.CO;2-Q)
- Shirtcliffe, N. J., McHale, G., Newton, M. I., Perry, C. C., & Roach, P. (2005). Porous materials show superhydrophobic to superhydrophilic switching. *Chemical Communications*, (25), 3135-3137. doi: 10.1039/B502896E. Repéré à <http://dx.doi.org/10.1039/B502896E>
- Sill, T. J., & von Recum, H. A. (2008). Electrospinning: applications in drug delivery and tissue engineering. *Biomaterials*, 29(13), 1989-2006. doi: 10.1016/j.biomaterials.2008.01.011. Repéré à <http://www.ncbi.nlm.nih.gov/pubmed/18281090>
- Srisitthiratkul, C., Yaipimai, W., & Intasanta, V. (2012). Environmental remediation and superhydrophilicity of ultrafine antibacterial tungsten oxide-based nanofibers under visible light source. *Applied Surface Science*, 259(0), 349-355. doi:

<http://dx.doi.org/10.1016/j.apsusc.2012.07.050>. Repéré à  
<http://www.sciencedirect.com/science/article/pii/S0169433212012378>

Strobel, M., Lyons, C. S., & Mittal, K. (1994). *Plasma surface modification of polymers: relevance to adhesion*. Vsp.

Sun, B., Long, Y. Z., Zhang, H. D., Li, M. M., Duvail, J. L., Jiang, X. Y., & Yin, H. L. (2014). Advances in three-dimensional nanofibrous macrostructures via electrospinning. *Progress in Polymer Science*, 39(5), 862-890. doi: <http://dx.doi.org/10.1016/j.progpolymsci.2013.06.002>. Repéré à <http://www.sciencedirect.com/science/article/pii/S0079670013000658>

Sun, D., Chang, C., Li, S., & Lin, L. (2006). Near-Field Electrospinning. *Nano Letters*, 6(4), 839-842. doi: 10.1021/nl0602701. Repéré à <http://dx.doi.org/10.1021/nl0602701>

Sundaram, H. S., Cho, Y., Dimitriou, M. D., Finlay, J. A., Cone, G., Williams, S., . . . Ober, C. K. (2011). Fluorinated Amphiphilic Polymers and Their Blends for Fouling-Release Applications: The Benefits of a Triblock Copolymer Surface. *ACS Applied Materials & Interfaces*, 3(9), 3366-3374. doi: 10.1021/am200529u. Repéré à <http://dx.doi.org/10.1021/am200529u>

Tai, M. H., Gao, P., Tan, B. Y. L., Sun, D. D., & Leckie, J. O. (2014). Highly Efficient and Flexible Electrospun Carbon-Silica Nanofibrous Membrane for Ultrafast Gravity-Driven Oil-Water Separation. *ACS Applied Materials & Interfaces*, 6(12), 9393-9401. doi: 10.1021/am501758c. Repéré à <http://dx.doi.org/10.1021/am501758c>

Tamborini, E., Ghofraniha, N., Oberdisse, J., Cipelletti, L., & Ramos, L. (2012). Structure of Nanoparticles Embedded in Micellar Polycrystals. *Langmuir*, 28(22), 8562-8570. doi: 10.1021/la301369z. Repéré à <http://dx.doi.org/10.1021/la301369z>

Tanaka, K., Takahara, A., & Kajiyama, T. (1998). Surface Molecular Aggregation Structure and Surface Molecular Motions of High-Molecular-Weight Polystyrene/Low-Molecular-Weight Poly(methyl methacrylate) Blend Films. *Macromolecules*, 31(3), 863-869. doi: 10.1021/ma9709866. Repéré à <http://dx.doi.org/10.1021/ma9709866>

- Tasuku, O., Bin, D., Yuji, S., & Seimei, S. (2007). Super-hydrophobic surfaces of layer-by-layer structured film-coated electrospun nanofibrous membranes. *Nanotechnology*, 18(16), 165607. Repéré à <http://stacks.iop.org/0957-4484/18/i=16/a=165607>
- Taylor, G. (1964). Disintegration of Water Drops in an Electric Field. *Proceedings of the Royal Society A: Mathematical, Physical and Engineering Sciences*, 280(1382), 383-397. doi: 10.1098/rspa.1964.0151
- Thorvaldsson, A., Edvinsson, P., Glantz, A., Rodriguez, K., Walkenström, P., & Gatenholm, P. (2012). Superhydrophobic behaviour of plasma modified electrospun cellulose nanofiber-coated microfibers. *Cellulose*, 19(5), 1743-1748. doi: 10.1007/s10570-012-9751-z. Repéré à <http://dx.doi.org/10.1007/s10570-012-9751-z>
- Tijing, L. D., Ruelo, M. T. G., Amarjargal, A., Pant, H. R., Park, C.-H., Kim, D. W., & Kim, C. S. (2012). Antibacterial and superhydrophilic electrospun polyurethane nanocomposite fibers containing tourmaline nanoparticles. *Chemical Engineering Journal*, 197, 41-48.
- Toncheva, A., Mincheva, R., Kancheva, M., Manolova, N., Rashkov, I., Dubois, P., & Markova, N. (2016). Antibacterial PLA/PEG electrospun fibers: Comparative study between grafting and blending PEG. *European Polymer Journal*, 75, 223-233. doi: <http://dx.doi.org/10.1016/j.eurpolymj.2015.12.019>. Repéré à <http://www.sciencedirect.com/science/article/pii/S0014305715300987>
- Tsai, P., Pacheco, S., Pirat, C., Lefferts, L., & Lohse, D. (2009). Drop Impact upon Micro- and Nanostructured Superhydrophobic Surfaces. *Langmuir*, 25(20), 12293-12298. doi: 10.1021/la900330q. Repéré à <http://dx.doi.org/10.1021/la900330q>
- Tuteja, A., Choi, W., Ma, M., Mabry, J. M., Mazzella, S. A., Rutledge, G. C., . . . Cohen, R. E. (2007). Designing superoleophobic surfaces. *Science*, 318(5856), 1618-1622.
- Utracki, L., & Favis, B. (1989). *Polymer alloys and blends* (Vol. 4). Marcel Dekker: New York.
- Valiquette, D., & Pellerin, C. (2011). Miscible and Core–Sheath PS/PVME Fibers by Electrospinning. *Macromolecules*, 44(8), 2838-2843. doi: 10.1021/ma102121t. Repéré à <http://dx.doi.org/10.1021/ma102121t>

- Vasita, R., Mani, G., Agrawal, C. M., & Katti, D. S. (2010). Surface hydrophilization of electrospun PLGA micro-/nano-fibers by blending with Pluronic® F-108. *Polymer*, 51(16), 3706-3714. doi: <http://dx.doi.org/10.1016/j.polymer.2010.05.048>. Repéré à <http://www.sciencedirect.com/science/article/pii/S0032386110004763>
- Wang, M., Fang, D., Wang, N., Jiang, S., Nie, J., Yu, Q., & Ma, G. (2014). Preparation of PVDF/PVP core-shell nanofibers mats via homogeneous electrospinning. *Polymer*, 55(9), 2188-2196. doi: <http://dx.doi.org/10.1016/j.polymer.2014.02.035>. Repéré à <http://www.sciencedirect.com/science/article/pii/S0032386114001372>
- Wang, N., Zhu, Z., Sheng, J., Al-Deyab, S. S., Yu, J., & Ding, B. (2014). Superamphiphobic nanofibrous membranes for effective filtration of fine particles. *Journal of Colloid and Interface Science*, 428, 41-48. doi: <http://dx.doi.org/10.1016/j.jcis.2014.04.026>. Repéré à <http://www.sciencedirect.com/science/article/pii/S0021979714002379>
- Wang, Q., Wang, X., Li, X., Cai, Y., & Wei, Q. (2011). Surface modification of PMMA/O-MMT composite microfibers by TiO<sub>2</sub> coating. *Applied Surface Science*, 258(1), 98-102. doi: <http://dx.doi.org/10.1016/j.apsusc.2011.08.013>. Repéré à <http://www.sciencedirect.com/science/article/pii/S0169433211012414>
- Wang, X., Ding, B., Yu, J., & Wang, M. (2011). Highly sensitive humidity sensors based on electro-spinning/netting a polyamide 6 nano-fiber/net modified by polyethyleneimine. *Journal of Materials Chemistry*, 21(40), 16231-16238. doi: 10.1039/C1JM13037D. Repéré à <http://dx.doi.org/10.1039/C1JM13037D>
- Wang, Y.-q., Wang, T., Su, Y.-l., Peng, F.-b., Wu, H., & Jiang, Z.-y. (2005). Remarkable Reduction of Irreversible Fouling and Improvement of the Permeation Properties of Poly(ether sulfone) Ultrafiltration Membranes by Blending with Pluronic F127. *Langmuir*, 21(25), 11856-11862. doi: 10.1021/la052052d. Repéré à <http://dx.doi.org/10.1021/la052052d>
- Wang, Y., Hong, X., Liu, B., Ma, C., & Zhang, C. (2008). Two-Dimensional Ordering in Block Copolymer Monolayer Thin Films upon Selective Solvent Annealing. *Macromolecules*, 41(15), 5799-5808. doi: 10.1021/ma800753a. Repéré à <http://dx.doi.org/10.1021/ma800753a>

- Wang, Z., Espín, L., Bates, F. S., Kumar, S., & Macosko, C. W. (2016). Water droplet spreading and imbibition on superhydrophilic poly(butylene terephthalate) melt-blown fiber mats. *Chemical Engineering Science*, 146, 104-114. doi: <http://dx.doi.org/10.1016/j.ces.2016.02.006>. Repéré à <http://www.sciencedirect.com/science/article/pii/S0009250916300513>
- Washburn, E. W. (1921). The Dynamics of Capillary Flow. *Physical Review*, 17(3), 273-283. Repéré à <http://link.aps.org/doi/10.1103/PhysRev.17.273>
- Wei, Q. F., Gao, W. D., Hou, D. Y., & Wang, X. Q. (2005). Surface modification of polymer nanofibres by plasma treatment. *Applied Surface Science*, 245(1-4), 16-20. doi: <http://dx.doi.org/10.1016/j.apsusc.2004.10.013>. Repéré à <http://www.sciencedirect.com/science/article/pii/S016943320401503X>
- Weijie, X., Anthony, A., James, J. Y., & Sang Jin, L. (2013). Controllable dual protein delivery through electrospun fibrous scaffolds with different hydrophilicities. *Biomedical Materials*, 8(1), 014104. Repéré à <http://stacks.iop.org/1748-605X/8/i=1/a=014104>
- Williams, M. L., Landel, R. F., & Ferry, J. D. (1955). The Temperature Dependence of Relaxation Mechanisms in Amorphous Polymers and Other Glass-forming Liquids. *Journal of the American Chemical Society*, 77(14), 3701-3707. doi: 10.1021/ja01619a008. Repéré à <http://dx.doi.org/10.1021/ja01619a008>
- Winchester, M. R., & Payling, R. (2004). Radio-frequency glow discharge spectrometry:: A critical review. *Spectrochimica Acta Part B: Atomic Spectroscopy*, 59(5), 607-666. doi: <http://dx.doi.org/10.1016/j.sab.2004.02.013>. Repéré à <http://www.sciencedirect.com/science/article/pii/S0584854704000709>
- Wu, J., Wang, N., Wang, L., Dong, H., Zhao, Y., & Jiang, L. (2012). Electrospun Porous Structure Fibrous Film with High Oil Adsorption Capacity. *ACS Applied Materials & Interfaces*, 4(6), 3207-3212. doi: 10.1021/am300544d. Repéré à <http://dx.doi.org/10.1021/am300544d>
- Wu, J., Wang, N., Zhao, Y., & Jiang, L. (2013). Electrospinning of multilevel structured functional micro-/nanofibers and their applications. *Journal of Materials Chemistry A*, 1(25), 7290-7305. doi: 10.1039/C3TA10451F. Repéré à <http://dx.doi.org/10.1039/C3TA10451F>

- Xianfeng, W., Bin, D., Jianyong, Y., Moran, W., & Fukui, P. (2010). A highly sensitive humidity sensor based on a nanofibrous membrane coated quartz crystal microbalance. *Nanotechnology*, 21(5), 055502. Repéré à <http://stacks.iop.org/0957-4484/21/i=5/a=055502>
- Xiao, K., Zhai, Y., Yu, J., & Ding, B. (2015). Nanonet-structured poly(m-phenylene isophthalamide)-polyurethane membranes with enhanced thermostability and wettability for high power lithium ion batteries. *RSC Advances*, 5(68), 55478-55485. doi: 10.1039/C5RA09325B. Repéré à <http://dx.doi.org/10.1039/C5RA09325B>
- Xue, Z., Cao, Y., Liu, N., Feng, L., & Jiang, L. (2014). Special wettable materials for oil/water separation. *Journal of Materials Chemistry A*, 2(8), 2445-2460. doi: 10.1039/C3TA13397D. Repéré à <http://dx.doi.org/10.1039/C3TA13397D>
- Yang, F., Wolke, J. G. C., & Jansen, J. A. (2008). Biomimetic calcium phosphate coating on electrospun poly( $\epsilon$ -caprolactone) scaffolds for bone tissue engineering. *Chemical Engineering Journal*, 137(1), 154-161. doi: <http://dx.doi.org/10.1016/j.cej.2007.07.076>. Repéré à <http://www.sciencedirect.com/science/article/pii/S1385894707005347>
- Yano, T., Yah, W. O., Yamaguchi, H., Terayama, Y., Nishihara, M., Kobayashi, M., & Takahara, A. (2011). Precise control of surface physicochemical properties for electrospun fiber mats by surface-initiated radical polymerization. *Polym J*, 43(10), 838-848. doi: <http://www.nature.com/pj/journal/v43/n10/supinfo/pj201180s1.html>. Repéré à <http://dx.doi.org/10.1038/pj.2011.80>
- Yoo, H. S., Kim, T. G., & Park, T. G. (2009). Surface-functionalized electrospun nanofibers for tissue engineering and drug delivery. *Advanced drug delivery reviews*, 61(12), 1033-1042. doi: <http://dx.doi.org/10.1016/j.addr.2009.07.007>. Repéré à <http://www.sciencedirect.com/science/article/pii/S0169409X09002324>
- Yuan, Y., Choi, S.-O., & Kim, J. (2016). Analysis of contact area between water and irregular fibrous surface for prediction of wettability. *RSC Advances*, 6(77), 73313-73322. doi: 10.1039/C6RA15389E. Repéré à <http://dx.doi.org/10.1039/C6RA15389E>
- Yue, M., Zhou, B., Jiao, K., Qian, X., Xu, Z., Teng, K., . . . Jiao, Y. (2015). Switchable hydrophobic/hydrophilic surface of electrospun poly (l-lactide) membranes obtained

by CF4 microwave plasma treatment. *Applied Surface Science*, 327, 93-99. doi: <http://dx.doi.org/10.1016/j.apsusc.2014.11.149>. Repéré à <http://www.sciencedirect.com/science/article/pii/S0169433214026476>

Zeleny, J. (1917). Instability of Electrified Liquid Surfaces. *Physical Review*, 10(1), 1-6. Repéré à <http://link.aps.org/doi/10.1103/PhysRev.10.1>

Zeng, J., Xu, X., Chen, X., Liang, Q., Bian, X., Yang, L., & Jing, X. (2003). Biodegradable electrospun fibers for drug delivery. *Journal of Controlled Release*, 92(3), 227-231. doi: 10.1016/s0168-3659(03)00372-9

Żenkiewicz, M. (2007). Methods for the calculation of surface free energy of solids. *Journal of Achievements in Materials and Manufacturing Engineering*, 24(1), 137-145.

Zhang, C., Salick, M. R., Cordie, T. M., Ellingham, T., Dan, Y., & Turng, L.-S. (2015). Incorporation of poly(ethylene glycol) grafted cellulose nanocrystals in poly(lactic acid) electrospun nanocomposite fibers as potential scaffolds for bone tissue engineering. *Materials Science and Engineering: C*, 49, 463-471. doi: <http://dx.doi.org/10.1016/j.msec.2015.01.024>. Repéré à <http://www.sciencedirect.com/science/article/pii/S092849311500034X>

Zhang, C., Wang, L., Zhai, T., Wang, X., Dan, Y., & Turng, L.-S. (2016). The surface grafting of graphene oxide with poly(ethylene glycol) as a reinforcement for poly(lactic acid) nanocomposite scaffolds for potential tissue engineering applications. *Journal of the Mechanical Behavior of Biomedical Materials*, 53, 403-413. doi: <http://dx.doi.org/10.1016/j.jmbbm.2015.08.043>. Repéré à <http://www.sciencedirect.com/science/article/pii/S1751616115003276>

Zhang, W., Yan, E., Huang, Z., Wang, C., Xin, Y., Zhao, Q., & Tong, Y. (2007). Preparation and study of PPV/PVA nanofibers via electrospinning PPV precursor alcohol solution. *European Polymer Journal*, 43(3), 802-807. doi: <http://dx.doi.org/10.1016/j.eurpolymj.2006.11.015>. Repéré à <http://www.sciencedirect.com/science/article/pii/S0014305706004009>

Zhao, F., Wang, X., Ding, B., Lin, J., Hu, J., Si, Y., . . . Sun, G. (2011). Nanoparticle decorated fibrous silica membranes exhibiting biomimetic superhydrophobicity and highly flexible properties. *RSC Advances*, 1(8), 1482-1488. doi: 10.1039/C1RA00605C. Repéré à <http://dx.doi.org/10.1039/C1RA00605C>

- Zhao, Z.-P., Li, M.-S., Li, N., Wang, M.-X., & Zhang, Y. (2013). Controllable modification of polymer membranes by long-distance and dynamic low-temperature plasma flow: AA grafting penetrated through electrospun PP fibrous membranes. *Journal of Membrane Science*, 440, 9-19. doi: <http://dx.doi.org/10.1016/j.memsci.2013.03.069>. Repéré à <http://www.sciencedirect.com/science/article/pii/S0376738813002809>
- Zhou, X., Liu, X., Xie, Z., & Zheng, Z. (2011). 3D-patterned polymer brush surfaces. *Nanoscale*, 3(12), 4929-4939. doi: 10.1039/C1NR11238D. Repéré à <http://dx.doi.org/10.1039/C1NR11238D>
- Zhu, L.-P., Yi, Z., Liu, F., Wei, X.-Z., Zhu, B.-K., & Xu, Y.-Y. (2008). Amphiphilic graft copolymers based on ultrahigh molecular weight poly(styrene-alt-maleic anhydride) with poly(ethylene glycol) side chains for surface modification of polyethersulfone membranes. *European Polymer Journal*, 44(6), 1907-1914. doi: <http://dx.doi.org/10.1016/j.eurpolymj.2008.03.015>. Repéré à <http://www.sciencedirect.com/science/article/pii/S0014305708001262>
- Zhu, M., Zuo, W., Yu, H., Yang, W., & Chen, Y. (2006). Superhydrophobic surface directly created by electrospinning based on hydrophilic material. *Journal of Materials Science*, 41(12), 3793-3797. doi: 10.1007/s10853-005-5910-z. Repéré à <http://dx.doi.org/10.1007/s10853-005-5910-z>